

This is a pre print version of the following article:

The 2.0–1.88 Ga Paleoproterozoic evolution of the southern Amazonian Craton (Brazil): An interpretation inferred by lithofaciological, geochemical and geochronological data / Roverato, M.; Giordano, D.; Giovanardi, T.; Juliani, C; Polo, L. - In: GONDWANA RESEARCH. - ISSN 1342-937X. - 70:(2019), pp. 1-21. [10.1016/j.gr.2018.12.005]

Terms of use:

The terms and conditions for the reuse of this version of the manuscript are specified in the publishing policy. For all terms of use and more information see the publisher's website.

15/05/2024 15:07

(Article begins on next page)

Manuscript Number: GR-D-18-00274R1

Title: The 2.0-1.88 Ga Paleoproterozoic evolution of the southern Amazonian Craton (Brazil): an interpretation inferred by lithofaciological, geochemical and geochronological data.

Article Type: Research Paper

Corresponding Author: Dr. Matteo Roverato, PhD

Corresponding Author's Institution: Yachaytech

First Author: Matteo Roverato, PhD

Order of Authors: Matteo Roverato, PhD; Daniele Giordano; Tommaso Giovanardi; Caetano Juliani; Liza Polo

Abstract: The study of Paleoproterozoic rocks is crucial for understanding Earth's tectonic evolution during the time when most of the modern crust and ore deposits were formed. The rocks of the Brazilian Amazonian Craton record some of the most-complete and best-preserved Paleoproterozoic magmatic and volcanic episodes on Earth. Following previous investigations, we present new lithofaciological and stratigraphic records of the felsic rocks of the Tapajós Mineral Province (TMP) (~ 2-1.88 Ga) and the São Felix do Xingú region (SFX) (~ 1.88 Ga) which, combined with new petrological and geochronological data, help providing a more complete understanding of the tectonic, magmatic and volcanological evolution of the Amazonian Craton. This magmatism/volcanism is thought to be formed in a late-/post-orogenic to extensional regime confirmed by the new geochemical data presented here. The transition from late-convergent to extensional tectonic setting could register the beginning of the taphrogenesis that marked the Amazonian Craton throughout the Mesoproterozoic. The volcanological approach of this contribution can serve as a strategy for the modelling of the evolution of Precambrian volcano-sedimentary basins around the world. The large amount of rocks analyzed are divided into primary and secondary volcanoclastic products depending on if they resulted from a direct volcanic activity (pyroclastic) or processes that reworked pyroclastic fragments. Furthermore, the deposits are subdivided into massive and stratified, depending on their primary mechanisms of transport and emplacement. By confirming the results from previous studies, our study permits to depict a more precise paleo-environmental picture of the processes that occurred in the Amazonian Craton during the Late-Paleoproterozoic. In particular, the presence of large regional-scale fissural systems and caldera collapses produced large silicic explosive volcanic eruptions, also accompanied by the emission of large volume effusive products. Although studies on the Amazonian Craton are still scarce and controversial, the present study provides new evidence that this volcanism may have formed one of the largest Silicic Large Igneous Provinces (SLIP) on earth. Our data also confirm that at least two major Paleoproterozoic periods of formation of volcanic rocks exist in the Amazonian craton. This point is of great relevance for any future interpretation of the geological evolution of this craton.

Response to Reviewers: To reviewer 1 Nils Lenhardt:

Dear reviewer,
we respected and changed most of the corrections suggested in
particularly we followed the suggestions to divide the lithofaciological
description and simplify the geological framework.
Thank you for the time you spent reading this long manuscript.

To reviewer 2 Roberto Dall'Agnol:

Dear reviewer,
thank you for your suggestions especially those related to the geological
framework and geochemical analyses. We considered and accepted most of
the changes suggested.
Now, the manuscript appears more clear.

Research Data Related to this Submission

There are no linked research data sets for this submission. The following
reason is given:

Data will be made available on request

Dear Editor of Gondwana Research,

Please find attached the manuscript: "*The 2.0-1.88 Ga Paleoproterozoic evolution of the southern Amazonian Craton (Brazil): an interpretation inferred by lithofaciological, geochemical and geochronological data.*" by Roverato M., Giordano D., Giovanardi T., Juliani C., and Polo L. which we would like to submit on Gondwana Research. This study documents in detail the extremely well preserved Paleoproterozoic architecture of a series of felsic volcanic and volcanoclastic rocks found in the southern part of the Amazonian Craton, Brazil. We aim to improve the current knowledge of the rare subaerial volcanism investigated in Precambrian volcanic regions by adding new textural data useful to better constrain this still poorly known volcanism. We provide also new geochemical and geochronological data that will increase the dataset of the study volcanic rocks. We use here a modern volcanological approach to describe the wide range of different lithofacies that our deposits display. We believe that this contribution will help to further our understanding of the geology of the Amazonian craton and, also, of other Precambrian volcanic areas worldwide.

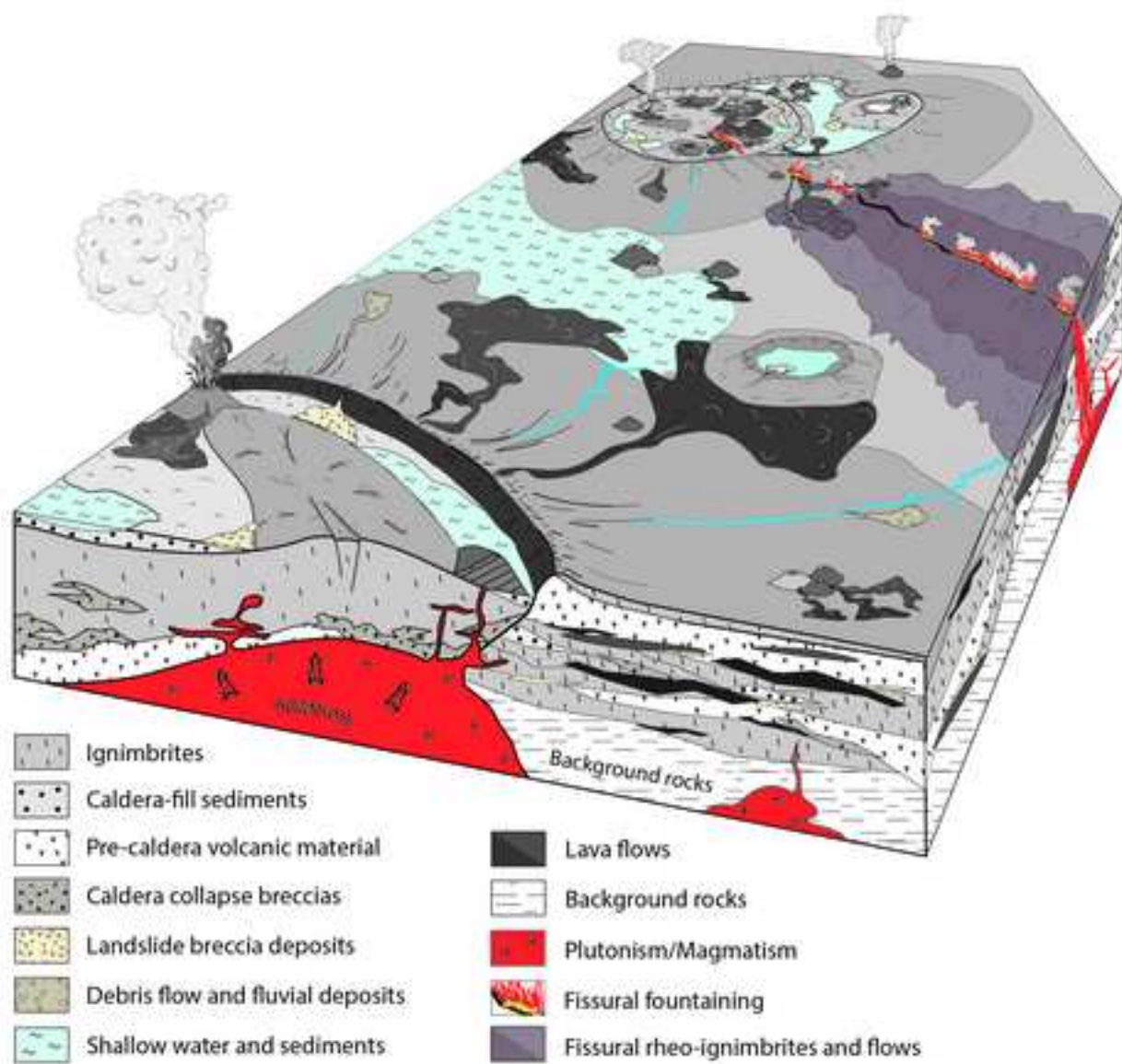
We hope that the manuscript will be of interest for a first class international journal like GR.

Yours sincerely,

Dr. Matteo Roverato

Highlights

- The modern lithofaciological approach is used here to describe the volcanic and volcanoclastic rocks of the Precambrian Amazonian Craton.
- The U-Pb geochronological data presented in the manuscript yielded three new ages of ca. 2.0 Ga and one new age of ca. 1.88 Ga that, linked with 31 geochemical analyses, increase the dataset available for the Amazonian craton and ancient terrains in general.
- The Paleoproterozoic volcanic activity that formed the large felsic rocks cropping out in the southern Amazonian craton is characterized by a fissure-fed and caldera volcanism with production of extensive lava flows and/or high-grade to rheomorphic ignimbrites, linked with other fragmental products of different type.



Reviewers' comments:

Reviewer #1: One of the main concerns of this manuscript is the lithofacies description and interpretation that oversimplifies the different lithofacies by only distinguishing them by their massive or stratified appearance. The observations and related interpretations seem to be of good value. However, I would suggest to make more subdivisions and adopt the terminology of McPhie et al. (1993) for non-genetic descriptive terms for each single lithofacies.

The manuscript contains too many different abbreviations for geological provinces, lithofacies types, etc. After a while, this appears rather confusing. Therefore, I would suggest to keep the abbreviations at a minimum, for instance for the lithofacies types and few other long terms that are constantly repeated throughout the text.

In the following paragraphs, some major suggestions are provided in detail. Further comments and suggestions (or questions) can be found in the attached commented manuscript.?

Author response:

Line 139:

Reviewer: What are the errors for the 2100 and 2875 Ma ages?

Line 148: What is the error for the 1880 Ma age?

Author: The reviewer further on suggests to simplify this chapter. We deleted the paragraph as suggested.

Lines 127-206:

Reviewer: A lot of information is presented here including many information on geochronology. Some of this information that is not particular of help for the understanding of the rest of the manuscript can probably be deleted or shortened. Furthermore, I suggest to show all mentioned locations on a map.

Author: Done! As suggested by Reviewer 1 we reduced this part by keeping some of the literature information useful to put our study in a wider context.

Rev: it would be good to see the detailed stratigraphy of the area: well we should wait for to more fieldwork.

Author: That's the problem, very few data are available nowadays, and actually this is one of the first work that try to present more detailed stratigraphy. We should organize a fieldwork there together!

line 226-229:

Rev: The way you describe the volcanoclastic rocks here, they are all fragmental rocks that are primary and syn-eruptive. However, effusive eruptions do not form fragments

Aut: yes they do! One example is a basal breccia of a thick lava flow. You can find a very well developed clastic deposit underneath the flow. In any case we deleted the point to avoid confusion.

Line 237:

Rev: Surely, no all volcanic products exhibit the same features. Otherwise, there would only be one lithofacies type. Please better describe what you mean.

Aut: Changed

Lines 239-243:

Rev: Not so many words are needed for this. Simply state that Table 1 shows all documented lithofacies including their descriptions and interpretations.

Aut: Done!

Lines 281-288

Rev: should be rephrased as they are difficult to read and understand. In particular, the paper of White and Houghton (2006) should be used here in order to define the terms pyroclastic and volcanoclastic. As it is, this part is not particularly clear. For once, effusive eruptions do not form volcanoclastic sediments. Furthermore, ignimbrites may also form due to PDCs.

Aut: Ok. We changed the sentence

Lines 297-486:

Rev.: There are some good observations and interpretations in here. However, the simplification into massive and stratified volcanoclastic rocks (containing everything from PDC deposits to autobreccias of a lava flow) and epiclastic rocks (containing everything from fluvial to mass-flow deposits) makes the chapter quite confusing. I suggest to make more subdivisions and describe the single lithofacies types one by one, probably adopting the non-genetic descriptive terms of McPhie et al. (1993). This way, the text may become slightly longer. However, the scientific value of the observations will significantly increase.

Aut.: Done! As the reviewer suggested, we divided the lithofacies descriptions and interpretations. Thank you for the suggestion!

Lines 785-789:

Rev: "Here we also image that an ideal late-convergent to extensional geotectonic environment was likely similar to that proposed in our discussion paragraph, where a post-orogenic to extensional regime for the period ~ 1.88 Ga was characterized by the emission of large volcanic felsic products." This sentence sounds very confusing and should be rephrased. For instance:

"The described volcano-sedimentary sequences that were characterized by the emission of large volcanic felsic products were formed in a post-orogenic to extensional regime during ~ 1.88 Ga."

Aut: Done! We changed the sentence!

Lines 789-791:

Rev:"With this contribution we want also stress the importance of the results obtained by investigating the lithofaciological character of the deposits instead of only carrying out geochemical studies." This should rather be obvious and can be omitted.

Aut: Done! We deleted the sentence

Reviewer #2: I appreciated your manuscript, in particular, the careful and detailed field and petrographic descriptions of lava flows and volcanoclastic sequences. Your data confirm the existence of, at least, two major Paleoproterozoic periods of formation of volcanic rocks in the Amazonian craton and this point is of great relevance for understanding the craton evolution. Your model to explain the origin of volcanic sequences is also a significant contribution. I made a series of comments and suggestions that I hope will help you to improve your manuscript. Most of them are not mandatory and should be evaluated for you. I have attached a pdf version indicating the main criticisms and indicating possible formal corrections.

Best regards,

Roberto Dall'Agnol

Author response:

1 - Abstract, p. 5, l. 41-45 - Please, rewrite. It is not clear.

Done

2 - Introduction, p. 5, l. 54-55 - I suggest to delete.

Done

3 - p. 5, l. 58-59 - References?

Done

4 - p. 5, l. 62 - the crust is...or the rocks are...???

Done

5 - p. 5, l. 63-67 - You are talking about the entire Amazonian craton but your references refer only to the regions of your direct interest. It is not reasonable to talk about mineral resources in the craton without any mention to the world-class mines of Carajás (iron, IOCG). I suggest to include also references of that province or to make clear that you are talking essentially about the Tapajós and Xingu regions.

Done

6 - p. 6, l. 71-74 - All this is the normal view of the Amazonian craton and it is correct in some degree. But I wonder if your contribution should not be directed to show that, in spite of the dominant conditions in the region, there are many areas where field information can be obtained and fresh rocks are available. This makes possible the petrological, geochemical and metallogenetic research on the craton that preserves better than one could imagine the signature of Precambrian events. You could illustrate this comment with the comprovod occurrence in the Tapajós province of Paleoproterozoic allunite (Juliani et al., 2005). In other words, better than reinforce the general view, you should show that many things are possible in the geological studies of the craton.

We deleted the sentence

7 - p. 6, l. 84-89 - This is remark is very important but it looks contradictory with you have said before (cf. my remark 6) about the geological research in Amazonia. Please, make consistent changing the previous generic and not representative description of Amazonian conditions.

Done!

8. p. 66, l. 89-90 - This statement was entirely true in the pioneer works of the research group but now it looks not very appropriate to say that they 'are novel in this area'. You have said before that the present work is a continuity of previous research developed by the group in the last 15 years.

Changed it!

9 - p. 6, l. 99-101 - This description of the Amazonian craton evolution is oversimplified and do not give a clear idea of the more recent tectonic models proposed to explain it. You should present it more critically. E.g., the existence of a large Archean platform is not entirely demonstrated. You are mentioning the models of tectonic-geochronologic provinces and the existence of domains formed after the Trans-Amazonian event in the following. These topics should be better integrated and more consistent.

10 - p. 7, l. 104-107 - The relevance of the Uatumã Group in the Paleoproterozoic evolution of the craton is clearly demonstrated but it cannot be said that "All volcano/plutonic rocks forming the craton are attributed to the Uatumã Supergroup". There are many magmatic units, including Paleoproterozoic ones, that have nothing to do with the Uatumã Supergroup. You should clarify these points, showing the relevance of the Uatumã event but with a more rigorous description of it.

11 - p. 7, l. 108-110 - Your statement is not helping to show the real stage of knowledge of the Amazonian craton. I would say that we have now a general picture of the craton evolution and there are some portions of it relatively well studied, side by side with poorly known areas.

These last 3 points (9,10,11) are related to the geological framework chapter. We changed the chapter in accordance with the correct suggestions of reviewer 2 and, also the points commented by reviewer 1 who suggests to simplify the information. As suggested by Reviewer 2 we also changed figure 1 so to provide the wider context of application of our research

12 - p. 7, l. 116-119 - Is this context of ocean-continent subduction and flat subduction consistent with the hypothesis of "The transition from late-convergent to extensional tectonic setting could register the beginning of the taphrogenesis that marked the Amazonian Craton throughout the Mesoproterozoic (your abstract)"?

Yes, because the volcanic rocks studied (specially the andesitic rocks well described in Fernandes et al., 2011 and Roverato et al., 2017, but also the felsic older rocks in TMP) are related to a continental arc tectonic environment. The idea is that the system passes from an ocean-continent flat-subduction setting to a post-orogenic /extensional tectonism (as proved by the presence of younger felsic A-type rocks in SFX)

13 - p. 8, l. 148 - Some authors employ the term 'aluminous' for some A-type granites that vary generally from metaluminous to mildly peraluminous (e.g., King et al., 1997; Lamarão et al., 2002). However, this is a not rigorous term because these A-type granites are typically low Al₂O₃ granites (Dall'Agnol and Oliveira, 2007, Lithos). King et al. (Australian Journal of Earth Sciences, 2001, 48, p.501) have abandoned and advised against the use of this term because 'aluminous' can be related to S-type peraluminous granites that are entirely distinct of the A-type granites. For this reason, I suggest to the authors to avoid the use of the term 'aluminous' for A-type granites.

This is the only point where we used this term. In any case due to changes, we deleted the entire paragraph

14 - p. 8, l. 151 - Please, verify the error of 1870 +- 0.008 Ma.
It is correct in Juliani et al., 2005

15 - p. 8, l. 158 and 160 - alkaline is ambiguous in this context because it can be confused with peralkaline. I suggest to delete alkaline.

Done

16 - p. 9, l. 172, Fig. 1 and 2 - The presentation of the figures is very poor and should be improved. In figure 1, only the Brazilian part of the Amazonian craton is represented and the reference of the model of geochronologic provinces adopted is not informed in the caption of the figure. The Rio Negro province is not correctly represented.

The schematic geologic maps of Figure 2 do not follow the classical conventions. The colors adopted for different geologic units are inappropriate. I suggest to revise entirely figures 1 and 2.

Improved fig 1 and 2. In figure 2 we added the location of the outcrops and rocks presented in the paper. I don t agree that about the geological unit, I'm using my symbols well expressed in the legend.

17 - p. 9, l. 178-181 - It would be more appropriate to say that the basement of the volcano-plutonic complex is not exposed. It could be similar to the Mesoarchean units of the Carajás province, as suggested by Nd TDM ages obtained by Teixeira et al. (2002) in andesites and rhyolites of Xingu area. It was published recently a synthesis of new geochronological data about the 1.88 Ga granites of the Carajás province (Teixeira et al., 2018, J South American Earth Sci). The authors have also presented a discussion about the relevance of the 1.88 Ga event in the craton and elsewhere.

We deleted the paragraph.

19 - p. 10, l. 217-220 - Independent of the degree of alteration and lithification, pyroclastic and volcanoclastic sequences need to be defined in the field, because they mix igneous and sedimentary features. Hence, I suggest you to emphasize the relevance of field observations in your work better than to put in relief the restrictions you had. Another point is that 'alteration' should be possibly mean hydrothermal alteration and it should be distinguished of weathering alteration because readers can suppose that your rocks were intensely weathered and you are clearly showing that you were able to collect fresh samples for petrographic, geochemical and geochronologic studies.

We deleted the paragraph as also suggested by the other reviewer.

20 - p. 10, l. 230 - Coastal? Is it accurate?

YES

22 - p. 11, l. 250, Fig. 3 and its caption - It should be given a general idea of the location and informed the point of sampling where the photographs were taken and the units presented in each case. This should be done also in the captions of figures 4 and 5.

Done and thank you for the suggestion

24 - p. 11, l. 264 - 265 - pervasive does not give an idea of abundance. 10 vol % to how much in vol %?

Done!

25 - p. 13, l. 312, Fig. 5B - There is an euhedral crystal in the central lower part of Figure 5B that is named plg (plagioclase). I suspect that it can be a crystal of alkali-feldspar. Please, verify.

Sure! Changed it!

26 - p. 13, l. 326 -330, Fig. 6 - It is important to indicate the location of that sequence in the geological map of Figure 2.

Done

27 - Fig. 8, 9, 10, 11 - You present an extremely valious register of field and macroscopic aspects of the studied volcanic sequences. It looks very important to me that the location of the documented points should be given. These points will be a relevant reference for future studies.

Done

28 - p. 18, l. 491, Fig. 12 and its caption - In the caption of the figure are mentioned the TAS, AFM and SiO₂-K₂O digrams. However, in the available version of your manuscript the Figure 12 is identical to Figure 13 and the diagrams mentioned in Figure 12 are not presented. Without the figures it is difficult to evaluate the consistence of your text.

Done

29 - p. 18, l. 489 Geochemistry, Table 2 - You should give information about the methods employed and the laboratory where the chemical analyses were done.

we have added a small 'Analytical Methods' chapter to the text.

30 - Chemical Analyzes, Table 2 - It should be included on Table 2 the classification and the volcanic facies of the analyzed rock. It is important to distinguish, if possible, the rocks with I-type and A-type affinity. The meaning of V, I and R should be explained in the foot of the table.

the meaning of VC, I and R is already in the figure caption. We have reformulated the text to make it more clear. We have also added the classification of I- and A-type affinity

31 - p. 19. l. 524 - 529, Fig. 14 - The distribution of the studied rocks in the Pearce's diagram of 1984 suggest in fact that they can be related to a post-collisional setting (cf. Pearce, 1996, Episodes).

we have added the diagram to Fig. 14 and add it to the chapter.

32 - p. 20-23, l. 571-659; 7. Discussion

7.1 Subduction-related to extensional setting - In general, this topic of discussion section is well organized and looks consistent to me. I have some remarks that hope can help you in the review.

- p. 20, l. 573-576, Fig. 14 - As mentioned before, if you consider Pearce (1996), the distribution of the whole of your samples suggest a post-collisional setting for the studied rocks.

we have taken it into account and added some paragraphs at the discussion.

p. 20, l. 576-577, Fig 14, diagram FeO_t/MgO vs. Zr+Nb+Ce+Y - The analyzed rocks plot mostly to the right of the fields of typical I and S granites because they are enriched in HFSE compared to these granites. It is not correct to say that your rocks have low HFSE. On the contrary, the relatively high HFSE contents distinguish your rocks of typical I and S granites and approach them of A-type rocks.

We agree. The sentence was not clear; we want to point out that TMP volcanics have enrichment in incompatible elements with respect HSFSE which suggest the occurrence of crustal component in the melt. We have rephrased the sentence to make it more clear and pointing that our samples have also high HSFSE content which shift the volcanics composition from the I- and S-type granites to the A-type field.

It is also relevant to mention that your ~2.0 Ga volcanic rocks are a little distinct in this respect of the Vila Riozinho formation rocks (Lamarão et al., 2002) that show a little lower HFSE contents when compared to your TMP samples. Besides, the hypothesis of a more evolved character for your rocks compared to VR of Lamarão et al. (2002), you should consider the possibility that the 2.0 Ga volcanism is not uniform in composition and advocate for TMP rocks an intermediate geochemical character between the VR and MA. The rocks of TMP analyzed (Fig. 2) are dispersed in a large area and not restricted to the VR type area. So, is it reasonable that some geochemical variations could occur.

notwithstanding we think that the TMP derived from more evolved melts with respect to the VR, as observed by higher Si, K, trace elements and evidences of fractional crystallization in the TMP melts, we agree that these features could be possibly related to 'heterogeneities' in the magmatism. We have added a paragraph to point out this possibility,

- p. 22, l. 631-639 - The 2.0-1.88 Ga event in the craton and also in the scale of the planet, as indicated by Antonio et al. (2018), has effectively great relevance. A similar discussion about the 1.88 Ga anorogenic granites of the Carajás province was recently presented (Teixeira et al., 2018; SAMES) and it can allow you to go deep in this point of the discussion.

we appreciate the indication and we have provided to discuss a little further the geodynamic setting of the TMP and SFX magmatism.

1
2 1
3 2 **The 2.0-1.88 Ga Paleoproterozoic evolution of the southern Amazonian Craton**
4 3 **(Brazil): an interpretation inferred by lithofaciological, geochemical and**
5 4 **geochronological data.**
6
7
8
9

10 6 Roverato^{*1,2} M., Giordano^{3,4} D., Giovanardi⁵ T., Juliani² C., Polo² L.
11 7

- 12 8 1. YachayTech University, School of Geological Sciences and Engineering, Hacienda San José,
13 9 Urcuquí, Ecuador.
14
15 10 2. ~~Departamento de Geologia Sedimentar e Ambiental (GSA)~~, Instituto de Geociências (IGC),
16 11 Universidade de São Paulo, INCT – Geociam, SP, 05508080, Brazil.
17
18 12 3. Università degli studi di Torino, Dipartimento di Scienze della Terra, via Valperga Caluso 35,
19 13 10125, Torino, Italy.
20
21 14 4. Centro Nazionale delle Ricerche (CNR), Istituto di Geoscienze e Georisorse (IGG), via G.
22 15 Moruzzi 1, 56124, Pisa, Italy.
23
24 16 5. Università di Modena e Reggio Emilia, Dipartimento di Scienze Chimiche e Geologiche, 41125,
25 17 Modena, via Campi 103, Italy.
26
27
28

29 19 *Corresponding Author: ~~matteomroverato1809@yachaytech.edu.egmail.com~~
30 20

31 21 Keywords: Paleoproterozoic volcanism; Amazonian craton; Fissure eruption; Felsic
32 22 volcanism; Lithofacies analyses
33
34
35
36
37
38

39 25 Abstract

40 26 The study of Paleoproterozoic rocks is crucial for understanding Earth's tectonic
41 27 evolution during the time when most of the modern crust and ore deposits were
42 28 formed~~Paleoproterozoic rocks represent some of the most interesting rocks to~~
43 29 ~~comprehend Earth's tectonic evolution during the Precambrian Supereon when most of~~
44 30 ~~modern crust and ore deposits formation occurred.~~ The rocks of the Brazilian Amazonian
45 31 Craton record one of the most-complete and best-preserved Paleoproterozoic magmatic
46 32 episodes on Earth. ~~Amazonian rocks record one amongst the most complete and best-~~
47 33 ~~preserved Paleoproterozoic magmatic episodes on Earth.~~ Following previous
48 34 investigations, we present new lithofaciological and stratigraphic records of the felsic
49 35 rocks of the Tapajos Mineral Province (TMP) (~ 2-1.88 Ga) and the São Felix do
50
51
52
53
54
55
56
57
58
59
60
61
62
63
64
65

Formatted: Default Paragraph
Font, Font: 12 pt

Formatted: Font: Times New
Roman, No underline, Not Highligh

Formatted: Font: Times New
Roman, No underline, Not Highligh

Formatted: Font: Times New
Roman, No underline

Xingu region (SFX) (~ 1.88 Ga) which, combined with new petrological and geochronological data, help providing a more complete understanding of the tectonic, magmatic and volcanological evolution of the Amazonian Craton. This magmatism/volcanism is thought to be formed in a late-/post--orogenic to extensional regime confirmed by the new geochemical data presented here. The transition from late-convergent to extensional tectonic setting could register the beginning of the taphrogenesis that marked the Amazonian Craton throughout the Mesoproterozoic. The modern volcanological approach of this contribution can serve as a model for the evolution of Precambrian volcano-sedimentary basins around the world. The large amount of rocks analyzed are divided into primary and secondary volcanoclastic volcanoclastic and sedimentary products depending on if they resulted from a direct volcanic activity (pyroclastic) or reworked processes that reworked pyroclastic fragments. In this second group are also included the epiclastic rocks constituted by all sediments that had been reworked before, independent of their source and composition. Furthermore, the deposits are divided in massive and stratified, depending on their different transport and emplacement mechanisms. By confirming the results from previous studies, our study permits to depict a more precise paleo-environmental picture of the processes that occurred in the Amazonian Craton during the Late-Paleoproterozoic. In particular, the presence of large regional-scale fissural systems with caldera collapses produced large silicic explosive volcanic eruptions, which were also accompanied by the emission of large volume effusive products. Although studies on the Amazonian Craton are still scarce and controversial, the present study provides new evidence that this volcanism may have formed one of the largest Silicic Large Igneous Provinces (SLIP) on earth.

1. Introduction

The Proterozoic Eon (2500 – 541 Ma) is the longest and youngest part of the Precambrian Supereon. This Eeon represents the time just before the proliferation of oxygen accumulation and complex life on Earth. This period was likely the most tectonically active in Earth's history. In fact, it is also the period during which the largest portion of the modern crust (43%) and mineral ores were produced (Condie, 2000). Studies by Condie (2000) and Rino et al. (2004) suggest that crust production took place episodically, forming predominantly granitoid crust and secondary volcanic and metamorphic rocks, some of which are extraordinarily well preserved.

Formatted: Font: Times New Roman, 12 pt, No underline

Formatted: Font: Times New Roman, 12 pt, No underline

Formatted: Indent: First line: 0 cm

1
2
3
4
5
6
7
8
9
10
11
12
13
14
15
16
17
18
19
20
21
22
23
24
25
26
27
28
29
30
31
32
33
34
35
36
37
38
39
40
41
42
43
44
45
46
47
48
49
50
51
52
53
54
55
56
57
58
59
60
61
62
63
64
65

70 The Amazonian Craton (AC) is one of the largest Precambrian terrains in the
71 world (4.6x10⁶ km²) (Almeida et al., 1981). It occupies approximately half of the
72 Brazilian territory and it is the location of important mineral resources such as gold,
73 iron, copper, and tin, among others (Faraco et al., 1997; Bahia and Quadros, 2000;
74 Juliani, 2002; Klein et al., 2002, ~~;~~ ~~Klein et al.,~~ 2004; Reis et al., 2006; Klien and
75 Carvalho, 2008; Monteiro et al., 2008; Juliani et al., 2014, Dall’Agnol et al., 2017).
76 Although the geological investigation of the AC has recently seen a renewed interest of
77 the national and international scientific community, mainly because of the massive
78 presence of ore deposits, a general consensus related to the interpretation of its
79 complex ~~-~~ Paleoproterozoic evolution is still missing. Ancient volcanic regions
80 represent a challenge for the understanding of emplacement dynamics especially when
81 the stratigraphic relationships are difficult to decipher or blurred by erosion or
82 vegetation cover ~~:-~~
83 ~~In fact, the difficult access to the outcrops, due to dense forest cover and to the~~
84 ~~presence of extensive water basins together with, in most cases, the bad preservation of~~
85 ~~the ancient outcrops with frequently obliterated structures and textures, significantly~~
86 ~~complicate this task.~~
87 The present work constitutes the natural prosecution of previous investigations, carried
88 out by our research group (Juliani et al., 2005, ~~;~~ ~~Juliani et al.,~~ 2010, 2014~~;~~ Fernandes et
89 al., 2011~~;~~ ~~Juliani et al.,~~ 2014; da Cruz et al., 2015; Roverato, 2016~~;~~ ~~;~~ 2015; ~~Roverato et~~
90 ~~al., 2016;~~ ~~Roverato, 2016;~~ Roverato et al., 2016, 2017), which are devoted to
91 characterize the dynamics of emplacement of Precambrian volcanic rocks and their
92 relationships to sedimentary facies. The study area comprises of the Tapajós Mineral
93 Province (TMP) and the São Felix do Xingú (SFX) region, Pará state, northern Brazil.
94 This contribution provides a means to interpret the volcanic processes active in this
95 region during the Precambrian, mainly based on field observation and detailed
96 lithofacies analyses. In addition, ~~-~~ new geochemical and geochronological data are
97 provided. The superb preservation of the rock textures investigated here is such that
98 they help us to better constrain the genetic mechanisms that brought to the formation of
99 the investigated felsic deposits. ~~-~~ Our study demonstrates how powerful is the approach
100 of rock structure and texture characterization to the interpretation of the eruptive
101 processes that governed the emplacement of volcanic and volcanoclastic sequences.
102 The detailed lithofacies characterization and the stratigraphic reconstruction are ~~novel~~
103 important in this area and constitute a powerful ~~new~~ key-tool to appropriately interpret

Formatted: No underline, Superscript

Formatted: No underline, Superscript

Formatted: Indent: First line: 0 cm

Formatted: No underline, Font color: Auto, Highlight

1
2 104 the evolution of Precambrian volcano-sedimentary basins. Such an approach would
3 105 turn to be useful when employed to investigate ancient terrains associated both to the
4 106 ancient Amazonian felsic volcanism and Precambrian terrains in general.
5
6 107

8 108 2. Geological evolution of the southern portion of the Amazonian craton

9
10 The AC (Almeida et al., 1981) is located in the northern part of South America
11 and is divided into two Precambrian shields, the Central-Brazil (or Guaporé, southern
12 portion) and Guiana Shields (northern portion), which are separated by the
13 Phanerozoic Amazonian Sedimentary Basin (Fig. 1) (Almeida et al., 1981). The entire
14 craton has become stable before the end of the Precambrian (Dall'Agnol et al., 1994).

15
16
17 The AC ~~(Almeida et al., 1981)~~ has been considered (Amaral, 1974; Hasui et al.,
18 1993; Costa and Hasui, 1997) as a large Archean platform that had been reworked
19 and reactivated during the ca. 2100 Ma Trans-Amazonian event ~~(Amaral, 1974; Hasui~~
20 et al., 1993; Costa and Hasui, 1997). The AC is located in the northern part of South
21 America and is divided into two Precambrian shields, the Central-Brazil (or Guaporé)
22 and Guiana Shields, which are separated by the Phanerozoic Amazonian Sedimentary
23 Basin (Fig. 1) (Tassinari and Macambira, 1999; Santos et al., 2000). All igneous rocks
24 forming the craton are attributed to the Uatumã Supergroup, which extends to an area
25 of at least 1,500,000 km² (Dall'Agnol et al., 1999; Lamarão et al., 1999).

26
27
28 Alternative ideas Although several approaches have been used to unravel the
29 complex tectonic evolution of these huge and frequently inaccessible territories, a clear
30 understanding of the geological past of this area is still largely unknown. Based on
31 geochronological and isotopic data, Teixeira et al. (1989), (Teixeira et al., 1989;
32 Tassinari and Macambira, (1999;), and Santos et al., (2000) divided the craton into
33 several, predominantly NW-oriented geochronological provinces, which have been
34 interpreted as successive continental accretionary events, followed by granitic
35 magmatism and tectonic reworking ~~(Tassinari and Macambira (1999), Santos,~~
36 (2003); and Vasquez et al., (2008) identified six and eight geochronological
37 provinces, respectively (Fig. 1).

38
39
40 In a recent review Teixeira et al. (2019) report that the AC is the host of four
41 LIP-scale (or SLIP) magmatic events discriminated by the Orocaima, Uatumã,
42 Avanavero and Rincón del Tigre events, among other intra-plate activity through time
43 and space. The igneous rocks described in the present manuscript are widely attributed
44 to the Uatumã event (Dall'Agnol et al., 1999; Lamarão et al., 1999). More recently,
45
46
47
48
49
50
51
52
53
54
55

Formatted: Indent: First line: 0 cm

Formatted: Adjust space between Latin and Asian text, Adjust space between Asian text and numbers

Formatted: No underline, Not Highlight

1
2 138 ~~The studied Juliani and Fernandes (2010), Fernandes et al. (2011) and Roverato et al.~~
3 139 ~~(2017) suggested that the entire region is located~~ between TMP and SFX, ~~which may~~
4 140 ~~beis considered to be~~ related to a continental arc, with a NE-SW arc migration ~~as~~
5 141 ~~suggested by Juliani and Fernandes (2010), Fernandes et al. (2011) and Roverato et al.~~
6 142 ~~(2017).~~ -According to these authors a migration from the Serra do Cachimbo graben (in
7
8 143 TMP where the subduction trench is located) towards the SFX could be explained by a
9
10 144 change in the subducting angle of the oceanic plate beneath the continental plate. This
11
12 145 is in agreement with the flat-subduction plate settings proposed by previous authors ~~in~~
13 146 ~~other parts of the world~~ (Ferrari et al., 2012; Gutscher et al., 2000; Kay et al., 2005;
14
15 147 Mori et al., 2007; Manea et al., 2012; ~~Fernandes et al., 2011; Juliani et al., 2014~~).
16
17 148

19 149 2.1. The TMP (Tapajós Mineral Province)

20
21 150 The TMP (Fig. 2a) is primarily situated in the Tapajós–Parima
22
23 151 geochronological/tectonic province (Santos et al., 2000) with the eastern part
24
25 152 belonging to the Amazonia Central geochronological/tectonic province (Fig. 1). Based
26
27 153 on Sm–Nd data and U–Pb ages (2100–1870 Ma), Santos et al. (2001, 2004) and
28
29 154 Vasquez et al. (2008), identified several different domains for the Tapajós–Parima
30
31 155 geochronological province and consider the TMP as a sequence of continental
32
33 156 magmatic arcs ~~(Ferreira et al., 2000; Santos et al., 2000, 2004; Vasquez et al., 2000;~~
34
35 157 ~~Klein et al., 2001; Lamarão et al., 1999, 2002).~~ ~~The oldest granitoids and gneisses in~~
36
37 158 ~~this region belong to the Cuiú–Cuiú magmatic arc complex; the Conceição tonalite~~
38
39 159 ~~(Cuiú–Cuiú magmatism) yielded a U–Pb zircon age of 2019 ± 23 Ma (Santos et al.,~~
40
41 160 ~~2000). The supracrustal sequences of the Jacareacanga Group are considered broadly~~
42
43 161 ~~coeval with the Cuiú–Cuiú complex. Both units are related to early stages of magmatic~~
44
45 162 ~~arc development (Ferreira et al., 2000; Klein et al., 2001). Detrital zircon ages of ca.~~
46
47 163 ~~2100 and ca. 2875 Ma have been obtained for the Jacareacanga Group (Santos et al.,~~
48
49 164 ~~2000). Stratigraphically above the Jacareacanga Group is the Vila Riozinho Formation,~~
50
51 165 ~~formed by ca. 2000–1990 Ma intermediate to felsic volcanic rocks (Lamarão et al.,~~
52
53 166 ~~2002). These units are intruded by the ca. 2000–1970 Ma syn- to late-orogenic calc-~~
54
55 167 ~~alkaline granitoids of the Creporizão suite (Lamarão et al., 1999; Vasquez et al., 2000).~~
56
57 168 ~~Following this first intrusive event, a second intrusive event was characterized by the~~
58
59 169 ~~1907 ± 9 and 1892 ± 6 Ma granitoid rocks of the Tropas Suite (Santos et al. 2001,~~
60
61 170 ~~2004). The ca. 1880 Ma Parauari suite corresponds to a younger generation of post-~~
62
63 171 ~~orogenic, calc-alkaline granitoids and is mainly exposed in the northeastern part of the~~
64
65

Formatted: Indent: First line: 0 cm

Formatted: Indent: First line: 1.27 cm

172 ~~region. The Maloquinha ca. 1880 Ma aluminous A-type granite plutons are also found~~
173 ~~in the province and closes the sequence.~~ Late Paleoproterozoic volcanism of the
174 Tapajós domain is represented ~~by the Vila Riozinho Formation, formed by ca. 2000-~~
175 ~~1990 Ma intermediate to acid volcanic rocks (Lamarão et al., 2002), and~~ by the Iriri
176 Group that can be divided into the Bom Jardim (Almeida et al., 2000), Salustiano
177 (1870 ± 0.008 Ma; Juliani et al., 2005) and Aruri (Pessoa et al., 1977) formations.
178 ~~-The Bom Jardim Formation (1898 ± 5 Ma, Santos et al., 2001) consists of~~
179 mafic to intermediate high-K to shoshonitic calc-alkaline rocks while the latter
180 formations are characterized by rhyolites, dacites and their pyroclastic and epiclastic
181 derivatives. Juliani et al. (2005) considered the Bom Jardim volcanism as a preliminary
182 step of the Iriri event representing pre-caldera volcanism followed by the Salustiano
183 and Aruri caldera-related felsic activity. Post-caldera volcanism is characterized by
184 ring-felsic volcanic structures that produced ~~alkaline~~ A-type (Vasquez and Dreher,
185 2011) rhyolitic lavas and volcanoclastic deposits. Lamarão et al. (2002, 2005) described
186 the ~~alkaline~~ felsic A-type Moraes Almeida volcanic sequence (1890 ± 6 Ma rhyolite,
187 1875 ± 4 Ma ignimbrite) represented by lavas and ignimbrites as part of the Iriri Group.
188 Juliani et al. (2014) consider these last A-type ~~alkaline~~ rocks as similar in composition
189 and age to the Santa Rosa Formation that crops out in the São Felix do Xingú region
190 (SFX), which is considered to have formed by the same fissural-type volcanism
191 (Juliani and Fernandes, 2010; Fernandes et al., 2011; Roverato et al., 2016).
192 Preliminary data indicate that these rocks, ~~for~~ both ~~-~~TMP and SFX, display a very low
193 grade of metamorphism, falling into the prehnite-pumpellyite field (Echeverri-Misas,
194 2010; Lagler et al., 2011; Fernandes et al., 2011).

196 2.2. The SFX (São Felix do Xingú region)

197 According to the work of Santos (2003) and Vasques et al. (2008) the SFX
198 region belongs to the Amazonia Central province (Fig. 1). The study area (Fig. 2b) is
199 located near to São Felix do Xingú ~~city~~, which corresponds to the southern portion
200 of the Carajás Province. ~~The geographical limits of SFX are still uncertain, mainly due~~
201 ~~to the difficult access to the area. The eastern limit is marked by the Archean TTG~~
202 ~~rocks several km east to Xingu River while the dense vegetation cover does not permit~~
203 ~~access to the south. The northern limit is roughly marked by the Archean Xingu~~
204 ~~complex and younger intrusive formations (Macambira and Vale, 1997). The basement~~
205 ~~of the SFX region is represented by the Archean Rio Maria Granite-Greenstone~~

Formatted: Indent: First line: 0 cm

1
2 206 ~~Terrain and the metavolcano-sedimentary units of the Itacaiúnas Supergroup (Araújo et~~
3 207 ~~al., 1988).~~ The Paleoproterozoic volcanic sequences in the SFX comprise the basal
4
5 208 Sobreiro and upper Santa Rosa formations (Macambira and Vale, 1997; Juliani and
6
7 209 Fernades, 2010), which are crosscut by the Sn-bearing A-type granitoids of the Velho
8
9 210 Guilherme Suite (Teixeira et al., 2002). Antonio et al. (2017) published the first U-Pb
10
11 211 ages on zircons for the Santa Rosa Formation with 1877.4 ± 4.3 Ma for a rhyolite and
12
13 212 1895 ± 11 Ma for a dike. Recent geochronological data on a felsic porphyritic dike
14
15 213 belonging to the Velho Guilherme suite yielded an age of 1857 ± 8.4 Ma (Shrimp U/Pb
16
17 214 zircon analyses; Roverato, 2016). Other available geochronological data yielded ca.
18
19 215 1880 ± 6 Ma (TIMS Pb–Pb in zircon) for the Sobreiro Formation and ca. 1879 ± 2 Ma
20
21 216 (TIMS Pb–Pb in zircon) for the Santa Rosa Formation (Fernandes et al., 2011; Pinho et
22
23 217 al., 2006; Teixeira et al., 2002). Despite their similar ages, their geochemical
24
25 218 compositions, geological features and eruption styles point to their non-cogeneticity
26
27 219 (Fernandes et al., 2011). ~~The Sobreiro Formation was defined for the first time by~~
28
29 220 ~~Macambira (1997) and Macambira and Vale (1997) as constituted by andesitic, trachy-~~
30
31 221 ~~andesitic and trachytic magmatism.~~ The Sobreiro Formation (SF) comprises basaltic
32
33 222 andesite, andesite and less dacite massive lava flows and volcanoclastic rocks with
34
35 223 high-K calc-alkaline signature (Fernandes et al., 2011; Roverato et al., 2017).
36
37 224 According to da Cruz et al. (2015) late- to post-magmatic hydrothermal alteration in
38
39 225 these rocks is responsible for a secondary paragenesis characterized by epidote,
40
41 226 chlorite, carbonate, clinozoisite, sericite, quartz, albite, hematite and pyrite. The Santa
42
43 227 Rosa Formation (SRF) is described by Fernandes et al. (2011) as characterized by four
44
45 228 lithological facies with A-type signature: (i) rhyolitic lava flow and thick dikes of
46
47 229 banded rhyolite and ignimbrite; (ii) highly rheomorphic felsic ignimbrite associated
48
49 230 with un-welded ash tuff; (iii) felsic crystal tuff, lapilli-tuff and co-ignimbritic breccias;
50
51 231 (iv) granitic porphyry stocks and dikes and subordinate equigranular granitic
52
53 232 intrusions.
54
55 233

234 ~~3. Results~~

235 ~~Lithofaciological, petrological, geochemical and geochronological analyses were~~
236 ~~carried out in the course of this study in order to understand the geodynamic evolution~~
237 ~~of the study area. 31 new geochemical data for the TMP rock samples are presented~~
238 ~~here and compared with published data of Lamarão et al. (2002) and SFX previous~~
239 ~~results (Fernandes et al. (2011)). The geochemical signature of SFX rock samples have~~

Formatted: Indent: First line: 0 cm

240 already recently been reported by Fernandes et al. (2011) who made unnecessary new
241 analysis for our study. Four new geochronological data of rock samples from the TMP
242 (3 samples) and SFX (1 sample) are also provided to compare with dating available for
243 the AC. Finally, so far it concerns with the lithofaciological analysis we remind that a
244 characterization of the granulometry of the deposits and of the shape of the fragments
245 was qualitatively defined in the field, since the degree of alteration and lithification
246 would have been impossible in the laboratory.

250 34. Lithofacies analyses and stratigraphy

251 Lithofaciological analyses were carried out in the course of this study in order
252 to understand the geodynamic evolution of the study area. Here we report on the
253 lithofacies analysis of rocks recognized during our field campaigns (and after in
254 petrological thin section) at the TMP and SFX provinces. Within the study area (TMP
255 and SFX), massive to banded lava flows and rheomorphic ignimbrites (Fig. 3) as well
256 as felsic volcaniclastic rocks of various origin (Figs. 4-8, 11) are frequently found.
257 Massive and banded lava flows and rheomorphic ignimbrites deposits (fig. 3) as well
258 as volcaniclastic felsic rocks of various origin (e.g. pumiceous, effusive, ignimbritic)
259 (fig. 4,5,6,7,8,11) are frequently found in both the studied areas (TMP and SFX).
260 Reworked (secondary) volcaniclastic rocks (Fig. 9,10) and sedimentary
261 alluvial/coastal clastic deposits (epiclastic) are also widely distributed in both TMP and
262 SFX areas. Primary volcaniclastic rocks are here defined as those fragmental
263 products formed during a syn-eruptive explosive or effusive events, which were
264 deposited regardless of whether their transport occurs through air, water, granular
265 debris or a combination of them (McPhie et al., 1993; White and Houghton, 2006,
266 Manville et al., 2009; Roverato et al., 2017). On the other hand, all the units deposited
267 as a consequence of a reworking process of pre-existing volcanic units are defined here
268 as sedimentary/reworked secondary volcaniclastic rocks. We also introduce into this
269 group all those epiclastic products that constitute sediments that had been reworked
270 before, independent of their source and composition. All TMP and SFX volcanic
271 products share the same features both at outcrop scale and at hand specimen scale and
272 for such a reason they will be presented together in the lithofaciological description. In
273 Table 1 we propose shows a description and interpretation of the volcaniclastic

Formatted: Indent: First line: 0 cm

Formatted: Font: Times New Roman, 12 pt, No underline

1
2 274 lithofacies, both primary (~~volcaniclastic~~) and ~~reworked (secondary sedimentary)~~, for
3 275 the deposits identified in the study areas. ~~In the following we will also provide an~~
4 276 ~~interpretation of the processes involved in their transport and emplacement.~~

6 277
7
8 278 ~~4.14.~~ Lava flows and rheo-ignimbrites

9 279 As already discussed by Roverato et al. (2016), the absence of unequivocal
10 280 vitroclastic textures complicates the distinction between volcaniclastic and layered lava
11 281 flows in general and, more in particular, for the ancient volcanic rocks investigated
12 282 here. Lava flows found in the TMP and SFX provinces have both massive and banded
13 283 structures (Ffig. 3) while still maintaining, in some cases, glassy (obsidian) and
14 284 aphanitic to porphyritic texture. Their composition varies from trachytic to rhyolitic with
15 285 various content of alkalis (see section 58). The phenocryst assemblage consists
16 286 mainly of plagioclase, quartz, Fe–Ti oxides and accessory-amount of zircon and
17 287 apatite. Plagioclase and bipiramidal quartz crystals (Ffig. 3a), with a maximum size of
18 288 3-4 mm, range from euhedral to anhedral, showing moderate to intense resorption.
19 289 Plagioclase shows sieve texture indicating non-equilibrium conditions likely
20 290 determined by magmatic transport. ~~Potassic-K-~~feldspar is also present as anhedral
21 291 crystals in the groundmass often associated with sericite as alteration phase. Samples
22 292 are generally affected by variable intensity of hydrothermal alteration. Plagioclase
23 293 phenocrysts, in particular, present diffuse potassic and minor propylitic alterations.
24 294 Abundant spherulites and lithophysae of variable size, from millimetric to decimetric,
25 295 were recognized in almost every sample and are thus common in these rocks (Ffig. 3b,
26 296 c). The spherulites (radiating fibers of K-feldspar and cristobalite), ranging from few
27 297 millimeters to 2 cm, are typically associated with perlitic fractures. Their content can
28 298 vary from 10 vol% to ~~pervasive-70%~~ in the investigated rocks. A large amount of the
29 299 spherulites developed into lithophysae commonly reaching 10-12 cm as a consequence
30 300 of cooling and degassing processes. In the obsidian-type lavas (Ffig. 3c), the
31 301 groundmass is characterized by a micro-granophiric-like devitrification texture
32 302 characterized by crystallization of amorphous quartz and alkali feldspar, a process that
33 303 occurred after the emplacement of lava bodies. Several rocks show textures that are not
34 304 easy to be associated to either lava flows or flows of fragmented material which
35 305 underwent rheomorphism (Ffig. 3d-g). Both banded lavas and rheo-ignimbrites display
36 306 folds (Ffig. 3d-g, see also Ffig. 11e) and sub-parallel bands on mm- to dm-scale,
37 307 planar to wavy (Ffig. 3e, see also Ffig. 6 and 7) (parataxitic fabric), that deform and

1
2 308 flattened around lithic fragments and crystals which alignment suggests the flow
3 309 direction. In thin sections, the bands are characterized by extremely flattened
4 310 vitroclastic textures with the former glass completely replaced by a mixture of quartz
5 311 and feldspar (Roverato et al., 2016).
6
7
8 312

9 313 ~~5.4.2. V~~Primary volcaniclastic rocks

10
11 314 We consider primary volcaniclastic rocks those dense, scoriaceous and
12 315 pumiceous products of fragmental character emplaced by ~~primary low intensity~~
13 316 explosive processes, ~~frequently associated to effusive manifestations or highly~~
14 317 ~~explosive events associated to fall out, small pyroclastic density currents (PDC) or~~
15 318 ~~ignimbrites~~. With pyroclastic we refer to fragmental material generated by any kind of
16 319 explosive volcanic activity and transported as ash-fall and pyroclastic density currents
17 320 ~~by an explosive volcanism~~ (Manville et al., 2009), which deposition occurs by
18 321 suspension settling, from traction, by en masse freezing, or any combination of these
19 322 (White and Houghton, 2006). Depending on the mechanism of transport and the
20 323 eruptive style these clastic rocks were distinguished into two different categories, i.e.
21 324 massive and stratified; and they can vary from well sorted, poorly sorted or unsorted.
22 325 The rocks are predominantly rhyolitic in composition (Fernandes et al., 2011, Roverato
23 326 et al., 2016) and there is no significant geochemical difference from the lava flows.
24 327 Nine main lithofacies (Lf) have been recognized for the volcaniclastic rocks: six of
25 328 them are massive and three are stratified.
26
27
28
29
30
31
32
33
34
35 329

36 330 ~~5.1. 4.2.1.~~Massive

37 331 Six massive lithofacies (mAL, mLA, mLB, l-gwLA, m-gwLA and h-gwLA)
38 332 were recognized during our field campaign, three of them belong to the welded
39 333 ignimbrites sub-group (Table 1). By using the granulometric classification proposed by
40 334 Fisher (1961), ash is defined as any fragment with size <2 mm, lapilli are fragments
41 335 with size between 2 to 64 mm and blocks (or bombs) have sizes > 64 mm. Massive
42 336 lithofacies includes all those deposits that display a massive coherent structure.
43 337 Outcrops of such kind of lithofacies are constituted by a high percentage of ash up to
44 338 block-rich textures. Most of the observed samples appear to have been affected by
45 339 devitrification processes of the juvenile pyroclastic fragments and matrix. The presence
46 340 of juvenile material linked with other observed textures such as broken crystals (Best
47 341 and Christiansen, 1997) and eutaxitic fabric allows us to confirm that the rocks

Formatted: Indent: First line: 0 cm

Formatted: Indent: First line: 0 cm

Formatted: Font: Not Italic, No underline

Formatted: Font: Not Italic

1 342 belonging to lithofacies mAL, mLA, l-gwLA, m-gwLA and h-gwLA are fragmental
2 343 and pyroclastic in origin. We discuss the meaning of Lf mLB below in section 5.1.2.

3 344
4 345 5.1.1. Lf mAL; mLA (massive Ash to Lapilli; massive Lapilli and Ash)

5 346 Description: the ash to lapilli (mAL) and lapilli and ash (mLA) deposits (Fig.
6 347 4a-e, Fig.6) are heterolithologic, matrix supported, containing angular to sub-rounded
7 348 medium to coarse devitrified lapilli (displaying axiolitic fabric), banded fragments,
8 349 occasional (or absent) lithics and angular-shaped broken crystals of plagioclase,
9 350 bipiramidal quartz and rare oxides (Fig. 5). In mLA, clasts <25 cm in size are
10 351 randomly immersed in the groundmass (Fig 4d and 4e, 11d). Some of them are altered
11 352 by carbonate minerals. Groundmass of mAL and mLA is formed by K-feldspar and
12 353 quartz crystals, devitrified ash fragments and sericite crystals as phase of alteration
13 354 (Fig. 5).

14 355 Interpretation: the general massive aspect and the poor sorting of mAL and
15 356 mLA point to a laminar granular flow transport regime and the fine content suggests
16 357 the deposition from a dilute fluid escape-dominated flow-boundary zone in which
17 358 turbulent shear-induced tractional segregation is suppressed (Branney and Kokelaar,
18 359 2002; Sulpizio et al., 2007, Roverato et al., 2017). These lithofacies are interpreted as
19 360 ash flow deposits suggesting the deposition from a pyroclastic density current (PDC)
20 361 (Lenhardt et al., 2011; Sulpizio et al., 2014; Roverato et al., 2017). The coarser
21 362 lithofacies mLA (fig. 4e) could be related to proximal co-ignimbritic breccias as result
22 363 of deposition by denser pyroclastic granular flows (Branney and Kokelaar, 2002). The
23 364 angular aspect of the clasts indicates short-period transport.

24 365
25 366 5.1.2. Lf mLB (massive Lapilli and Block)

26 367 Description: this lithofacies (fig. 4f, fig.7) represents monolithologic coarse-
27 368 grained rocks having high-clast content (clast:matrix ratios up to 3:1). Angular/sub-
28 369 angular coarse lapilli and blocks up to 50-60 cm of devitrified banded or massive lava
29 370 fragments are immersed in a devitrified fine lapilli and coarse ash matrix.

30 371 Interpretation: the blocky and monolithologic coarse-grained aspect of the
31 372 lithofacies mLB and its position underneath thick flow-deposits is attributed to the
32 373 basal auto-brecciation of lava flows and/or rheo-ignimbrite flows. Despite the
33 374 lithofacies is likely a consequence of an effusive volcanic activity (in the lava-flow

case) it is considered anyway as part of the volcaniclastic group due to its fragmental character.

5.1.3. *Lf l-gwLA; m-gwLA; h-gwLA* (welded Ignimbrites)

Description: all massive deposits displaying welding characteristics have been grouped in the “welded ignimbrites” group (table 1), following the idea of “grade of welding” (Walker, 1983) (i.e. the amount of welding and compaction exhibited by deposits). The rocks are matrix-supported with sub-rounded to angular lapilli and ash lithic clasts, euhedral, subhedral and broken crystals (plagioclase and less quartz) and deformed devitrified juvenile fragments (*fiamme*). Slightly- (low-grade, *l-gwLA*), medium- (medium-grade, *m-gwLA*), well-stretched (high-grade, *h-gwLA*) *fiamme* (Fig. 6), as well as, devitrified shards define the eutaxitic fabric (Roverato et al., 2016). These fragments varying from millimetric to 3–4 cm in size are immersed in a homogeneous micro-granophiric-like devitrified groundmass (see Roverato et al., 2016 for details). Figure 6 shows a stratigraphic column representing a 35 m thick sequence of ignimbrite deposits found in the TMP, displaying very low-grade to high-grade welded fabric where the grade of welding increases toward the top of the succession. The very top of the sequence is characterized by columnar jointing.

Interpretation: the massive aspect and the poor sorting of the lithofacies *l-gwLA*, *m-gwLA* and *h-gwLA* point to a laminar granular flow transport regime, interpreted to be deposited from a pyroclastic density current (PDC). The welded character of these lithofacies is indicative of hot PDC emplacement and compaction that result into the low- up to high-grade eutaxitic fabric. This process is favored by loading-compaction, low-viscosity fragments, high temperature (i.e. > 900°C), cooling of gas-permeable fragments (pumices) and dissolved water (Branney and Kokelaar, 2002; Roverato et al., 2016 and references therein).

~~Six massive lithofacies were recognized during our field campaign, three of them belong to the ignimbrites sub-group (Table 1). By using the granulometric classification proposed by Fisher (1961), ash is defined as any fragment with size < 2 mm, lapilli are fragments with size between 2 to 64 mm and blocks (or bombs) have sizes > 64 mm. Massive lithofacies includes all those deposits that display a massive coherent structure. Outcrops of such kind of lithofacies are constituted by a high percentage of ash up to block rich textures. The ash to lapilli (mAL) and lapilli and ash~~

Formatted: Indent: First line: 0 cm

Formatted: Font: Not Italic, No underline

Formatted: Font: Not Italic, No underline

Formatted: Font: Not Italic, Font color: Black

Formatted: Font color: Auto

Formatted: Font: Not Italic, Font color: Auto

Formatted: Indent: First line: 0 cm

1
2 409 (mLA) deposits (fig. 4a/b/c/d/e, fig.6) are heterolithologic, matrix supported,
3 410 containing angular to sub-rounded medium to coarse devitrified lapilli (displaying
4 411 axiolitic fabric), banded fragments, occasional (or absent) lithics and angular shaped
5 412 broken crystals of plagioclase, bipiramidal quartz and rare oxides (fig. 5). In mLA,
6 413 elasts <25 cm in size are randomly immersed in the groundmass (Fig 4d/e, 11d). Some
7 414 of them are altered by carbonate minerals. Groundmass of mAL and mLA is formed by
8 415 K-feldspar and quartz crystals, devitrified ash fragments and sericite crystals as phase
9 416 of alteration (Fig. 5). mLB (massive Lapilli and Block) facies (fig. 4f, fig.7) represent
10 417 monolithologic coarse-grained rocks having high-clast content (clast:matrix ratios up
11 418 to 3:1). Angular/sub-angular coarse lapilli and blocks up to 50-60 cm of devitrified
12 419 banded or massive lava fragments are immersed in a devitrified fine lapilli and coarse
13 420 ash matrix.

21 421
22 422 All massive deposits displaying welding characteristics have been grouped in
23 423 the “ignimbrites” group (table 1), following the idea of “grade of welding” (Walker,
24 424 1983) (i.e. the amount of welding and compaction exhibited by deposits). The rocks
25 425 are matrix supported with sub-rounded to angular lithic clasts, euhedral, subhedral and
26 426 broken crystals (plagioclase and less quartz) and deformed devitrified juvenile
27 427 fragments (fiamme). Slightly (low grade, l-gwLA), medium (medium grade, m-
28 428 gwLA), well stretched (high grade, h-gwLA) fiamme (Fig. 6), as well as, devitrified
29 429 shards define the eutaxitic fabric (Roverato et al., 2016). These fragments varying from
30 430 millimetric to 3–4 cm in size are immersed in a homogeneous micro-granophiric like
31 431 devitrified groundmass (see Roverato et al., 2016 for details). Figure 6 shows a
32 432 stratigraphic column representing a 35 m thick sequence of ignimbrite deposits found
33 433 in the TMP, displaying very low grade to high grade welded fabric where the grade of
34 434 welding increases toward the top of the succession. The very top of the sequence is
35 435 characterized by columnar jointing.

46 436 47 437 4.2.2. Interpretation —

48 438 Most of the observed samples appear to have been affected by devitrification
49 439 processes of the juvenile pyroclastic fragments and matrix. The presence of juvenile
50 440 material linked with other observed textures such as broken crystals (Best and
51 441 Christiansen, 1997) and eutaxitic fabric allows us to confirm that the rocks belonging
52 442 to lithofacies mAL, mLA, l-gwLA, m-gwLA and h-gwLA are fragmental and

pyroclastic in origin. The general massive aspect and the poor sorting of mAL and mLA point to a laminar granular flow transport regime and the fine content suggests the deposition from a dilute fluid escape dominated flow boundary zone in which turbulent shear induced tractional segregation is suppressed (Branney and Kokelaar, 2002; Sulpizio et al., 2007, Roverato et al., 2017). These lithofacies are interpreted as ash flow deposits suggesting the deposition from a pyroclastic density current (PDC) (Lenhardt et al., 2011; Sulpizio et al., 2014; Roverato et al., 2017). The coarser lithofacies mLA (fig. 4e) could be related to proximal co-ignimbritic breccias as result of deposition by denser pyroclastic granular flows (Branney and Kokelaar, 2002). The angular aspect of the clasts indicates short period transport. The blocky aspect of the lithofacies mLB is attributed to the basal auto-brecciation of lava flows and/or rheo-ignimbrite flows. The welded character of the lithofacies l-gwLA, m-gwLA and h-gwLA is indicative of hot PDC emplacement and compaction that result into the low-up to high grade eutaxitic fabric. This process is favored by loading compaction, low-viscosity fragments, high temperature (i.e. > 900°C), cooling of gas permeable fragments (pumices) and dissolved water (Branney and Kokelaar, 2002; Roverato et al., 2016 and references therein).

5.4.2.23. Stratified

These lithofacies, although commonly associated with ignimbrites, are not very spread in the studied areas. We also didn't find any alternation between massive and stratified deposits even if this association is a common occurrence in PDC deposits (Sulpizio et al., 2014; Roverato et al., 2017), alternating dilute (stratified deposits resulting) and concentrated (massive deposits resulting) regimes during transport (Sulpizio et al., 2014). Just one example has been found in TMP and is reported in the stratigraphic reconstruction of fig.11.

5.2.1 Lf sA; xsA; dsAL (stratified Ash; cross-stratified Ash; diffusely stratified Ash to lapilli)

Description: The stratified samples and outcrops analyzed comprise well sorted very fine to fine ash organized in millimetric to sub-millimetric parallel (sA) or cross-stratified (xsA) layers, with sharp or gradational changes in grain size (Fig. 8). The fragments are represented by devitrified shards, crystals (plagioclase), and rare (or absent) lithics (fig. 8d) immersed in a devitrified groundmass. Diffuse-stratified

Formatted: Font color: Black

Formatted: Indent: First line: 0 cm

Formatted: Indent: First line: 0 cm

1
2 477 lithofacies dsAL display a coarser character with coarse lithic and devitrified ash and
3 478 lapilli fragments forming well developed parallel continuous meter-long stratification
4
5 479 (or very-low angle cross-stratification) at centimeter scale (fig. 11b), with gradational
6
7 480 changes in grain-size. The sorting varies from well to moderate.
8
9 481

10 482 11 483 4.2.4. Interpretation:

12 484 tThe fine parallel layering of shards material displayed by lithofacies sA is
13
14 485 interpreted here as being deposited under the product of sedimentation by the upper
15
16 486 and highly dilute ash-cloud that accompany a pyroclastic-density current. We don't
17
18 487 exclude the direct sedimentation from tephra fall-out activity. Cross-stratified (Lf xsA)
19
20 488 and diffuse-stratified (Lf dsAL) deposits indicate tractive processes usually attribute to
21
22 489 pyroclastic surge-type depositional condition from dilute currents (Cas and Wright
23
24 490 1987; Lenhardt et al., 2011; Roverato et al., 2017). We interpreted these as pyroclastic
25
26 491 surge deposits although Lf dsAL could also be the product of coarse ash fall-out
27
28 492 processes. Pyroclastic surge deposits usually display small volume and rarely reach
29
30 493 more than 10 km from their source (Lenhardt et al., 2011). Conversely, fall-out
31
32 494 deposits could emplace tens of kilometers from their source.
33
34 495

35 496 6.——4.3. Secondary volcanoclastic/epiclastic Sedimentary rocks

36 497 The nomenclature of Fisher et al. (1961) is applied also for the **sedimentary**
37
38 498 **secondary volcanoclastic** rocks as follow: silt ($2 <> 64 \mu\text{m}$), sand ($64 \mu\text{m} <> 2 \text{ mm}$), gravel
39
40 499 ($2 <> 64 \text{ mm}$), cobble ($64 <> 256 \text{ mm}$). These rocks are considered as the product of
41
42 500 reworking and erosive processes. The clasts belonging to this group show a wide range
43
44 501 of composition, size and shape variations. Based on their component, texture and
45
46 502 fabric, we recognized five massive, both matrix- and clast-supported, and four
47
48 503 stratified lithofacies (fig. 9).

49 504 50 505 6.3.1.1. Massive

51 506 6.1.1. Lf mS (massive Sand)

52 507 Description: this lithofacies consists of reddish moderately to well-sorted,
53
54 508 massive, fine- to medium grained sand forming parallel strata intercalated to clast-
55
56 509 supported conglomerate deposits (Lf csG) (fig. 9a). The sandstone strata extend tens of
57
58 510 meters and present thinness between 0.4-0.8 m. Lf mS is predominantly composed of

Formatted: Font: Not Italic, No underline, Font color: Auto

Formatted: Font: Not Italic, No underline, Font color: Auto

Formatted: Indent: First line: 0 cm

Formatted: Font: Not Italic, No underline, Font color: Auto

Formatted: Font: Not Italic

1
2 511 quartz, feldspar and minor rock fragments. Contacts between mS and csG are sharp
3 512 with rare slightly erosional surfaces. The tops of the sandstone are characterized by the
4
5 513 presence of centimeters ripples (fig. 9b).

6 514 Interpretation: the massive sand (mS) and the small ripples found at the top of
7
8 515 the strata indicate low energy under tractional currents in shallow water conditions
9
10 516 (Collison and Thompson, 1982; Lenhardt et al., 2011). The alternation of Lf csG and
11 517 mS indicates changes in energy conditions of sedimentation. We interpret these
12 518 oscillations as belonging to a subaqueous-subaerial fan-delta interface setting where
13 519 continental supply of material alternates to under-water sand accumulation (Lf mS).

16 520 17 18 521 6.1.2. Lf csG (clast supported Gravel)

19 522 Description: this lithofaciesThe Lf esG (Fig. 9a, c, d) is massive, clast to matrix
20 523 supported, with heterolithic felsic rounded high-spherical coarse gravel with a
21 524 sandy inter-clast matrix. Clasts are mainly characterized by massive and banded
22 525 medium- to coarse-size felsic lava fragments (and rare quartz; size does not exceed 5
23 526 cm) and present rounded with low- to high-sphericity. We found lithofacies csG also
24 527 associated to xsSG (see below section 6.2.2.) (Ffig. 9c, 10b).

28 528 Interpretation: lithofacies csG is dominated by water flow processes where
29 529 matrix plays a secondary role. The clast-supported character and less matrix content
30 530 indicates that water removed the finer particles during transport and deposition. Lf csG
31 531 display rounded clasts and well-sorting indicative of good selection during transport
32 532 and emplacement. The rounded character of csG and the presence of matrix in the
33 533 deposits suggest a laminar debris-flow regime in medial reaches of stream-dominated
34 534 fluvial/alluvial fans (Mueller and Corcoran, 1998).

39 535 40 41 536 6.1.3. Lf csGS (clast supported Gravel to Sand)

42 537 Description: Lf csGS (Ffig. 9e, 11c) is massive, moderately well-sorted and
43 538 clast-supported. Clasts (gravel to sand) present sub-rounded to sub-angulours with
44 539 low/medium sphericity with maximum size of 2-3 cm. The rocks belonging to this
45 540 lithofacies are mainly formed by massive felsic lava fragments with different color and
46 541 crystallinity.

49 542 Interpretation: Lf csGS is dominated by water flow processes where matrix
50 543 plays a secondary role. The clast-supported character and less matrix content indicates
51 544 that water removed the finer particles during transport and deposition. This lithofacies

Formatted: Level 1, Adjust space between Latin and Asian text, Adjust space between Asian text and numbers

Formatted: Indent: First line: 0 cm

1
2
3
4
5
6
7
8
9
10
11
12
13
14
15
16
17
18
19
20
21
22
23
24
25
26
27
28
29
30
31
32
33
34
35
36
37
38
39
40
41
42
43
44
45
46
47
48
49
50
51
52
53
54
55
56
57
58
59
60
61
62
63
64
65

represents deposition within a debris-flow dominated fluvial/alluvial environment.
Poor sorting, clast-supported and sub-angular clasts point to deposition by localized
laminar hyperconcentrated-flows in volcanic fans fringing flanks of volcanic edifices.
Single cross-beds are usually ca. 1 cm thick

6.1.4. Lf csGC (clast supported Gravel and Cobble)

Description: Lithofacies csGC (Fig. 9f) is massive, low-sorted and clast-supported. The clast population is characterized by sub-rounded, low/medium sphericity, massive felsic porphyritic fragments with maximum size up to 20 cm. This lithofacies has an interstitial matrix characterized by medium to coarse sand.

~~4.3.2. Interpretation:~~

~~Lf esG, esGS and csGC (fig. 9a/d/f) is~~ dominated by water flow processes where matrix plays a secondary role. The clast-supported character and less matrix content indicates that water removed the finer particles during transport and deposition. ~~This Lf esG display rounded clasts and well sorting indicative of good selection during transport and emplacement. The rounded character of esG and the presence of matrix in the deposits suggest a laminar debris flow regime in a medial reaches of stream-dominated fluvial/alluvial fans (Mueller and Corcoran, 1998). The alternation of Lf esG and mS (fig. 9a) indicates changes in energy conditions of sedimentation. We interpret these oscillations as belonging to a subaqueous subaerial fan-delta interface setting where continental supply of material alternates to under-water sand accumulation (Lf mS). The massive sand grain size (mS) and the small ripples found at the top of the strata indicate low energy under-tractional currents in shallow water conditions (Collison and Thompson, 1982; Lenhardt et al., 2011). Lithofacies esGS and esGC represents~~ deposition within a debris-flow dominated fluvial/alluvial environment. Poor sorting, clast-supported and sub-angular clasts likely points to deposition by localized laminar hyperconcentrated flows (esGS) and non-cohesive debris-flows (esGC) in volcanic fans fringing flanks of volcanic edifices. Single cross-beds are usually ca. 1 cm thick.

~~6.4.3.23. Stratified~~

6.2.1 Lf xsS (cross-stratified Sand)

Formatted: Indent: First line: 0 cm

Formatted: None, Don't adjust space between Latin and Asian text, Don't adjust space between Asian text and numbers

Formatted: Font: Not Italic, No underline, Font color: Auto

Formatted: None, Don't adjust space between Latin and Asian text, Don't adjust space between Asian text and numbers

Formatted: Font: Not Italic, No underline, Font color: Auto

Formatted: Font: Not Italic

Formatted: Indent: First line: 0 cm

Formatted: Font: Not Italic, No underline, Font color: Auto

Formatted: Font: Not Italic, No underline, Font color: Auto

Formatted: Font: Not Italic

1
2 579 Description: Lithofacies cross-stratified ~~Ssandstone (xsS)~~ (Fig. 10a) consist of
3 580 white to brownish low-angle cross-stratified coarse quartzitic sandstone. The
4 581 sandstones are characterized by lobe to sheet-shaped bodies. Major bedsets are
5 582 recognized ranging in thickness from 0.5 to 1.5 m, composed of fine-grained sandstone
6 583 dominated by medium-angle cross strata (18-20°). Single cross-beds are usually 0.7-
7 584 1cm thick. The outcrops displaying this lithofacies extend tens of meters with sharp
8 585 upper and lower contact.

9
10
11
12 586 Interpretation: the cross-stratification of xsS is interpreted as formed in fluvial
13 587 channels attesting the deposition from crested dune bed-forms that formed under
14 588 condition of lower flow regime (Collinson, 1996; Miall, 1996; Capuzzo and Wetzel,
15 589 2004; Went, 2016). The deposition of medium-angle cross-bedding within large-scale
16 590 examples of beds indicates that these larger beds are likely a product of bar migration.
17 591 The beds are interpreted as channel-fill deposits (Lenhardt et al., 2017) related to a
18 592 fluvial environment likely associated to meandering or braided rivers. Shoreline
19 593 deposition developed around margins of immature marine basins is also considered.

20
21
22
23
24
25 594 ▲
26
27 595 6.2.2. Lf xsSG (cross-stratified Sand and Gravel)

28 596 Description: Lf xsSG ~~Lf xsSG~~ (Fig. 10b) is characterized by crystal-lithic fine
29 597 to coarse sand and fine gravel (max 5-6 mm in size) organized in cross-bedded
30 598 stratification. Clasts display medium roundness and sphericity and are mostly
31 599 composed by felsic fragments. Stratification is defined by alternating of well to poorly
32 600 sorted, fine to coarse millimeters-thick strata. The finer black layers are formed by sub-
33 601 millimetric hematite sand.

34
35
36
37
38 602 Interpretation: Lf xsSG correspond to cross-stratified water reworked deposits.
39 603 The cross-stratified thicker fine gravelly strata, alternated with sandy layers laterally
40 604 discontinuous, were interpreted as different pulses as the result of rapid deposition
41 605 from hyperconcentrated flows (Zanchetta et al., 2004) in a stream-dominated
42 606 fluvial/alluvial setting. Alternation with csG (Fig. 9c) represents difference of energy
43 607 condition.

44
45
46
47
48 608 ▲
49 609 6.2.3. Lf dsSt (diffusely layered Silt)

50
51 610 Description: ~~Lf dsSt~~ this lithofacies consists of parallel, lenticular, truncated,
52 611 and locally low-angle cross-stratified multicolor millimetric well-sorted fine- to very
53 612 fine-grained sand and silt strata (Fig. 10c). Within the sandy bedset, a thinning- and

Formatted: Font color: Custom
Color(RGB(35,31,32))

Formatted: Indent: First line: 0 cm

Formatted: Font color: Text 1

Formatted: Indent: First line: 0 cm

1
2 613 fining-upward trend may be distinguished. Small and straight groove marks have been
3 614 detected and reduced tiny slump folding is also presence in some parts.

4
5 615 Interpretation: lithofacies dsSt displays diffuse fine stratification with tiny
6 616 ripples, suggesting transport and sedimentation in shallow water. The thin sheet-shaped
7 617 is interpreted as flood sediments (Lenhardt et al., 2011). These deposits are interpreted
8 618 to have been formed in low energy lacustrine environment or ponds (Collinson, 1996;
9 619 Roverato et al., 2017) characterized by small turbidities successions affected by
10 620 scouring and tiny deformations (slumps) of the sediments.

11 621

12 622 6.2.4. Lf bChS (bedded Chert and Sand)

13 623 Description: tThe bedded chert lithofacies (with sand) (bChS) (Ffig. 10d) crops out in
14 624 both regions and it is characterized by outcrops that can be traced on strike for
15 625 hundreds of meters. The facies consist of thin laminated pinkish chert (layers < 1mm in
16 626 thickness) with darker laminae intercalated, formed predominantly by hematite
17 627 (Lenhardt et al., 2017). The layers are composed by microcrystalline quartz. In some
18 628 portions, these lithofacies are associated with fine to medium sand composed mainly
19 629 by quartz and less volcanic fragments.

20 630

21 631

22 632 4.3.4 _- Interpretation: this lithofacies is interpreted as inorganic precipitation of silica
23 633 in a closed lake basin mainly due to its association with volcanic rocks and fine
24 634 sandstone (Blatt et al., 1980; Eriksson et al., 1994). The picture in figure 10d shows
25 635 elongated ripped-up millimetric fragments of chert immersed in the sandstone eroded
26 636 by low-energy stream flow or local lacustrine turbidites. As suggests by Lenhardt et al.
27 637 (2017) the chert may have formed during repeated pulses of hydrothermal fluids that
28 638 circulated into the lake water during hiatuses in the volcanism (Van Kranendonk,
29 639 2006).

30 640

31 641 7. Analytical methods for geochemistry and geochronology

32 642 A total of 19 new samples (9 volcaniclastics and 10 lava flows) from the
33 643 Tapajos region (associated with the data published in Roverato et al., 2016; Table 2)
34 644 were analysed for bulk rock major and trace elements. Major element bulk rock
35 645 analyses were performed by X-ray fluorescence, using a wavelength dispersive Philips
36 646 PW 2400 spectrometry, using fused glass disks according to procedures described by

Formatted: Indent: First line: 0 cm

Formatted: Font: Not Italic, No underline, Font color: Auto

Formatted: No underline, Font color: Text 1

Formatted: No underline, Font color: Text 1

Formatted: Font color: Text 1

Formatted: Left, Indent: First line: 1.27 cm, Line spacing: 1.5 lines

1 647 Mori et al. (1999). Accuracy was greater than 2%. Trace element analyses in selected
2
3 648 samples were performed by Inductively Coupled Plasma-Mass Spectrometry (ICP-MS)
4
5 649 using the procedure described by Navarro et al. (2008). Accuracy, determined with
6
7 650 respect to the reference standards BHVO-2 and BR, was 0.5–2%.

8 651 Zircon grains were examined with a FEI-QUANTA 250 scanning electron
9
10 652 microscope equipped with secondary-electron and cathodoluminescence (CL) detectors
11
12 653 at the Instituto de Geociências - Centro de Pesquisas Geocronológicas - Universidade
13 654 de São Paulo (IGc-CPGeo-USP); the most common conditions used in CL analysis
14 655 were 60 μ A of emission current, 15.0 kV of accelerating voltage, 7 μ m of beam
15 656 diameter, 200 μ s of acquisition time, and a resolution of 2048x1887 pixels and 345 dpi.
16
17 657 Selected samples were analyzed for U-Pb isotopes using a SHRIMP-IIe also at IGc-
18
19 658 CPGeo-USP, following the analytical procedures of Williams (1998) as reported by
20
21 659 Giovanardi et al. (2015). Correction for common Pb is based on the measured ^{204}Pb ,
22 660 and the typical error for the $^{206}\text{Pb}/^{238}\text{U}$ ratio is less than 2%; U abundance and U-Pb
23
24 661 ratios were calibrated against the TEMORA-II standard. The dataset consists of 56 new
25
26 662 U-Pb SHRIMP-II analyses and is reported in Table 3. Thirty-five analyses were
27
28 663 performed on zircon grains from the Tapajos region as follow: 11 analyses on sample
29 664 NP380-C, 11 analyses on sample NP183 and 13 analyses on sample NP396-B. Eleven
30 665 analyses were performed on zircon grains from Xingu sample XU08. For all samples,
31 666 $^{207}\text{Pb}/^{235}\text{U}$ and $^{206}\text{Pb}/^{238}\text{U}$ concordia ages (with 95% of confidence level and 2σ error)
32
33 667 are calculated using Isoplot 4.1 software (Ludwig, 2009).
34
35 668

36 669
37
38 670 ~~The cross-stratification of lithofacies xsS is interpreted as formed in fluvial~~
39
40 671 ~~channels attesting the deposition from crested dune bedforms that formed under~~
41
42 672 ~~condition of lower flow regime (Collinson, 1996; Miall, 1996; Capuzzo and Wetzel,~~
43
44 673 ~~2004; Went, 2016). The deposition of medium-angle cross-bedding within large-scale~~
45
46 674 ~~examples of beds indicates that these larger beds are likely a product of bar migration.~~
47
48 675 ~~The beds are interpreted as channel-fill deposits (Lenhardt et al., 2017) related to a~~
49
50 676 ~~fluvial environment likely associated to meandering or braided rivers. Shoreline~~
51
52 677 ~~deposition developed around margins of immature marine basins is also considered. Lf~~
53
54 678 ~~xsSG correspond to cross-stratified water-reworked deposits. The cross-stratified~~
55
56 679 ~~thicker fine-gravelly strata, alternated with sandy layers laterally discontinuous, were~~
57
58 680 ~~interpreted as different pulses as the result of rapid deposition from hyperconcentrated~~

Formatted: Font: Not Italic, No underline, Font color: Auto

1
2 681 | flows (Zanchetta et al., 2004) in a stream-dominated fluvial/alluvial setting.
3 682 | Alternation with csG (fig. 9c) represents difference of energy condition. Lithofacies
4 683 | dsSt display diffuse fine stratification with tiny ripples, suggesting transport and
5 684 | sedimentation in shallow water. The thin sheet-shaped is interpreted as flood sediments
6 685 | (Lenhardt et al., 2011). These deposits are interpreted to have been formed in low
7 686 | energy lacustrine environment or ponds (Collinson, 1996; Roverato et al., 2017)
8 687 | characterized by small turbidities successions affected by scouring and tiny
9 688 | deformations (slumps) of the sediments. The Lf bChS is interpreted as inorganic
10 689 | precipitation of silica in a closed lake basin mainly due to its association with volcanic
11 690 | rocks and fine sandstone (Blatt et al., 1980; Eriksson et al., 1994). The picture in figure
12 691 | 10d shows elongated ripped-up millimetric fragments of chert immersed in the
13 692 | sandstone eroded by low-energy stream flow or local lacustrine turbidites. As suggests
14 693 | by Lenhardt et al. (2017) the chert may have formed during repeated pulses of
15 694 | hydrothermal fluids that circulated into the lake water during hiatuses in the volcanism
16 695 | (Van Kranendonk, 2006).
17
18
19
20
21
22
23
24
25
26
27
28
29

30 698 | 8.5. Geochemistry of the TMP samples

31 699 | Independently of their nature (lavas or volcaniclastic), the rocks of the TMP
32 700 | follow a typical calc-alkaline trend (Fig. 12). They are mostly rhyolitic in composition
33 701 | (Table 2), with four exceptions which fall in the trachytic field. In addition, their low
34 702 | LOI values (0.32-3.51%) and the low FeO content (0.78 – 3.26%) together with the
35 703 | negative correlation FeO vs SiO₂ appears to indicate that the investigated volcanic
36 704 | rocks neither underwent significant alteration processes nor they belong to sedimentary
37 705 | suites which commonly contain water rich clay minerals. TMP volcaniclastic and lava
38 706 | flows show similar negative correlation between TiO₂, Al₂O₃, MgO, FeO, CaO, Na₂O
39 707 | and P₂O₅ with SiO₂. A negative correlation between K₂O and SiO₂ also exists for the
40 708 | volcanoclastic, but not for the lava flows. The similar trends observed suggest that both
41 709 | these kind of rocks are originated by similar the same magmatic sources. Such a
42 710 | conclusion is supported by similar variation paths, although with different values, of
43 711 | minor and trace elements (Figs. 13). In particular, TMP lava flows show LREE
44 712 | enrichment ((La/Yb)_N=10.68-21.45; normalization to Chondrite I from Anders &
45 713 | Ebihara, 1982) and a negative Eu anomaly which increases from trachytes
46 714 | ((Eu/Eu*)_N=0.89-0.78) to rhyolites ((Eu/Eu*)_N=0.69-0.31) (Fig. 13). The Eu negative
47
48
49
50
51
52
53
54
55
56
57
58
59
60
61
62
63
64
65

Formatted: Indent: First line: 0 cm

715 anomaly, shown from all the samples, is expression of feldspar fractionation. On the
 716 other hand, volcanoclastic rocks show similar LREE enrichment ($(La/Yb)_N=11.12-$
 717 28.10) and negative Eu anomaly ($(Eu/Eu^*)_N=0.97-0.37$) (Fig. 13). In addition,
 718 volcanoclastics have higher LREE abundances with respect to lavas (La between 35.5-
 719 91.3 ppm and between 40.5-71.9 ppm, respectively) while they have similar MREE
 720 and HREE contents (Yb between 1.56-3.43 ppm and between 1.83-4.11 ppm,
 721 respectively). Volcanoclastics commonly show higher Rb (121-272.9 ppm) and Pb
 722 (4.5-137.1 ppm) with respect to lavas (Rb=96.1-232 ppm and Pb=2.7-45.8 ppm).
 723 Volcanoclastics are enriched in LILE, Th and U with respect to MORB (Fig. REE13;
 724 normalization to MORB from Hoffman, 1988), with the exception of Sr, which
 725 commonly show a pronounced negative anomaly ($(Sr/Sr^*)_N=0.55-0.05$). The Sr
 726 negative anomaly is consistent with feldspar fractionation. Negative anomalies are also
 727 present for Nb and Ta, while Ba and Pb are commonly enriched (Fig. 13). Lavas show
 728 a similar trace pattern, but higher values dispersion (Fig. REE13). The Ba enrichment
 729 is less pronounced with respect to volcanoclastics (Ba between 75-1965 ppm and 310-
 730 2245 ppm, respectively) and the Nb/Ta ratio show higher dispersion (3.29-14.63 and
 731 6.73-13.9, respectively), indicating more limited fractionation of feldspar. According
 732 to the fractionation of feldspar, the trachytes have less pronounced negative Sr
 733 anomalies with respect rhyolites ($(Sr/Sr^*)_N=0.61-0.35$ and $0.34-0.04$, respectively).
 734 Geochemical affinity of Tapajos volcanoclastics and lava flows suggests that the
 735 magmatism occurred in active continental margin setting (Fig. 14). Using the tectonic
 736 discriminant diagrams of $Zr+Nb+Ce+Y$ (ppm) vs FeO_{tot}/MgO (wt.%), Yb vs Ta and
 737 Th-Ta-Hf/3 (Wahlen et al., 1987; Pearce et al., 1984; Wood, 1980), the magmatism in
 738 the Tapajos region appears related to a syn- to post-collisional setting with few samples
 739 falling into the intraplate field (Fig. 14). According to the refined diagram Nb+Y vs Rb
 740 of Pearce (1996), all the Tapajos volcanics, together with the majority of volcanic
 741 rocks from the Sobreiro formation (Fernandes et al., 2011) are consistent with a late- to
 742 post-collisional setting (Fig. 14).

96. U-Pb zircon Geochronology

746 Zircons from Tapajos samples are colorless, sometimes fractured and euhedral
 747 to sub-euhedral. They can contain inclusions of apatite or spinel and are display
 748 commonly low emission in Cathodoluminescence (CL). All crystals show magmatic

1
2 749 oscillatory zoning and commonly a dark core which, in most cases, appears to be
3 750 homogenous. Nonetheless, in few cases an inner core with discordant and partially
4 751 reabsorbed domains is recognized. Some of the zircons also show a bright CL rim with
5 752 transgressive or sub-concordant contacts with the inner oscillatory zoning. Zircons
6 753 from sample XU08 from the Xingu region are colourless, rarely fractured and sub-
7 754 euhedral. Inclusions of apatite or spinel are also observed sometimes. Crystals are
8 755 medium in CL emissions and commonly show a homogeneous core and a concordant
9 756 magmatic oscillatory zoning. Few zircons show a core with discordant zoning. No
10 757 transgressive bright CL rims were recognized. Analyses were carried out on zircons
11 758 that do not show transgressive or resorption features and discordant inner cores.
12 759 Zircons from sample NP183 (Ignimbrite) provide 4 discordant ~~ages~~ and 7 concordant
13 760 analyses that provide ~~for~~ an upper intercept at 1984 ± 8.5 Ma (95% confident decay-
14 761 const. errs included, MSWD 1.09) and a concordia age at 1986 ± 8.2 Ma (2σ , decay-
15 762 const. errs included, MSWD 1.08, Probability of concordance = 0.30; Fig. 15). Single
16 763 spot $^{206}\text{Pb}/^{207}\text{Pb}$ ages range between 2010 ± 17 Ma and 1909 ± 53 Ma with an average
17 764 age of 1985 ± 11 Ma (95% confident decay-const. errs included, MSWD 1.6,
18 765 Probability of concordance = 0.15; Fig. 15). Zircons from sample NP380 (Ignimbrite)
19 766 show slightly older single spot $^{206}\text{Pb}/^{207}\text{Pb}$ ages between 2023 ± 31 Ma and 1981 ± 24
20 767 Ma with an average age of 1998 ± 5.9 Ma (95% confident decay-const. errs included,
21 768 MSWD 0.74, Probability of concordance = 0.68; Fig. 14). Analyses are slightly
22 769 discordant (up to 4%) providing an upper intercept at 1998 ± 7.7 Ma (95% confident
23 770 decay-const. errs included, MSWD 0.74). Zircons from sample NP396 (Banded lava)
24 771 provide 5 discordant ages and 8 concordant analyses, which provide ~~for~~ an upper
25 772 intercept at 1994 ± 8.2 Ma (95% confident decay-const. errs included, MSWD 1.40)
26 773 and a concordia age at 1997 ± 7.0 Ma (2σ , decay-const. errs included, MSWD 5.70,
27 774 Probability of concordance = 0.02; Fig. 15). Single spot $^{206}\text{Pb}/^{207}\text{Pb}$ ages range between
28 775 2014 ± 14 Ma and 1973 ± 8 Ma with an average age of 1994 ± 8.7 Ma (95% confident
29 776 decay-const. errs included, MSWD 1.6, Probability of concordance = 0.12; Fig. 14).
30 777 Pooling together the analyses of the Tapajós samples provides an average age of 1991
31 778 ± 12 Ma (2σ , MSWD 1.50, Probability of concordance = 0.06). Zircons from sample
32 779 XU08 (Lava flow) provide a concordia age at 1882 ± 6.4 Ma (2σ , decay-const. errs
33 780 included, MSWD 2.70, Probability of concordance = 0.10; Fig. 16). Single spot
34 781 $^{206}\text{Pb}/^{207}\text{Pb}$ ages range between 1899 ± 10 Ma and 1875 ± 13 Ma, with an average at

1 782 1884 ±5.2 Ma (95% confident decay-const. errs included, MSWD 0.60, Probability of
2 concordance = 0.82).

3 783
4 784

5 785 107. Discussion

6 786 ~~7.1~~ 10.1. Subduction-related to extensional setting

7 787 The geochemistry of the TMP samples presented in this work display a high-K
8 788 calc-alkaline signature (Fig. 12); ~~most of them are related to a volcanic are setting~~
9 789 ~~(fig. 14), although few samples display a geochemical signature that vary from the~~
10 790 ~~trend and they majorly~~ fall into the A-type intra-plate granite field and tectonic
11 791 discriminant diagrams suggest a late- to post-collisional setting for the TMP volcanism
12 792 (Fig. 14). This interpretation is also supported by enrichment in low-HSFE and the
13 793 high-LILE, Th, U and LREE contents of our samples, which suggest a strong crustal
14 794 component in the parent melt, consistent with a subduction/post orogenic
15 795 geodynamic setting (Fig. 12), and the high HSFE which shifted the TMP volcanics
16 796 composition in the A-type granites showing however FeO/MgO which are low and
17 797 comparable with I- and S-types granites (Fig. 14). Similar features are. ~~These two~~
18 798 ~~distinct signatures are also well~~ reported in previous works (Lamarão et al., 1999;
19 799 Lamarão et al., 2002) for volcanics in the Tapajós region, which are grouped into the
20 800 Vila Riozinho (VR) and Maraes Aldeida (MA) formations, respectively. The Vila
21 801 Riozinho rocks are intermediate to felsic in composition (Lamarão et al., 2002) with a
22 802 calc-alkaline signature, while the rhyolites and ignimbrites of Moraes Almeida are
23 803 slightly enriched in silica compared to the rhyolites of Vila Riozinho and are
24 804 geochemically similar to evolved A-type granites (Lamarão et al., 2002). Our results
25 805 show similarities with these data, suggesting that our specimens could be part of the
26 806 VR and/or MA formations. The identification of two volcanic series has important
27 807 implications for the understanding of the magmatic evolution of the Amazonian craton
28 808 in late Paleoproterozoic. A model for the evolution of the TMP involves a first stage of
29 809 subduction-related magmatism followed by an intracontinental magmatism related to a
30 810 distensional event (Lamarão et al., 2002). Geochronological analyses by Lamarão et al.
31 811 (2002) yielded ages of ca. 2 Ga for the VR rocks and ca. 1.88-1.87 Ga for the MA
32 812 volcanism. The three new U-Pb geochronological analyses reported in this study yielded
33 813 ages of ca. 2000 Ma (fig. 15) are, concordant with the ages presented by Lamarão et al.
34 814 (2002) for the VR magmatism, thus suggesting that the TMP rocks could be part of the
35 815 VR volcanic sequence. However, TMP rocks are geochemically more evolved with

Formatted: Indent: First line: 0 cm

Formatted: No underline, Font color: Text 1

Formatted: Normal, No bullets or numbering

Formatted: Font: Not Italic, No underline, Font color: Auto

Formatted: Font color: Text 1

1
2 816 respect to VR in terms of SiO₂ (63.8-76.6 wt.% and 54.4-71.8 wt.%, respectively),
3 817 K₂O (2.3-7.1 wt.% and 2.1-5.8 wt.%, respectively) and REE abundances (Fig. 12) and
4 818 are more similar to MA rocks (Fig-s. 11, 12 and 13). In particular, REE patterns of the
5 819 TMP samples are comparable with the rocks of the MA formation (Fig. 12) while they
6 820 are more enriched in REE with respect to VR rocks. Conversely, TMP rocks are
7 821 enriched in Ba (Fig. 12), while ~~MA~~ are depleted, and have compositions for Rb/Zr
8 822 and Nb, considered as a proxy for arc maturity (Brown et al., 1984), similar to VR and
9 823 different from MA (Rb/Zr between 0.3-1.1 in TMP, 0.2-0.7 in VR and 0.2-1.7 in MA;
10 824 Lamarão et al., 2002). Thus, according to geochronological and petrological data, we
11 825 proposed that the TMP rocks in this study ~~represent the more felsic and evolved facies~~
12 826 ~~of the VR magmatism and~~ must be ascribed ~~at this~~ to the VRs formation. Geochemical
13 827 differences in our rocks and VR volcanics could be explained by a more evolved
14 828 character of the TMP rocks. The ~~The~~ evidences of plagioclase fractionation from the
15 829 parent melts of the TMP (negative Eu and Sr anomalies, Fig. 12) and their absence in
16 830 less evolved VR rocks reinforce this interpretation, and suggest fractional
17 831 crystallization as the prominent process controlling the VR magmatism evolution.
18 832 However, we want to point out that due to the large area covered by the presented
19 833 investigation (Fig. 2), together with the VR area, the geochemical variations between
20 834 our rocks (TMP) and VR could be the result of local/regional heterogeneities in the
21 835 magmatism. This hypothesis is supported by the intermediate characteristics of the
22 836 TMP samples with respect to the VR and MA volcanics (Figs 11, 12 and 13).

23 837 Recently, new authors (Juliani et al., 2014) suggest the geochemical and
24 838 geochronological signature of the MA ~~(TMP)~~ formation could be correlated to the felsic
25 839 Santa Rosa (SR) formation cropping out in the SFX region. Our new U-Pb
26 840 geochronological analyses on one rock sample from the SR formation yielded an
27 841 average age of 1884 ± 5.2 Ma (Fig. 168) that is consistent with previous Pb-Pb ages on
28 842 other locations. Juliiani and Fernandes (2010) published two Pb-Pb ages on zircons of
29 843 1879 ± 2 Ma and 1884 ± 1.7 for a rhyolite and an ash tuff, respectively. Recently
30 844 Antonio et al. (2017) publishes the first U-Pb ages on zircons for the Santa Rosa
31 845 Formation with 1877.4 ± 4.3 Ma for a rhyolite and 1895 ± 11 Ma for a dike. All
32 846 geochronological results support a ca. 1880 Ma age for the emplacement of these
33 847 rocks.

34 848 The southern Amazonian craton, as well as other ~~P~~recambrian terrains
35 849 worldwide (Condie, 2002; Hoffman, 1988; Zhao et al., 2002), are considered to be

1
2 850 characterized by a series of orogenic to post-orogenic events from 2.0 up to 1.88 Ga.
3 851 The amalgamation of cratonic blocks worldwide established connections between
4
5 852 South America and West Africa and other cratonic terrains such as Western Australia
6
7 853 and South Africa, Laurentia and Baltica, Siberia and Laurentia, Laurentia and Central
8
9 854 Australia, etc (Zhao et al., 2002). These late-Paleoproterozoic collisional processes
10
11 855 likely formed the controversial supercontinent Columbia (Zhao et al., 2004). This
12
13 856 period also coincides with a major peak in orogenic gold resources (Goldfarb et al.,
14
15 857 2001, Juliani et al., 2014) and understanding the geodynamic of this period is crucial
16
17 858 for economic interests. Antonio et al. (2017) highlight that for the period 1.88 Ga,
18
19 859 many cratonic terrain have been characterized by extensive magmatism. These authors
20
21 860 report as examples the 1880 Ma NE-trending Ghost dike swarm and the 1880 Ma
22
23 861 Circum-Superior LIP in the Canadian shield (Minifie et al., 2013), the 1880 Ma
24
25 862 Southern Bastar- Cuddapah LIP in India (French et al., 2008), the Mashonaland sills
26
27 863 and the Post-Waterberg dolerites in Kalahari craton (Hanson et al., 2004), an extensive
28
29 864 A-type magmatism in Baltica and in Siberia. The A-type affinity of the 1.88 Ga rocks
30
31 865 is widely described by other authors in different regions into the Amazonian craton
32
33 866 (Ferron et al., 2010; Pierosan et al., 2011; Fernandes et al., 2011; Klein et al., 2012;
34
35 867 Barreto et al., 2014; Teixeira et al., 2018). Currently, the significance of the 1.88 Ga A-
36
37 868 type magmatism in the Amazonian craton is still matter of debate, also due to the
38
39 869 extremely large aerial cover which interested several different domains with different
40
41 870 basements and geologic evolutions. For example, studies on the Carajas region suggest
42
43 871 that the 1.88 Ga anorogenic magmatism in this domain was provoked by delamination
44
45 872 and fusion of the Archean basement by a mantle plume which originated an
46
47 873 extensional setting (Dell'Agnol et al., 2005; Silva et al., 2016; Teixeira et al., 2018;
48
49 874 Teixeira et al., 2019).
50
51 875 Conversely, the geochemical features of the TMP and SFX magmatism
52
53 876 presented in this work and in literature (Lamarão et al., 2002, 2005; Fernandes et al.,
54
55 877 2011) mainly support an extensional regime of these regions related to a late- to post-
56
57 878 collisional event, being possibly related to the end of the subduction process.-
58
59 879 According to these authors we suggest that the A-type rocks emplaced during
60
61 880 the period 1.88 Ga in both TMP and SFX are related to an intraplate environment in an
62
63 881 extensional regime.The transition from convergent (syn/post-orogenic) to extensional
64
65 882 tectonic setting could register the beginning of the taphrogenesis that marked the
66
67 883 Amazonian Craton throughout the Mesoproterozoic (Brito Neves, 1999; Lamarão et

Formatted: Font: (Default) Times New Roman, No underline, Font color: Text 1

Formatted: Font: (Default) Times New Roman, Font color: Text 1, English (United States)

Formatted: Font: (Default) Times New Roman, No underline, Font color: Auto

Formatted: Font: (Default) Times New Roman, No underline

Formatted: Font: (Default) Times New Roman, No underline, Font color: Auto

Formatted: Font: (Default) Times New Roman, No underline

Formatted: Font: (Default) Times New Roman, No underline, Font color: Auto

1
2
3
4
5
6
7
8
9
10
11
12
13
14
15
16
17
18
19
20
21
22
23
24
25
26
27
28
29
30
31
32
33
34
35
36
37
38
39
40
41
42
43
44
45
46
47
48
49
50
51
52
53
54
55
56
57
58
59
60
61
62
63
64
65

884 al., 2002). The ca. 1.88 Ga felsic magmatism in different provinces of the Amazonian
885 craton could represent the oldest magmatism related to this event. It should be
886 mentioned that in term of textural features, the products emitted during the transition
887 between the post-collisional to extensive events don't display substantial variations. In
888 other words, the lithofaciological signature of the volcanic and volcanoclastic rocks that
889 characterized the 2 Ga VR event (subduction related) is similar for those products
890 erupted during the 1.88-1.87 Ga extensional volcanism that characterized the MA and
891 SR events. Moreover, the post-orogenic to extensional setting emphasizes the
892 continental setting where the studied volcanic products have been emitted. Following
893 the idea of Roverato et al. (2017) for the Late-Paleoproterozoic andesitic Sobreiro
894 Formation, we stress the lack of any evidences in favour of subaqueous eruptions for
895 the emitted felsic products such as pillow lavas as well as hyaloclastites. This suggests
896 the subaerial character of the volcanism and its emitted products acted in both regions.

Formatted: Font: (Default) Times New Roman, No underline

Formatted: Font: (Default) Times New Roman, No underline

Formatted: Font: (Default) Times New Roman, No underline, Font color: Auto

Formatted: Font: (Default) Times New Roman, No underline, Font color: Auto

107.2. Eruptive style and emplacement

Formatted: Indent: First line: 0 cm

899 The study areas are widely characterized by volcanic deposits whose eruptive
900 style is hard to differentiate. Distinguishing between banded lavas and high grade
901 ignimbrites is, sometime, extremely challenging (Henry and Wolff, 1992; Manley,
902 1995). This is made even more complicated when the investigated deposits are ancient
903 and the outcrops intensely eroded, such as those Precambrian terrains investigated here
904 (Lenhardt et al., 2012; Roverato et al., 2016; Lenhardt et al., 2017). Evidences in the
905 field show that a great volume of the volcanic activity is represented by the emission of
906 lava flows and/or high-grade to rheomorphic ignimbrites, although an important
907 amount of other fragmental products of different type (Lf mAL, mLA, l-g/m-g/h-
908 gwAL) are also well represented in both regions. High-grade welded and rheomorphic
909 (up to lava-like) ignimbrites share similar features with lavas, displaying banding and
910 ductile folds formed by the elongation of fiamme and vesicles (Schmincke and
911 Swanson, 1967; Chapin and Lowell, 1979; Wolff and Wright, 1981; Branney et al.,
912 1992; Sumner and Branney, 2002; Pioli and Rosi, 2005; Andrews and Branney, 2011;
913 Brown and Bell, 2013). Although the ignimbrites investigated here have a fragmental
914 derivation their origin largely differ from those characteristic of fallout deposits that
915 form by a sustained column explosive-driven eruption. High-grade welded and
916 rheomorphic ignimbrites are correlated with highly explosive plinian-type eruptions

Formatted: Font: Not Italic, No underline

Formatted: Font: Not Italic, No underline

1 917 which produce, during their column collapse stage, large PDC. In addition, high-grade
2 918 rheomorphism of silicic products, either deriving from an explosive or effusive
3 919 eruption, are favored by high temperature low-viscosity emplacement conditions and
4 920 the presence of some residual water. The high temperatures condition of our deposits is
5 921 also confirmed by the pervasive presence of spherulites and lithophysae formed during
6 922 the slow-cooling regimes of large silica-rich lavas and welded ignimbrites (Lofgren,
7 923 1971; Breitzkreuz, 2013). The eruptive scenario showed in figure 17 giving origin to the
8 924 frequent eruption of large volume and high discharge rate lava flows and ignimbrites
9 925 was likely characterized by fissure-fed and caldera collapses systems as those
10 926 described by previous authors (Legros et al., 2000; Aguirre et al., 2003; Cas et al.,
11 927 2011; Lesti et al., 2011; Lenhardt et al., 2012; Willcock et al., 2013). Eruptions fed by
12 928 extensive fissures of large size, in fact, appear to be the most favourable volcanic
13 929 systems to minimize cooling during emplacement and produce an alternance of low-
14 930 height sustained column eruptions feeding PDC and eruptions characterized by the
15 931 effusion of low viscosity lava flows, coulees and domes, while maintaining high
16 932 discharge rates (e.g. Bachmann et al., 2000; Aguirrez-Diaz & Labarthe-Hernandez,
17 933 2003; Polo et al., 2018a, b; Simões et al., 2017). The sustained fountaining and
18 934 entrainment of air in the eruptive jet is strongly influenced by the geometry of the
19 935 conduit (Legros et al., 2000) as well as the transition from sustained to collapsing
20 936 eruptive column. A wide-geometry conduit would impede much air entrainment into
21 937 the pyroclastic fountain and, at the same time, would favors magmatic escape of
22 938 volcanic gases, favoring the low fountaining and promoting a “boil-over” style
23 939 eruption (Branney and Kokelaar, 1992, 2002; Lenhardt et al., 2017) with high
24 940 discharge rate. Moreover, the low air injection would inhibit the dilution of the
25 941 eruptive material making it thermodynamically isolated from the surrounding
26 942 environment (Lesti et al., 2011), preserving the high temperatures and enhancing the
27 943 agglutination of fragments (welding) (e.g. Quane and Russell, 2004; Russell and
28 944 Quane 2005; Giordano et al., 2005). When the low-altitude pyroclastic fountaining or
29 945 the emission of high temperature lavas would be maintained for long time the high
30 946 flow-mobility is ensured (Sulpizio et al., 2014). If the material supply from the vent
31 947 continues for long time and with high discharge rate, the mobility could be maintained
32 948 even on very low slope angles (Sulpizio et al., 2014; Giordano et al., 2017; Kolzenburg
33 949 et al., 2017), and flowing various kilometers up to hundreds of kilometers far from the
34 950 vent (Aguirre-Diaz et al., 2008; Cas et al., 2011; Giordano et al., 2017). This could

1
2 951 explain the presence of large silicic volcanic areas characteristic of the ancient
3 952 Amazonian volcanism (Roverato et al., 2016). Although, volcanoclastic rocks seem to
4 953 be volumetrically less important in the study areas than the lava flows and/or
5 954 rheomorphic ignimbrites the recognition of fragmental rocks during our field
6 955 campaigns is important to understand their significance into our paleogeographic
7
8 956 reconstruction (Fig. 17). An idealized deposit sequence of a caldera forming eruption
9 957 displays an air-fall deposit overlain by an ignimbrite (Druitt and Sparks, 1984) and the
10 958 transition from the sustained column phase to the pyroclastic flow phase is often
11 959 accompanied by a strong increase in the discharge rate (Bursik and Woods, 1996). The
12 960 stratigraphic sequence of figure 11 shows this association of a possible air-fall deposit
13 961 (Lf dsAL) linked with pyroclastic flow-dominated deposits (Lf mAL and *m-gwLA*). In
14 962 some cases, pyroclastic eruptions commonly precede lava emplacement (Fink 1983;
15 963 Heiken and Wohletz 1987). The sequence presented in figure 7 shows a low-grade
16 964 welded ignimbrite deposit (Lf *l-gwAL*) overlaid by a thick banded body that we are
17 965 interpreting here as a lava flow. At the base of the banded lava is a breccia (Lf mLB)
18 966 consisting of clasts of a mix of lava textural types, including massive, vesicular, flow
19 967 banded and flow-folded, glassy, pumiceous and devitrified. Autobrecciation in lavas or
20 968 rheomorphic ignimbrites occurs when more rigid layers and the external parts are
21 969 broken in response to the applied shear stress locally exceeding the tensile strength
22 970 (Fink and Manley; 1987). Some polymictic breccia deposits (Lf mLA) are
23 971 characterized by lithic angular clasts and devitrified fragments that could point to co-
24 972 ignimbritic breccias with short transport of the emitted material. These deposits could
25 973 be also related to collapse-caldera-breccias falling down into the caldera ring during
26 974 the roof subsidence (Fig. 8). Air-fall (sA) and dilute pyroclastic flow (xsA) deposits
27 975 (surge type) crop out in both regions. These, linked with the glassy and lithic
28 976 pyroclastic material described above, are evidence of intense explosive phases from
29 977 more sustained column eruptions of smaller intra-caldera volcanic centers and/or
30 978 associated to events of caldera collapse (Fig. 17).

980 107.2.1 The sedimentary response

981 Sets of small basins intra-calderas and probable relatively immature shallow
982 marine deposits are interpreted as forming part of a tectonically unstable setting of a
983 young extensional environment that characterized the southern Amazonian craton
984 during the Paleoproterozoic. Reworked sediments can accumulate into volcano-

Formatted: Font: Not Italic, No underline

Formatted: Font: Not Italic

1 985 tectonic depressions created by the eruption, which often collects an intra-caldera lake
2 986 (Heiken et al., 2000 Németh et al., 2009, Manville et al., 2009). The sedimentation into
3 987 intra-volcano shallow-water lacustrine basins would have be facilitated (Fig. 17). The
4 988 alternation of subaerial to shallow-water sedimentation displayed by the alternation of
5 989 Lf mS and csG is indicative of this volcano-tectonic depressions, which could be also
6 990 interpreted as immature marine depressions. Subaerial and subaqueous talus coarse-
7 991 grained up to finer grained turbidites (dsSt) and suspension deposits formed during
8 992 quiescent periods into lakes or pounds is also inferred (Bacon et al., 2002). Silica-rich
9 993 accumulations into shallow water basins (Chipera et al., 2008; Manville et al., 2009)
10 994 deriving from hydrothermal activity in a dynamic volcanic context is also thought to be
11 995 responsible for the formation of chert accumulation (Lf bChS). Post caldera uplifting
12 996 (Fig. 17), resurgence or central volcanism could also contribute to produce new
13 997 sediments to be reworked and transported. Fluvial erosion and reworking of primary
14 998 deposits produced wide range of different sediments from localized cross-bedded,
15 999 well-sorted sand (Lf xsS) and gravel (Lf xsSG) beds to massive clast-supported sand
16 1000 and gravel (Lf csGS, csG) and cobble (Lf csGC) deposits. Fluvial deposits occur
17 1001 throughout all successions, representing periods of stream and river reworking and re-
18 1002 establishment after an eruptive phase (Zernack et al., 2011; Roverato et al., 2017).
19 1003 Debris-flows, hyperconcentrated flows, sheet-floods and active sandy braided river
20 1004 systems existed and the probable absence of vegetation during the Precambrian
21 1005 (Oberholzer and Eriksson, 2000; Roverato et al., 2017) permitted that copious rainfalls
22 1006 easily reworked the available sediments.
23
24
25
26
27
28
29
30
31
32
33
34
35
36
37

38 1008 119. Conclusion 39 1009

40 1010 This study is the result of the lithofaciological analysis carried out during the
41 1011 2013, 2014 and 2015 field campaigns in the Amazon Craton in the TMP and SFX
42 1012 regions and the successive geochemical and geochronological analysis of samples
43 1013 collected in the field. This work constitutes a further step ahead toward the
44 1014 comprehension of significance, chronostratigraphic distribution and the dynamic of
45 1015 eruption and emplacement of felsic volcanic products in the region. Our results
46 1016 complete previous studies and confirm that products present in the Amazonia Craton
47 1017 could be related either to caldera-type systems (e.g. Lamarão et al., 2002; Juliani et al.,
48 1018 2005; Lamarão et al., 2005; Pierosan et al., 2011) and to fissure-fed eruptive
49
50
51
52
53
54
55
56
57
58
59
60
61
62
63
64
65

1
2 1019 environment following the model proposed by Aguirre-Diaz and Labarthe-Hernandez
3 1020 (2003) for the “Sierra Madre Occidental” formation and by Juliani and Fernandes
4 1021 (2010) for the Xingu region. The two models are in fact very similar only differing for
5 1022 the size of the hypothesized magma chambers and the shape of the fissural vents. The
6 1023 described volcano-sedimentary sequences that were characterized by the emission of
7 1024 large volcanic felsic products were likely formed in a late- to post-orogenic (~ 2 Ga) to
8 1025 extensional regimes (~ 1.88 Ga).

9
10
11
12
13
14 1027 ~~Here we also image that an ideal late-convergent to extensional geotectonic~~
15 1028 ~~environment was likely similar to that proposed in our discussion paragraph, where a~~
16 1029 ~~post-orogenic to extensional regime for the period ~1.88 Ga was characterized by the~~
17 1030 ~~emission of large volcanic felsic products. With this contribution we want also stress~~
18 1031 ~~the importance of the results obtained by investigating the lithofaciological character of~~
19 1032 ~~the deposits instead of only carrying out geochemical studies.~~

20
21
22
23
24
25 1034 Acknowledgments

26 1035 This work was supported by the project CAPES/CNPq 402564/2012-0 (Programa
27 1036 Ciências sem Fronteiras) to Caetano Juliani and Matteo Roverato. M. Roverato
28 1037 acknowledges the grant of the Brazilian CAPES/ CNPq Programa Ciências Sem
29 1038 Fronteiras, Atração de Jovem Talento 402564/2012-0. We acknowledge the CNPq/CT-
30 1039 Mineral (Proc. 550.342/ 2011-7) and the INCT-Geociam (573733/2008-2) —
31 1040 (CNPq/MCT/ FAPESPA/PETROBRAS). Furthermore, the first author would like to
32 1041 thank Jeovaci Jr. Martins da Rocha, Diego Felipe Gomez Gutierrez, Lucas Villela
33 1042 Cassini for the help in the field -and Carlos Marcelo Diaz Fernandez for the help ~~in the~~
34 1043 ~~field~~ and very useful discussions. Dr. Giordano acknowledges the financial support for
35 1044 this research from the CAPES project (proposal 302827) of the Ciências Sem
36 1045 Fronteiras program (Brazil) and the local research funds (2012, 2013, 2014) of the
37 1046 University of Turin (Ex60-2015). We are indebted to ~~.....~~ Nils Lenhardt and Roberto
38 1047 Dall’Agnol..... for the dedication in reviewing this manuscript and important
39 1048 comments and reviews, which improved considerably this work. ,.....

40
41
42
43
44
45
46
47
48
49
50
51 1050
52 1051 References

53 1052
54 1053 Aguirre-Diaz, G.J., Labarthe-Hernández, G., 2003. Fissure ignimbrites: fissure-source

Formatted: Indent: First line: 0.75 cm

- 1
2 1054 origin for voluminous ignimbrites of the Sierra Madre Occidental and its
3 1055 relationship with Basin and Range faulting. *Geology* 31, 773-776.
4
5 1056 Aguirre-Diaz, G.J., Labarthe-Hernández, G., Tristán-González, M., Nieto-Obregón, J.,
6 1057 Isaac Gutiérrez-Palomares, I., 2008. The ignimbrite flare-up and graben calderas
7 1058 of the Sierra Madre Occidental, Mexico. In: Martí, J., Gottsman, J. (Eds.), *Caldera*
8 1059 *Volcanism: Analysis, Modelling and Response*. *Developments in Volcanology* 10,
9 1060 143-180.
10
11 1061 Almeida, F.F.M., Hasui, Y., Brito Neves, B.B., Fuck, R.A., 1981. Brazilian structural
12 1062 provinces: an introduction. *Earth Science Reviews* 17, 1-29.
13
14 1063 Almeida, M.E., Brito, M.F.L., Ferreira, A.L., Monteiro, M.A.S., 2000. Projeto Especial
15 1064 Província Mineral do Tapajós. *Geologia e recursos minerais da Folha Vila Mamãe*
16 1065 *Anã (SB.21-V-D)*. Estados do Pará e Amazonas. CPRM, Brasília. [CD-ROM].
17
18 1066 Amaral, G., 1974. *Geologia Pré-Cambriana da Região Amazônica*. Tese de Livre
19 1067 Docência, IG/USP (212 pp.).
20
21 1068 Anders, E., Ebihara, M., 1982. Solar system abundances of the elements. *Geochim.*
22 1069 *Cosmochim. Ac.* 46, 2363-2380.
23
24 1070 Andrews, G.D.M., Branney, M.J., 2011. Emplacement and rheomorphic deformation
25 1071 of a large, lava-like rhyolitic ignimbrite: Grey's Landing, southern Idaho.
26 1072 *Geological Society of America Bulletin* 123, 725-743.
27
28 1073 Antonio, P., D'Agrella-Filho, M.S., Trindade, R.I.F., Nédélec, A., de Oliveira, D.C., da
29 1074 Silva, F.F., Roverato M., Lana, C., 2017. Turmoil before the boring billion:
30 1075 Paleomagnetism of the 1880–1860 Ma Uatumã event in the Amazonian craton.
31 1076 *Gondwana Research* 49, 106-129.
32
33 1077 Araújo, O.J.B., Maia, R.G.N., Jorge, João, X.S., Costa, J.B.S., 1988. A
34 1078 megaestruturação arqueana da folha Serra dos Carajás. In: SBG (Ed.), *Congresso*
35 1079 *Latinoamericano de Geologia*, seventh ed. Belém. 324-333.
36
37 1080 Bacon, C.R., Gardner, J.V., Mayer, L.A., Buktenica, M.W., Dartnell, P., Ramsey,
38 1081 D.W., Robinson, J.E., 2002. Morphology, volcanism, and mass wasting in Crater
39 1082 Lake, Oregon. *Geological Society of America bulletin* 114, 675-692.
40
41 1083 Bahia, R.B.C., Quadros, M.L.E.S., 2000. *Geologia e recursos minerais da Folha*
42 1084 *Caracol SB.21-X-C*. Estados do Pará e Amazonas. Escala 1:250.000. Brasília:
43 1085 CPRM, 2000. 1 CD ROM.
44
45 1086 Barreto, C.J.S., Lafonb, J.M., da Rosa Costac L.T., Fernandes-Limad, E., 2014.
46 1087 Palaeoproterozoic (~1.89 Ga) felsic volcanism of the Iricoumé Group, Guyana

- 1
2 1088 Shield, South America: geochemical and Sm-Nd isotopic constraints on sources
3 1089 and tectonic environment. *International Geology Review*, 2014.
4
5 1090 <http://dx.doi.org/10.1080/00206814.2014.930800>
6
7 1091 Best, M.G., Christiansen, E.H., 1997. Origin of broken phenocrysts in ash-flow tuffs.
8 1092 *GSA Bulletin*, 109 (1), 63-73.
9
10 1093 Blatt, H., Middleton, G., Murray, R., 1980. *Origin of Sedimentary Rocks*. Prentice-
11 1094 Hall, Englewood Cliffs, 634.
12
13 1095 Branney, M.J., Kokelaar, B.P., 1992. A reappraisal of ignimbrite emplacement:
14 1096 progressive aggradation and changes from particulate to non-particulate flow
15 1097 during emplacement of high-grade ignimbrite. *Bull. Volcanol.* 54, 504-520.
16
17
18 1098 Breitzkreuz, C., 2013. Spherulites and lithophysae—200 years of investigation on high
19 1099 temperature crystallization domains in silica-rich volcanic rocks. *Bull. Volcanol.*
20 1100 75:705.
21
22
23 1101 Brito-Neves, B.B., 2011. The Paleoproterozoic in the South-American continent:
24 1102 Diversity in the geologic time. *Journal of South American Earth Sciences* 32, 270-
25 1103 286.
26
27 1104 Brown, D.J., Bell, B.R., 2013. The emplacement of a large, chemically zoned,
28 1105 rheomorphic, lava-like ignimbrite: the Sgurr of Eigg Pitchstone, NW Scotland.
29 1106 *Journal of the Geological Society* 170, 753-767.
30
31 1107 Brown, G.C., Thorpe, R.S., Webb, P.C., 1984. The geochemical characteristics of
32 1108 granitoids in contrasting arcs and comments on magma sources. *Journal of the*
33 1109 *Geological society* 141, 413-426.
34
35
36 1110 Bursik, M.I., Woods, A.W., 1996. The dynamics and thermodynamics of large ash
37 1111 flows. *Bull. Volcanol.* 58, 175-193.
38
39
40 1112 Capuzzo, N., Wetzel, A., 2004. Facies and basin architectural of the Late
41 1113 Carboniferous Salvan-Dorénaz continental basin (Western Alps,
42 1114 Switzerland/France). *Sedimentology* 51, 675-697.
43
44
45 1115 Cas, R.A.F., Wright, J.V., 1987. *Volcanic Successions, Modern and Ancient*. Unwin
46 1116 Hyman, Boston. 528.
47
48 1117 Cas, R.A.F., Wright, H.M.N., Folkes, C.B., Lesti, C., Porreca, M., Giordano, G.,
49 1118 Viramonte, J.G., 2011. The flow dynamics of an extremely large volume
50 1119 pyroclastic flow, the 2.08-Ma Cerro Galán Ignimbrite, NW Argentina, and
51 1120 comparison with other flow types. *Bull. Volcanol.* 73, 1583-1609.
52
53
54
55
56
57
58
59
60
61
62
63
64
65

- 1
2 1121 Chipera, S.J., Goff, F., Goff, C.J., Fittipaldo, M., 2008. Zeolitization of intracaldera
3 1122 sediments and rhyolitic rocks in the 1.25 Ma lake of Valles caldera, New Mexico,
4 1123 USA. *Journal of Volcanology and Geothermal Research* 178, 317-330.
5
6 1124 Collinson, J.D., 1966. Antidune bedding in the Namurian of Derbyshire, England:
7 1125 *Geologie en Mijnbouw* 45, 262-264.
8
9 1126 Collinson, J.D., Thompson, D.B., 1982 *Sedimentary structures*: London, Allen and
10 1127 Unwin, 194.
11
12 1128 Condie, K.C., 2000. Episodic continental growth models: after thoughts and
13 1129 extensions. *Tectonophysics* 322, 153-162.
14
15 1130 Condie, K.C., 2002. Continental growth during a 1.9-Ga superplume event. *Journal of*
16 1131 *Geodynamics* 34, 249-264.
17
18 1132 Costa, J.B.S., Hasui, Y. 1997. Evolução geológica da Amazônia. In: M.L. Costa &
19 1133 R.S. Angélica (Ed.), *Contribuições à geologia da Amazônia*, 16-90.
20
21 1134 Da Cruz, R.S., Fernandes, C.M.D., Villas, R.N.N., Juliani, C., Monteiro, L.V.S.,
22 1135 Almeida, T.I.R., Lagler, B., Carneiro, C.C., Misas, C.M.E., 2015. A study of the
23 1136 hydrothermal alteration in Paleoproterozoic volcanic centers, São Felix do Xingu
24 1137 region, Amazonian Craton, Brazil, using short-wave infrared spectroscopy. *J.*
25 1138 *Volc. Geoth. Res.* 304, 324-335.
26
27 1139 Dall’Agnol, R., Lafon, J.M., Macambira, M.J.B., 1994. Proterozoic anorogenic
28 1140 magmatism in the Central Amazonian Craton: geochronological and geochemical
29 1141 aspects. *Mineral. Petrol.* 50, 113-138.
30
31 1142 Dall’Agnol, R., Costi, H.T., Leite, A.A.S., Magalhães, M.S., Teixeira, N.P., 1999.
32 1143 Rapakivi granites from Brazil and adjacent areas. *Precambrian Research* 95, 9-39.
33
34 1144 Dall’Agnol, R., Teixeira, N.P., Rämö, O.T., Moura, C.A.V., Macambira, M.J.B.,
35 1145 Oliveira, D.C., 2005. Petrogenesis of the paleoproterozoic, rapakivi, A-type granites
36 1146 of the Archean Carajás metallogenic province, Brazil. *Lithos* 80, 101-129.
37
38 1147 Dall’Agnol, R., da Cunha, I.R.V., Guimarães, F.V., de Oliveira, D.C., Teixeira,
39 1148 M.F.B., Feio, G.R.L., Lamarão, C.N., 2017. Mineralogy, geochemistry, and
40 1149 petrology of Neoproterozoic to magnesian granites of Carajás province,
41 1150 Amazonian Craton: The origin of hydrated granites associated with charnockites.
42 1151 *Lithos* 277, 3-32.
43
44 1152 Druitt, T.H., Sparks, R.S.J., 1984. On the formation of calderas during ignimbrite
45 1153 eruptions. *Nature* 310, 679-681.
46
47 1154 Echeverri-Misas, C.M., 2010. Geologia e gênese do depósito de Au-(Cu) do Palito,
48
49
50
51
52
53
54
55
56
57
58
59
60
61
62
63
64
65

Formatted: Font: 12 pt, No underline, Font color: Auto

Formatted: Font: 12 pt, No underline, Font color: Auto

Formatted: Font: 12 pt, No underline, Font color: Auto

Formatted: Font: 12 pt, No underline, Font color: Auto

Formatted: Font: 12 pt, No underline, Font color: Auto

- 1
2 1155 Província Aurífera do Tapajós. Dissertação de Mestrado, IG/USP.
- 3 1156 Eriksson, P.G., Engelbrecht, J.P., Res, M., Harmer, R.E., 1994. The Bushy Bend lavas,
4
5 1157 a new volcanic member of the Pretoria Group, Transvaal Sequence. S. Afr. J.
6
7 1158 Geol. 97, 1-7.
- 8 1159 Faraco, M.T.L., Carvalho, J.M.A., Klein, E.L., 1997. Carta metalogenética da
9
10 1160 Província Auréfera do Tapajós, in: Costa, M.L.C., Ange´lica, R.S. (Eds.),
11 1161 Contribuic,ões a` Geologia da Amazônia. Sociedade Brasileira de Geologia,
12 1162 Belém, Brazil 1, 423-437.
- 13 1163 Fernandes, C.M.D., Juliani, C., Monteiro, L.V.S., Lagler, B., Misas, C.M.E., 2011.
14 1164 High-K calc-alkaline to A-type fissure-controlled volcano-plutonism of the São
15 1165 Félix do Xingu region, Amazonian craton, Brazil: Exclusively crustal sources or
16 1166 only mixed Nd model ages? Journal of South America Earth Science 32 (4), 351-
17 1167 368.
- 18 1168 Ferrari, L., Orozco-Esquivel, T., Manea, V.C., Manea, M., 2012. The dynamic history
19 1169 of the Trans-Mexican Volcanic Belt and the Mexico subduction zone.
20 1170 Tectonophysics 522-523, 122-149.
- 21 1171 Ferreira, A.L., Almeida, M.E., Brito, M.F.L., Monteiro, M.A.S., 2000. Projeto Especial
22 1172 Província Mineral do Tapajós. Geologia e recursos minerais da Folha
23 1173 Jacareacanga (SB.21-Y-B). Estados do Pará e Amazonas. Escala 1:250.000. Nota
24 1174 explicativa e mapas, CPRM, Brasília. [CD ROM].
- 25 1175 Ferron, J.M.T.M., Bastos-Neto, A.C., Lima, E.F., Nardi, L.V.S., Costi, H.T., Pierosan,
26 1176 R., Prado, M., 2010. Petrology, geochemistry, and geochronology of
27 1177 Paleoproterozoic volcanic and granitic rocks (1.89–1.88 Ga) of the Pitinga
28 1178 Province, Amazonian Craton, Brazil. Journal of South American Earth Sciences
29 1179 29, 483-497.
- 30 1180 Fink, J., 1983. Structure and emplacement of a rhyolitic obsidian flow: little Glass
31 1181 Mountain, Medicine Highland, northern California. GSA Bull. 94, 362-380.
- 32 1182 Fink, J.H., Manley, C.R., 1987. Origin of pumiceous and glassy textures in rhyolite
33 1183 flows and domes: Geological Society of America Special Paper 212, 77-88.
- 34 1184 Fisher, R.V., 1961. Proposed classification of volcanoclastic sediments and rocks.
35 1185 Geological Society of America Bulletin 72, 1409-1414.
- 36 1186 French, J.E., Heaman, L.M., Chacko, T., Srivastava, R.K., 2008. 1891–1883 Ma
37 1187 Southern Bastar–Cuddapah mafic igneous events, India: a newly recognized large
38 1188 igneous province. Precambrian Research 160, 308-322.

- 1
2 1189 Giordano, D., La Felice, S., Arzilli, F., De Cristofaro, S.P., Masotta, M., Polo L.
3 1190 (2017). Il vulcanismo effusivo acido del Monte Amiata: stima delle condizioni
4 1191 pre- e sin-eruttive ed implicazioni vulcanologiche. Effusive acidic volcanism of
5 1192 Monte Amiata: estimates of pre- and syn-eruptive conditions and volcanological
6 1193 implications. Monografia Il Vulcano di Monte Amiata, ISBN 978-88-99742-32-4,
7 1194 171-193.
- 11 1195 Giordano, D., Nichols, A.R.L., Dingwell, D.B., 2005. Glass transition temperatures of
12 1196 natural hydrous melts: a relationship with shear viscosity and implications for the
13 1197 welding process. Jour. Volc Geoth. Res. 142, 105-118.
- 16 1198 [Giovanardi, T., Girardi, V.A.V., Correia, C.T., Sinigoi, S., Tassinari, C.C.G.,](#)
17 1199 [Mazzucchelli, M., 2015. U-Pb zircons SHRIMP data from the Cana Brava](#)
18 1200 [Layered Complex: New constraints for the mafic-ultramafic intrusions of Northern](#)
19 1201 [Goiás, Brazil. Open Geosci 7, 197-206.](#)
- 22 1202 Goldfarb, R., Groves, D., Gardoll, S., 2001. Rotund versus skinny orogens: well-
23 1203 nourished or malnourished gold? Geology 29, 539-542.
- 25 1204 Gutscher, M.A., Maury, R., Eissen, J.P., Bourdon, E., 2000. Can slab melting be
26 1205 caused by flat subduction? Geology 28, 535-538.
- 28 1206 Hanson, R.E., Gose, W.A., Crowley, J.L., Ramezani, J., Bowring, S.A., Bullen, D.S.,
29 1207 Hall, R.P., Pancake, J.A., Mukwakwami, J., 2004. Paleoproterozoic intraplate
30 1208 magmatism and basin development on the Kaapvaal Craton: age, paleomagnetism
31 1209 and geochemistry of ~1.93 to ~1.87 Ga post-Waterberg dolerites. South African
32 1210 Journal of Geology 107, 233-254.
- 36 1211 Hasui, Y., Haraly, N.L.E., Schobbenhaus, C., 1993. Megaestruturação Pré-Cambriana
37 1212 do território brasileiro baseada em dados geofísicos e geológicos. Geociências 12,
38 1213 7-31.
- 41 1214 Heiken, G, Wohletz, K., 1987. Tephra deposits associated with silicic domes and lava
42 1215 flows. GSA Special Paper 212.
- 44 1216 Heiken, G., Krier, D., McCormick, T., Snow, M.G., 2000. Intracaldera volcanism and
45 1217 sedimentation — Creede caldera, Colorado. In: Bethke, P.M., Hay, R.L. (Eds.),
46 1218 Ancient Lake Creede: Its volcano-tectonic setting, history of sedimentation, and
47 1219 relation to mineralization in the Creede Mining District. Geological Society of
48 1220 America Special Paper, 346. Boulder, Colorado, 127-157.
- 52 1221 Hofmann, A.W., 1988. Chemical differentiation of the Earth: The relationship between
53 1222 mantle, continental crust and oceanic crust. EPSL 90, 297-314.

- 1
2 1223 Hollocher, K., Robinson, P., Walsh, E., Roberts, D., 2012. Geochemistry of
3 1224 amphibolite-facies volcanics and gabbros of the Støren Nappe in extensions west
4 1225 and southwest of Trondheim, Western Gneiss Region, Norway: a key to
5 1226 correlations and paleotectonic settings. *American Journal of Science* 312, 357-
6 1227 416.
- 9 1228 Juliani, C., 2002. Alteração hidrotermal e metalogênese em sistemas vulcano-
10 1229 plutônicos paleoproterozóicos na Província Aurífera do Tapaj, Cráton Sul
11 1230 Amazônico, Pará. Tese de Livre-Docência, IG/USP.
- 14 1231 Juliani, C., Vasquez, M.L., Klein, E.L., Villas, R.N., Echeverri-Misas, C.M., Santiago,
15 1232 E.S.B., Monteiro, L.V.S., Carneiro, C.C., Fernandes, C.M.D., Usero, G., 2014.
16 1233 Metalogenia da Província Tapajós. In: Silva M.G.; Jost H.; Kuyumajian R.M.
17 1234 (Org.). *Metalogênese das Províncias Tectônicas Brasileiras*. 1 ed. : CPRM —
18 1235 Serviço Geológico do Brasil 1, 51-90.
- 22 1236 Juliani, C., Rye, R.O., Nunes, C.M.D., Snee, L.W., Correa Silva, R.H., Monteiro,
23 1237 L.V.S., Bettencourt, J.S., Neumann, R., Neto, A.A., 2005. Paleoproterozoic high
24 1238 sulphidation mineralization in the Tapajós gold province, Amazonian Craton,
25 1239 Brazil: geology, mineralogy, alunite argon age, and stable-isotope constraints.
26 1240 *Chemical Geology* 215, 95-125.
- 30 1241 Juliani, C., Fernandez C.M.D., 2010. Well-preserved Late Paleoproterozoic volcanic
31 1242 centers in the São Félix do Xingu region, Amazonian Craton, Brazil. *Journal of*
32 1243 *Volcanology and Geothermal Research* 191, 167-179.
- 35 1244 Kay, S.M., Godoy, E., Kurtz, A., 2005. Episodic arc migration, crustal thickening,
36 1245 subduction erosion, and magmatism in the south_central Andes. *Geological*
37 1246 *Society of America Bulletin* 117, 67-88.
- 39 1247 Klein, E.L., Almeida, M.E., and Costa, L.T.R., 2012. The 1.89-1.87 Ga Uatumã Silicic
40 1248 Large Igneous Province, northern South America: Large Igneous Provinces
41 1249 Commission: <http://www.largeigneousprovinces.org/12nov> (accessed 12 January
42 1250 2012).
- 46 1251 Klein, E.L., Santos, R.A., Fuzikawa, K., Angélica, R.S., 2001. Hydrothermal fluid
47 1252 evolution and structural control of the brittle-style Guarim lode-gold
48 1253 mineralisation, Tapajós Province, Amazonian Craton, Brazil. *Miner. Depos.* 36,
49 1254 149-164.
- 52 1255 Klein, E.L., Vasquez, M.L., Rosa-Costa, L.T., Carvalho, J.M.A., 2002. Geology of
53 1256 Paleoproterozoic gneiss- and granitoid-hosted gold mineralization in Southern

- 1
2 1257 Tapajós Gold Province, Amazonian Craton, Brazil. *Intern. Geol. Rev.*, 44, 544-
3 1258 558.
4
5 1259 Klein, E.L., Rosa-Costa, L.T., Carvalho, J.M.A., 2004. Estudo de inclusões fluidas em
6 1260 veio de quartzo aurífero do prospecto Patinhas, Província Aurífera do Tapajós,
7 1261 Cráton Amazônico. *RBG* 34, 59-66.
8
9 1262 Lagler, B., Juliani, C., Pessoa, F.F., Fernandes, C.M.D., 2011. Petrografia e
10 1263 geoquímica das sequências vulcânicas Paleoproterozóicas na região de Vila
11 1264 Tancredo, São Félix do Xingu (PA). In: *SBGq, Congr. Bras. Geoquí.*, 13, e Simp.
12 1265 Países do Mercosul, 3, Gramado, RS. Anais, [CD-ROM].
13
14 1266 Lamarão, C.N., Dall'Agnol, R., Lafon, J.M., Lima, E.F., 1999. As associações
15 1267 vulcânicas e plutônicas de Vila Riozinho e Morais Almeida, Província Aurífera do
16 1268 Tapajós, SW do estado do Pará. In: *Simpósio sobre Vulcanismo e Ambientes*
17 1269 *Associados. 1, Gramado*/RS, Boletim de resumos*, 93 (in Portuguese).
18
19 1270 Lamarão, C.N., Dall'agnol, R., Lafon, J.M., Lima, E.F., 2002. Geology, geochemistry,
20 1271 and Pb-Pb zircon geochronology of the Paleoproterozoic magmatism of Vila
21 1272 Riozinho, Tapajós Gold Province, Amazonian craton, Brazil. *Prec. Res.* 119, 189-
22 1273 223.
23
24 1274 Lamarão, C.N., Dall'agnol, R., Pimentel, M.M., 2005. Nd isotopic composition of
25 1275 Paleoproterozoic volcanic rocks of Vila Riozinho: Implications for the crustal
26 1276 evolution of the Tapajós gold province, Amazon craton. *J. South Am. Earth Sci.*
27 1277 18, 277-292.
28
29 1278 Legros, F., Kelfoun, K., 2000. On the ability of pyroclastic flows to scale topographic
30 1279 obstacles. *J. Volcanol. Geotherm. Res.* 98, 235-241.
31
32 1280 Lenhardt, N., Hornung, J., Hinderer, M., Böhnell, H., Torres-Alvarado, I.S., Trauth, N.,
33 1281 2011. Build-up and depositional dynamics of an arc front volcanoclastic complex:
34 1282 the Miocene Tepoztlan Formation (Transmexican Volcanic Belt, Central Mexico).
35 1283 *Sedimentology* 58, 785-823.
36
37 1284 Lenhardt, N., Eriksson, P., Catuneanu, O., Bumby, A.J., 2012. Nature of and controls
38 1285 on volcanism in the ca. 2.32-2.06 Ga Pretoria Group, Transvaal Supergroup,
39 1286 Kaapvaal Craton, South Africa. *Precambrian Research* 214-215, 106-123.
40
41 1287 Lenhardt, N., Masango S.M., Jolayemi, O.O., Lenhardt, S.Z., Peeters, G.J., Eriksson,
42 1288 P.G., 2017. The Palaeoproterozoic (~2.06 Ga) Rooiberg Group, South Africa:
43 1289 Dominated by extremely high-grade lava-like and rheomorphic ignimbrites? New
44 1290 observations and lithofacies analysis. *Journal of African Earth Sciences* 131, 213-
45
46
47
48
49
50
51
52
53
54
55

- 1
2 1291 232.
- 3 1292 Lesti, C., Porreca, M., Giordano, G., Mattei, M., Cas, R.A.F., Wright, H.M.N., Folkes,
4
5 1293 C.B., Viramonte, J., 2011. High-temperature emplacement of the Cerro Galán and
6
7 1294 Toconquis Group ignimbrites (Puna plateau, NW Argentina) determined by TRM
8
9 1295 analyses. Bull. Volcanol. 73, 1535-1565.
- 10 1296 Lofgren, G., 1971. Spherulite textures in glassy and crystalline rocks. J. Geophys. Res. ◀
11 1297 76, 5635-5648.
- 12 1298 [Ludwig, K.R., 2009. Isoplot 4.1. A geochronological toolkit for Microsoft Excel.](#)
13 1299 [Berkeley Geochronology Center special publication 4, 76.](#)
- 14
15
16 1300 Macambira, E.M.B., 1997. Geologia e aspectos metalogenéticos dos elementos do
17
18 1301 grupo de platina no complexo máfico-ultramáfico da serra da Onça – sul do Pará.
19 1302 Tese de Mestrado, UFPA, Belém, Pará, Brasil.
- 20
21 1303 Macambira, E.M.B., Vale, A.G., 1997. Programa Levantamentos Geológicos Básicos
22 1304 do Brasil. São Félix do Xingu. Folha SB-22-Y-B. Estado do Pará, CPRM, Brasília
23 1305 (in Portuguese).
- 24
25 1306 Manea, V.C., Pérez-Gussinyé, M., Manea, M., 2012. Chilean flat-slab subduction
26
27 1307 controlled by overriding plate thickness and trench rollback. Geology 40 (1), 35-
28 1308 38.
- 29
30 1309 Manville, V., Németh, K., Kano, K., 2009. Source to sink: A review of three decades
31 1310 of progresss in the understanding of volcanoclastic processes, deposits, and
32 1311 hazards. Sedimentary Geology 220, 136-161.
- 33
34
35 1312 McPhie, J., Doyle, M., Allen, S.R., 1993. Volcanic textures: A guide to the
36 1313 interpretation of textures in volcanic rocks, Centre for Ore Deposit and
37 1314 Exploration Studies. University of Tasmania, 198.
- 38
39
40 1315 Miall, A.D., 1996. The Geology of Fluvial Deposits: Sedimentary Facies, Basin
41 1316 Analysis, and Petroleum Geology. Springer-Verlag, New York. 582.
- 42
43 1317 Minifie, M.J., Kerr, A.C., Ernst, R.E., Hastie, A.R., Ciborowski, T.J.R., Desharnais,
44 1318 G., Millar, I.L., 2013. The northern and southern sections of the western ca. 1880
45 1319 Ma Circum-Superior Large Igneous Province, North America: the Pickle Crow
46 1320 dyke connection? Lithos 174, 217-235.
- 47
48
49 1321 [Monteiro, L.V.S., Xavier, R.P., de Carvalho, E.R., Hitzman, M.W., Johnson, C.A., de](#)
50 1322 [Souza Filho, C.R., Torresi, I., 2008. Spatial and temporal zoning of hydrothermal](#)
51 1323 [alteration and mineralization in the Sossego iron oxide-copper-gold deposit,](#)
52 1324 [Carajás Mineral Province, Brazil: paragenesis and stable isotope constraints.](#)
53
54
55

Formatted: Normal, Left, Indent:
Left: 0 cm, Hanging: 0.75 cm,
Line spacing: 1.5 lines, No
widow/orphan control, Don't adjust
space between Latin and Asian
text, Don't adjust space between
Asian text and numbers

1 1325 | [Miner Deposita 43, 129-159.](#)

2

3 1326 | Mori, L., Gómez-Tuena, A., Cai, Y., Goldstein, S., 2007. Effects of prolonged flat

4 1327 | subduction on the Miocene magmatic record of the central Trans-Mexican

5 1328 | Volcanic Belt. *Chemical Geology* 244, 452-473.

6

7 1329 | [Mori, P.E., Reeves, S., Correia, C.T., Haukka, M., 1999. Development of a fused glass](#)

8 1330 | [disc XRF facility and comparison with the pressed powder pellet technique at](#)

9 1331 | [Instituto de Geociências. Rev. Bras. Geociências, 29, 441-446.](#)

10

11 1332 | Mueller, W.U., Concoran, P.L., 1998. Late-orogenic basins in the Archaean Superior

12 1333 | Province, Canada: characteristics and inferences. *Sedimentary Geology* 120, 177-

13 1334 | 203.

14 1335 | Mueller, W.U., Chown, E.H., Thurston, P.C., 2000a. Processes in physical

15 1336 | volcanology and volcanoclastic sedimentation: modern and ancient. *Precambrian*

16 1337 | *Research* 101, 81-85.

17 1338 | [Navarro, M.S., Andrade, S., Ulbrich, H.H.G.J., Gomes, C.B., Girardi, V.A.V., 2008.](#)

18 1339 | [The analysis of rare earth elements with ICP-MS in basaltic and related rocks:](#)

19 1340 | [testing the efficiency of sample decomposition procedures. Geostand. Geoanal.](#)

20 1341 | [Res. 32\(2\),167-180.](#)

21

22 1342 | Németh, K., Cronin, S.J., Stewart, R.B., Charley, D., 2009. Intra- and extra- caldera

23 1343 | volcanoclastic facies architecture of a frequently active mafic island-arc volcano,

24 1344 | Ambryn Island, Vanuatu. *Sedimentary Geology* 220, 256-270.

25 1345 | Oberholzer, J.D., Eriksson, P.G., 2000. Subaerial volcanism in the Palaeoproterozoic

26 1346 | Heekpoort Formation (Transvaal Supergroup), Kaapvaal craton. *Precambrian*

27 1347 | *Research* 101, 193-210.

28 1348 | Pearce, J.A., Harris, N.B.W., and Tindle, A.G., 1984. Trace element discrimination

29 1349 | diagrams for the tectonic interpretation of granitic rocks. *Journal of Petrology* 25,

30 1350 | 956-983.

31 1351 | [Pearce, 1996.....](#)

32

33 1352 | Pessoa M.R., Santiago A.F., Andrade A.F., Barreto E.L., Nascimento J.O., Santos

34 1353 | J.O.S., Oliveira J.R., Lopes R.C., Prazeres W.V. 1977. Projeto Jamanxim.

35 1354 | CPRM/DNPM, 1-3, 614.

36 1355 | Pierosan, R., Lima, E.F., Nardi, L.V.S., Bastos Neto, A.C., Campos, C.P., Jarvis, K.,

37 1356 | Ferron, J.M.T.M., Prado, M., 2011. Geochemistry of Palaeoproterozoic volcanic

38 1357 | rocks of the Iricoumé Group, Pitinga Mining District, Amazonian craton, Brazil:

39 1358 | *International Geology Review* 53, 946-979.

- 1
2 1359 Pinho, S.C.C., Fernandes, C.M.D., Teixeira, N.P., Paiva Jr., A.L., Cruz, V.L.,
3 1360 Lamarão, C.N., Moura, C.A.V., 2006. O magmatismo paleoproterozóico da região
4 1361 de São Félix do Xingu, Província Estanífera do Sul do Pará: Petrografia e
5 1362 geocronologia. *Revista Brasileira de Geociências* 36, 793-802.
6
7 1363 Pioli, L., Rosi, M., 2005. Rheomorphic structures in a high-grade ignimbrite: the
8 1364 Nuraxi tuff, Sulcis volcanic district (SW Sardinia, Italy). *Journal of Volcanology*
9 1365 and *Geothermal Research* 142, 11-28.
10
11 1366 Polo, L.A., Giordano, D., Janasi, V., Freitas-Guimaraes, L., 2017(a). Effusive silicic
12 1367 volcanism in the Paraná Magmatic Province, South Brazil: Physico-chemical
13 1368 conditions of storage and eruption and considerations on the rheological behaviour
14 1369 during emplacement. *J. Volcanol. Geoth. Res.* 355, 115-135.
15
16 1370 Polo L.A., Janasi V., Giordano D., Lima E.F., Cañon-Tapia E., Roverato M., 2017(b).
17 1371 Effusive silicic volcanism in the Paraná Magmatic Province, South Brazil:
18 1372 Evidence for locally-fed lava flows and domes from detailed field work. *J.*
19 1373 *Volcanol. Geoth. Res.* 355, 204-218.
20
21 1374 Quane, S. L., Russell, J. K., 2005. Welding: Insights from high-temperature analogue
22 1375 experiments. *Journal of Volcanology and Geothermal Research* 142 (1-2), 67-87.
23
24 1376 Reis, N.R., Almeida, M.E., Ferreira, A.L., Riker, S.R., 2006. *Geologia e Recursos*
25 1377 *Minerais do Estado do Amazonas. Sistema de Informações Geográficas*
26 1378 1:1.000.000. CPRM, Manaus, 144.
27
28 1379 Rino, S., Tsuyoshi, K., Windley, B.F., Katayama, I., Motoki, A., Hirata, T., 2004.
29 1380 Major episodic increases of continental crustal growth determined from zircon
30 1381 ages of river sands; implications for mantle overturns in the Early Precambrian.
31 1382 *Physics of the Earth and Planetary Interiors* 146, 369-394.
32
33 1383 Roverato, M., Capra, L., Sulpizio, R., Norini, G., 2011. Stratigraphic reconstruction of
34 1384 two debris avalanche deposits at Colima Volcano (Mexico): insights into pre-
35 1385 failure conditions and climate influence. *J. Volc. Geoth. Res.* 207 (1), 33-46.
36
37 1386 Roverato, M., Cronin, S., Procter, J., Capra, L., 2014. Textural features as indicators of
38 1387 debris avalanche transport and emplacement, Taranaki volcano. *Geol. Soc. Am.*
39 1388 *Bull.* B30946-1
40
41 1389 Roverato, M., 2016. The Montesbelos mass-flow (southern Amazonian craton, Brazil):
42 1390 a Paleoproterozoic volcanic debris avalanche deposit? *Bull. Volcanol.* 78, 49.
43
44 1391 Roverato, M., Giordano, D., Echeverri-Misas, CM., Juliani, C., 2016.
45 1392 Paleoproterozoic felsic volcanism of the Tapajós Mineral Province, Southern
46
47
48
49
50
51
52
53
54
55

- 1
2 1393 Amazon Craton, Brazil. *Journal of Volcanology and Geothermal Research* 310,
3 1394 98-106.
4
5 1395 Roverato, M., Juliani, C., Marcelo Dias-Fernandes, C., Capra, L., 2017.
6 1396 Paleoproterozoic andesitic volcanism in the southern Amazonian craton, the
7 1397 Sobreiro Formation: new insights from lithofacies analysis of the volcanoclastic
8 1398 sequences. *Precambrian Research* 289, 18-30.
9
10 1399 Russell, J. K., Quane, S. L., 2005. Rheology of welding: Inversion of field constraints.
11 1400 *Journal of Volcanology and Geothermal Research* 142 (1-2), 173-191.
12
13 1401 Santos, J.O.S., Hartmann, L.A., Gaudette, H.E., Groves, D.I., McNaughton, N.J.,
14 1402 Fletcher, I.R., 2000. A new understanding of the provinces of the Amazon craton
15 1403 based on integration of field mapping and U-Pb and Sm-Nd geochronology.
16 1404 *Gondwana Research* 3, 453-488.
17
18 1405 Santos, J.O.S., Groves D.I., Hartmann L.A., Moura M.A., McNaughton, N.J. 2001.
19 1406 Gold deposits of the Tapajós and Alta Floresta Domains, Tapajós-Parima orogenic
20 1407 belt, Amazon Craton, Brazil. *Mineralium Deposita* 36, 278-299.
21
22 1408 Santos, J.O.S., 2003. Geotectônica dos Escudos da Guiana e Brasil Central. In: L.A.
23 1409 Bizzi, C. Schobbenhaus, R.M. Vidotti, J.H. Gonçalves (Eds.). *Geologia, tectônica*
24 1410 *e recursos minerais do Brasil. Texto, mapas e SIG. CPRM - Serviço Geológico do*
25 1411 *Brasil, Brasília* 169-226.
26
27 1412 Santos, J.O.S., Van Breemen, O.B., Groves, D.I., Hartmann, L.A., Almeida, M.E.,
28 1413 McNaughton, N.J., Fletcher, I.R., 2004. Timing and evolution of multiple
29 1414 Paleoproterozoic magmatic arcs in the Tapajós Domain, Amazon Craton:
30 1415 constraints from SHRIMP and TIMS zircon, baddeleyite and titanite U-Pb
31 1416 geochronology. *Prec. Res.* 13, 73-109.
32
33 1417 [Silva, F.S., Oliveira, D.C., Antonio, P.Y., D'Agrella-Filho, M., Lamarão, C.N., 2016.](#)
34 1418 [Bimodal magmatism of the Tucuma area, Carajás Province: U-Pb geochronology,](#)
35 1419 [classification and processes. *J. S. Am. Earth Sci.* 72, 95-114.](#)
36
37 1420 Simões, M.S., Lima, E.F., Sommer, C.A., Rossetti, L.M.M., 2017. Structures and
38 1421 lithofacies of inferred silicic conduits in the Paraná-Etendeka LIP, southernmost
39 1422 Brazil. *Journal of Volcanology and Geothermal Research* 355, 319-336.
40
41 1423 Sulpizio, R., Mele, D., Dellino, P., La Volpe, L., 2007. Deposits and physical
42 1424 properties of pyroclastic density currents during complex Subplinian eruptions: the
43 1425 AD 472 (Pollena) eruption of Somma-Vesuvius, Italy. *Sedimentology* 54, 607-
44 1426 635.
45
46
47
48
49
50
51
52
53
54
55
56
57
58
59
60
61
62
63
64
65

- 1
2 1427 Sumner, J.M., Branney, M.J. 2002. The emplacement history of a remarkable
3 1428 heterogeneous, chemically zoned, rheomorphic and locally lava-like ignimbrite:
4 1429 'TL' on Gran Canaria. *Journal of Volcanology and Geothermal Research* 115,
5 1430 109-138.
6
7
8 1431 Tassinari, C.C.G., Macambira, M.J.B., 1999. Geochronological provinces of the
9 1432 Amazonian craton. *Episodes* 22, 174-182.
10
11 1433 Teixeira, W., Tassinari, C.C.G., Cordani, U.G., Kawashita, K., 1989. A review of the
12 1434 geochronology of the Amazonian craton: tectonic implications. *Precambrian Res.*
13 1435 42, 213-227. Teixeira, M.F.B., Dall'Agnol, R., Santos, J.O.S., Oliveira, D.C.,
14 1436 Lamarão, C.N., McNaughton, N.J., 2018. Crystallization ages of Paleoproterozoic
15 1437 A-type granites of Carajás province, Amazon craton: Constraints from U-Pb
16 1438 geochronology of zircon and titanite. *J. of South American Earth Sciences* 88,
17 1439 312-331.
18
19 1440 Teixeira, N.P., Bettencourt, J.S., Moura, C.A.V., Dall'Agnol, R., Macambira, E.M.B.,
20 1441 2002. Archean crustal sources for Paleoproterozoic tin-mineralized granites in the
21 1442 Carajas Province, SSE Para, Brazil: Pb-Pb geochronology and Nd isotope
22 1443 geochemistry. *Precambrian Research* 119, 257-275.
23
24 1444 Teixeira, W., Tassinari, C.C.G., Cordani, U.G., Kawashita, K., 1989. A review of the
25 1445 geochronology of the Amazonian craton: tectonic implications. *Precambrian Res.*
26 1446 42, 213-227.
27
28 1447 Teixeira, W., Nelson, J.R., Bettencourt, J.S., Klein, E.L., Oliveira, D.C., 2019.
29 1448 Intraplate Proterozoic magmatism in the Amazonian Craton reviewed:
30 1449 geochronology, crustal tectonics and global matches. In book: *Dyke Swarms of the*
31 1450 World: A Modern Perspective. DOI:10.1007/978-981-13-1666-1_4
32
33
34
35
36
37
38
39
40
41 1452 Van Kranendonk, M.J., 2006. Volcanic degassing, hydrothermal circulation and the
42 1453 flourishing of early life on Earth: a review of the evidence from c. 3490-3240 Ma
43 1454 rocks of the Pilbara Supergroup, Pilbara Craton, Western Australia. *Earth Science*
44 1455 *Rev.* 74, 197-240.
45
46
47 1456 Vasquez, M.L., Klein, E.L., Macambira, M.J.B., Santos, A., Bahia, R.B.C., Ricci, P.,
48 1457 dos, S.F., Quadros, M.L.E.S., 2000. Geochronology of granitoids, mafic intrusions
49 1458 and mineralizations of the Tapajós Gold Province - Amazonian Craton - Brazil. In:
50 1459 *Inter. Geol. Congr. 31, Abstracts, [CD-ROM]*.
51
52
53 1460 Vasquez, M.L., Sousa, C.S., Carvalho, J.M.A., 2008. Mapa Geológico e de Recursos

Formatted: Font color: Auto

Formatted: Font: (Default) Times New Roman, 11 pt, No underline

- 1
2 1461 Minerais do Estado do Pará, escala 1:1.000.000. Programa Geologia do Brasil,
3 1462 Belém, CPRM.
4
5 1463 Vasquez, M.L., Dreher, A.M. 2011. Uma avaliação da estratigrafia dos eventos
6 1464 magmáticos de 1900-1860 Ma do Cráton Amazônico. In: SBG, Simp. Geol.
7 1465 Amaz. 12, Bol. Res. [CD ROM].
8
9 1466 Walker, G.P.L., 1983. Ignimbrite types and ignimbrite problems. J. Volcanol.
10 1467 Geotherm. Res. 17, 65-88.
11
12 1468 Went, D.J., 2016 Alluvial fan, braided river and shallow-marine turbidity current
13 1469 deposits in the Port Lazo and Roche Jagu formations, Northern Brittany:
14 1470 relationships to andesite emplacements and implications for age of the Plourivo-
15 1471 Plouézec Group. Geol. Mag. 1-24, Cambridge University Press 2016.
16
17 1472 White, J.D.L., Houghton, B.F., 2006. Primary volcanoclastic rocks. Geological Society
18 1473 of America Bulletin 34, 677-680.
19
20 1474 Willcock, M.A.W., Cas, R.A.F., Giordano, G., Morelli, C., 2013. The eruption,
21 1475 pyroclastic flow behaviour, and caldera in-filling processes of the extremely large
22 1476 volume (N1290 km³), intra- to extra-caldera, Permian Ora (Ignimbrite) Formation,
23 1477 Southern Alps, Italy. J. Volcanol. Geotherm. Res. 265, 102-126.
24
25 1478 [Williams, I.S., 1998. U-Th-Pb geochronology by ion microprobe. In: McKibben, M.A.,](#)
26 1479 [Shanks, W.C.P., Ridley, W.I. \(eds\) Applications of Microanalytical Techniques to](#)
27 1480 [Understanding Mineralizing Processes, Rev Econ Geol vol 7. Soc. Econ. Geol,](#)
28 1481 [Littleton, 1-35.](#)
29
30 1482 Wolff, J.A., Wright, J.V., 1981. Rheomorphism of welded tuffs. Journal of
31 1483 Volcanology and Geothermal Research 10, 13-34.
32
33 1484 Zanchetta, G., Sulpizio, R., Di Vito, M.A., 2004. The role of volcanic activity and
34 1485 climate in alluvial fan growth at volcanic areas: an example from southern
35 1486 Campania (Italy). Sedimentary Geology 168, 249-280.
36
37 1487 Zernack, A.V., Cronin, S.J., Neall, V.E., Procter, J.N., 2011. A medial to distal
38 1488 volcanoclastic record of an andesitic stratovolcano: detailed stratigraphy of the
39 1489 ring-plain succession of south-west Taranaki, New Zealand: International Journal
40 1490 of Earth Sciences 100, 1937-1966.
41
42 1491 Zhao, G., Cawood, P.A., Wilde, S.A., Sun, M., 2002. Review of global 2.1–1.8 Ga
43 1492 orogens: implications for a pre-Rodinia supercontinent. Earth-Science Reviews 59,
44 1493 125-162.
45
46 1494 Zhao, G., Sun, M., Wilde, S.A., Li, S., 2004. A Paleo-Mesoproterozoic supercontinent:

1
2 1495 assembly, growth and breakup. Earth-Science Reviews 67, 91-123.

3 1496
4 1497
5 1498
6

7 1499 Figure Captions

8 1500
9 1501 Figure 1: location map of the northern South America and the Amazonian Ceraton and
10 1502 divided into several its geochronological provinces and other domains according to
11 1503 Santos et al. (2000); TMP = Tapajós Mineral Province, SFX = São Felix do Xingú
12 1504 Region. ; G = Guyana, GF = French Guyana, S = Suriname.
13
14
15

16
17 1506 Figure 2: distribution map of the outcrops analyzed during the field campaigns in both
18 1507 regions a) Tapajós Mineral Province (TMP) and b) São Felix do Xingú region (SFX);
19 1508 PW=distribution of the Santa Rosa formation inferred during the present work;
20 1509 F=distribution of the Santa Rosa formation inferred by Fernandes et al. (2011);
21 1510 BIF=Banded Iron Formation; red and white dot refers to primary andesitic deposits
22 1511 analyzed in Roverato et al. (2017).- In both figures are reported the outcrops described
23 1512 in the paper.
24
25
26
27
28

29 1513
30 1514 Figure 3: massive and banded lavas and rheo-ignimbrite (?) deposits. a) Np173
31 1515 (7°33'52.31" S, 55°10'58.80" W), b) Xu23 (6°41'08.65" S, 52°25'55.67" W), c) Xu101
32 1516 (6°52'12.82" S, 52°09'16.12" W), d) Xu52 (6°28'19.32" S, 51°50'08.90" W), e), f), g)
33 1517 Np396 (6°32'41.06" S, 55°23'59.37" W); see Fig. 2 for the outcrops location. For the
34 1518 lithofacies description and more details see the text.
35
36
37
38

39 1520 Figure 4: massive primary volcanoclastic rocks with different proportion of ash, lapilli
40 1521 and blocks. All the deposits are interpreted to be emplaced from pyroclastic density
41 1522 currents except (f) that is interpreted as a basal-breccia of a lava body. a) Xu104
42 1523 (6°52'22.96" S, 52°08'15.91" W), -b) Np183 (7°32'04.13" S, 55°08'50.02" W), c)
43 1524 Np93 (6°44'16.60" S, 55°27'12.96" W), d) Xu29 (6°41'42.51" S, 52°01'23.06" W), e)
44 1525 Xu07 (6°41'56.36" S, 52°08'42.27" W) f) Xu192 (6°31'31.92" S, 53°02'36.60" W);
45 1526 see Fig. 2 for the outcrops location. For the lithofacies description see the text and
46
47
48
49

50 1527 Table 1.
51
52

53 1529 Figure 5: microphotographs of different massive ash and lapilli ignimbrite deposits in
54
55

1
2 1530 thin section: a) broken crystals suggesting the fragmental character of the rock; b)
3 1531 detail of a devitrified juvenile ~~(?)~~ fragment displaying axiolitic fabric; c) banded sub-
4 1532 millimetric to millimetric lithic fragments immersed in a devitrified groundmass.
5
6 1533
7
8 1534 Figure 6: reconstructed schematic stratigraphic column and associated photographs
9
10 1535 representing the evolution of ignimbrite deposits cropping out in the TMP (Np183;
11 1536 7°32'04.13" S, 55°08'50.02" W); note the increase of welding from the base to the top.
12
13 1537
14 1538 Figure 7: schematic stratigraphic column and relative photographs of a >150 m thick
15 1539 felsic banded lava(s) cropping out in SFX (Xu192; 6°31'31.92" S, 53°02'36.60" W)
16 1540 overlying a basal breccia (Lf ~~m~~LB) and an ignimbrite deposit characterized by a low
17 1541 grade of welding (Lf *l-gw*LA).
18
19 1542
20
21 1543 Figure 8: stratified primary volcanoclastic rocks, a) related to sedimentation by highly
22 1544 dilute ash-cloud (Np130; 6°54'16.09" S, 55°10'59.38" W) and, b) ~~-~~attribute to
23 1545 pyroclastic surge-type depositional condition from dilute currents (XU162;
24 1546 6°32'28.39" S, 52°25'26.07" W); see Fig. 2 for the outcrops location. ~~-~~ Relative thin
25 1547 section microphotographs (~~c~~*b*/*d*) showing micrometric shards. For the lithofacies
26 1548 description see the text and Table 1.
27
28 1549
29
30 1550 Figure 9: massive sedimentary rocks. ~~(a)~~ ~~-~~The alternation of lithofacies *csG* and *mS*
31 1551 indicates changes in energy conditions of sedimentation belonging to a subaqueous-
32 1552 subaerial fan-delta interface (Np146; 6°42'58.24" S, 55°28'53.49" W); ~~(b)~~ ~~d~~Detail of
33 1553 centimeters ripples of Lf *mS* (Np89; 6°54'39.36" S, 55°26'12.28 W); ~~(c)~~ ~~-~~Lf *csG* is
34 1554 also associated to Lf *xsSG* (see stratified rocks in section 6.2) (Np27; 8°08'18.43" S,
35 1555 54°54'37.33" W); ~~(d)~~ ~~Np27, ~~e~~/~~f~~~~ ~~(e)~~ Xu209 (6°13'55.26" S, 52°42'29.25" W), ~~(f)~~
36 1556 Np158 (7°03'33.79" S, 55°24'11.84" W); ~~t~~The rounded and clast supported character
37 1557 of these lithofacies is linked with fluvial/alluvial deposition by debris-flow dominated
38 1558 processes; see Fig. 2 for the outcrops location. ~~-~~For a more detailed lithofacies
39 1559 description see the text and Table 1.
40
41 1560
42
43 1561 Figure 10: stratified sedimentary rocks. ~~(a)~~ The quartzitic sandy cross-bedded
44 1562 lithofacies is interpreted as formed in fluvial channel or around margins of immature
45 1563 marine basins (?) (Xu 201; 6°16'12.95" S, 52°52'18.84" W); ~~(b)~~ ~~t~~The cross-stratified

Formatted: Font: Not Italic, No underline

1
2 1564 | water reworked lithofacies is linked with stream-dominated fluvial/alluvial settings
3 1565 | [\(Np82; 8°03'40.79" S, 54°50'43.52" W\);](#) ~~-(c)-~~ ~~t~~The silty sedimentation likely belong to
4 1566 | a lacustrine environment characterized by small turbidities [\(Np158; 7°03'33.79" S,](#)
5 1567 | [55°24'11.84" W\);](#) ~~-(d)-~~ ~~t~~The top of the photographs shows the Lf *bChs* interpreted as
6 1568 | inorganic precipitation of silica (chert) in a closed lake basin; white arrows show
7 1569 | fragments of the chert deposit eroded by low-energy sandy stream flows or local
8 1570 | lacustrine turbidites [\(Np90; 6°49'50.20" S, 55°28'15.47" W\);](#) see Fig. 2 for the
9 1571 | [outcrops location.](#) For a more detailed lithofacies description see the text and Table 1.
10
11
12
13
14
15
16
17 1574 | Figure 11: sketch of a wide (300 x 80 m) outcrop in the TMP [\(Np407; 6°40'35.21" S,](#)
18 1575 | [55°21'14.63" W\).](#) The stratigraphic sequence is tilted showing sub-vertical contacts of
19 1576 | the different deposits. The sequence is interpreted displaying at the base banded (or
20 1577 | rheo-ignimbrite) and massive lava flows passing to fragmental deposits to the top. ~~(a)~~
21 1578 | ignimbrite medium-grade welded; b) the diffuse-stratified lithofacies indicates tractive
22 1579 | processes usually attribute to pyroclastic surge-type depositional condition from dilute
23 1580 | currents; c) sedimentary clast-supported deposit ~~(see descriptions in chapter 4.3);~~ d)
24 1581 | non-welded lapilli to ash ignimbrite; e) banded lava o highly reomorphic ignimbrite
25 1582 | (lava-like). For a more detailed lithofacies description see the text and Table 1.
26
27
28
29
30
31
32
33 1584 | Figure 12: classification diagrams for the Tapajos volcanics (TMP-V) and lava flow
34 1585 | (TMP-LF). TAS diagram with limits of alkaline series from Kuno (1968), dashed line,
35 1586 | and Irvine and Baragar (1971), solid line. AFM diagram with alkaline field from Irvine
36 1587 | and Baragard (1971). SiO₂ vs K₂O classification diagram (Ewart, 1982). Literature
37 1588 | values are from: VR (a) Vila Rozinho and MA (a) Moraes Almeida volcanic sequences
38 1589 | from Lamarão et al. (2002); [SF \(b\) Sobreiro Formation and;](#) SRF (b) Santa Rosa
39 1590 | Formation from Fernandes et al. (2011).
40
41
42
43
44
45
46 1592 | Figure 13: REE and spider-diagrams of volcanics and lava flow rocks from the Tapajos
47 1593 | region (TMP-V and TMP-LF). REE data are normalized to Chondrite I (CI; values
48 1594 | from Ander and Ebihara, 1982) and trace elements are normalized to Mid Ocean Ridge
49 1595 | Basalt (MORB; values from Hoffman, 1988). Literature values are from: VR (a) Vila
50 1596 | Rozinho and MA (a) Moraes Almeida volcanic sequences are average values from
51 1597 | Lamarão et al. (2002); SRF (b) Santa Rosa Formation from Fernandes et al. (2011)

1 1598 divided in -V volcanoclastics and -LF lava flow. Due to the lack of literature data,
2 1599 comparison of VR (a) and MA (a) is reported only for REE diagram.

3 1600

4 1601 Figure 14: tectonic affinity discriminant diagrams for the Tapajos volcanics (TMP-V)
5 1602 and lava flow (TMP-LF). Zr+Nb+Ce+Y (ppm) vs FeO_{tot}/MgO (wt.%) diagram. Yb vs
6 1603 Ta diagram. La/Yb vs Nb/La diagram. Th-Ta-Hf/3 diagram. Literature values are from:
7 1604 VR (a) Vila Rozinho and MA (a) Moraes Almeida volcanic sequences from Lamarão
8 1605 et al. (2002); SF (b) Sobreiro Formation and SRF (b) Santa Rosa Formation from
9 1606 Fernandes et al. (2011).

10 1607

11 1608 Figure 15: geochronological U-Pb data from Tapajos zircons. Average ²⁰⁶Pb/²⁰⁷Pb age
12 1609 (errors are calculated as 2σ) of the three samples. Probability density plot of ²⁰⁶Pb/²⁰⁷Pb
13 1610 ages. Calculated concordia age for sample NP396 (lava flow) and NP183 (ignimbrite).

14 1611

15 1612 Figure 16: geochronological U-Pb data from Xingu zircons. Calculated concordia age
16 1613 for ignimbrite sample XU-08. Probability density plot of ²⁰⁶Pb/²⁰⁷Pb ages.

17 1614

18 1615 Figure 17: pelegographic reconstruction of the fissural and calderic volcanic activity
19 1616 during the Late-Paleoproterozoic in the southern part of the Amazonian craton. In the
20 1617 foreground is shown a section of a caldera and a post-caldera ignimbrite uplift that
21 1618 could facilitate the production of new sediments to be reworked and transported. The
22 1619 rising magma could form sporadic intra-caldera domes and volcanic centers as also
23 1620 shown in the background calderas. Reworked sediments can accumulate into volcano-
24 1621 tectonic depressions, which often collects intra-caldera lakes. In the background a
25 1622 fissure-fed volcanism is the responsible of the emission of lava flows and/or high-
26 1623 grade to rheomorphic ignimbrites. Fluvial deposits that occur throughout all
27 1624 successions represent periods of stream and river reworking. The area in punctuated by
28 1625 little scoria cones and maars that contribute to the amount of the fragmental products
29 1626 well represented in the study regions.

30 1627

31 1628

32 1629

33 1630

34 1631 Tables

1
2
3
4
5
6
7
8
9
10
11
12
13
14
15
16
17
18
19
20
21
22
23
24
25
26
27
28
29
30
31
32
33
34
35
36
37
38
39
40
41
42
43
44
45
46
47
48
49
50
51
52
53
54
55
56
57
58
59
60
61
62
63
64
65

1632
1633 Table 1: Summary of the main characteristics of volcanoclastic lithofacies of the
1634 primary and secondary felsic products analyzed and their interpretation.

1635
1636 Table 2: Major and trace element bulk rock composition of Tapajos samples. Class
1637 identify the lithological features of the rocks: VC: volcanoclastic; I: ignimbrite; R:
1638 rhyolite; Type identify the geochemical affinity according to the granite classification
1639 (Zr+Nb+Ce+Y (ppm) vs FeO_{tot}/MgO (wt.%) diagram, Fig. 14): I is for I-type granites
1640 and A is for A-type granites; b.d.l. is below detection limits; Mg# is calculated as Mg²⁺
1641 /(Fe²⁺_t + Mg²⁺); (*) major elements analyses already published in Roverato et. (2016).
1642 ~~Table 2: Major and trace element bulk rock composition of Tapajos samples. VC:~~
1643 ~~volcanoclastic; I: ignimbrite; R: rhyolite; b.d.l. is below detection limits; Mg# is~~
1644 ~~calculated as Mg²⁺ / (Fe²⁺_t + Mg²⁺); (*) major elements analyses already published in~~
1645 ~~Roverato et. (2016).~~

1 **The 2.0-1.88 Ga Paleoproterozoic evolution of the southern Amazonian Craton**
2 **(Brazil): an interpretation inferred by lithofaciological, geochemical and**
3 **geochronological data.**

4
5
6
7 Roverato*^{1,2} M., Giordano^{3,4} D., Giovanardi⁵ T., Juliani² C., Polo² L.
8
9

- 10
11 1. YachayTech University, School of Geological Sciences and Engineering, Hacienda San José,
12 Urcuquí, Ecuador.
13
14 2. Instituto de Geociências (IGC), Universidade de São Paulo, INCT – Geociam, SP, 05508080,
15 Brazil.
16
17 3. Università degli studi di Torino, Dipartimento di Scienze della Terra, via Valperga Caluso 35,
18 10125, Torino, Italy.
19
20 4. Centro Nazionale delle Ricerche (CNR), Istituto di Geoscienze e Georisorse (IGG), via G.
21 Moruzzi 1, 56124, Pisa, Italy.
22
23 5. Università di Modena e Reggio Emilia, Dipartimento di Scienze Chimiche e Geologiche, 41125,
24 Modena, via Campi 103, Italy.
25
26
27
28

29
30 *Corresponding author: matteoverato1809@gmail.com
31

32
33 **Keywords:** Paleoproterozoic volcanism; Amazonian craton; Fissure eruption; Felsic
34 volcanism; Lithofacies analyses
35

36
37
38
39 **Abstract**
40

41 The study of Paleoproterozoic rocks is crucial for understanding Earth's
42 tectonic evolution during the time when most of the modern crust and ore deposits
43 were formed. The rocks of the Brazilian Amazonian Craton record some of the most-
44 complete and best-preserved Paleoproterozoic magmatic and volcanic episodes on
45 Earth. Following previous investigations, we present new lithofaciological and
46 stratigraphic records of the felsic rocks of the Tapajós Mineral Province (TMP) (~ 2-
47 1.88 Ga) and the São Felix do Xingú region (SFX) (~ 1.88 Ga) which, combined with
48 new petrological and geochronological data, help providing a more complete
49 understanding of the tectonic, magmatic and volcanological evolution of the
50 Amazonian Craton. This magmatism/volcanism is thought to be formed in a late-/post-
51 orogenic to extensional regime confirmed by the new geochemical data presented here.
52
53
54
55
56
57
58
59
60
61

1
2
3
4
5
6
7
8
9
10
11
12
13
14
15
16
17
18
19
20
21
22
23
24
25
26
27
28
29
30
31
32
33
34
35
36 The transition from late-convergent to extensional tectonic setting could register the
37 beginning of the taphrogenesis that marked the Amazonian Craton throughout the
38 Mesoproterozoic. The volcanological approach of this contribution can serve as a
39 strategy for the modelling of the evolution of Precambrian volcano-sedimentary basins
40 around the world. The large amount of rocks analyzed are divided into primary and
41 secondary volcanoclastic products depending on if they resulted from a direct volcanic
42 activity (pyroclastic) or processes that reworked pyroclastic fragments. Furthermore,
43 the deposits are subdivided into massive and stratified, depending on their primary
44 mechanisms of transport and emplacement. By confirming the results from previous
45 studies, our study permits to depict a more precise paleo-environmental picture of the
46 processes that occurred in the Amazonian Craton during the Late-Paleoproterozoic. In
47 particular, the presence of large regional-scale fissural systems and caldera collapses
48 produced large silicic explosive volcanic eruptions, also accompanied by the emission
49 of large volume effusive products. Although studies on the Amazonian Craton are still
50 scarce and controversial, the present study provides new evidence that this volcanism
51 may have formed one of the largest Silicic Large Igneous Provinces (SLIP) on earth.
52 Our data also confirm that at least two major Paleoproterozoic periods of formation of
53 volcanic rocks exist in the Amazonian craton. This point is of great relevance for any
54 future interpretation of the geological evolution of this craton.

55

56 1. Introduction

57 The Proterozoic Eon (2500 – 541 Ma) is the longest and youngest part of the
58 Precambrian Supereon. This Eon represents the time just before the proliferation of
59 oxygen accumulation and complex life on Earth. This period was likely the most
60 tectonically active in Earth's history. In fact, it is also the period during which the
61 largest portion of the modern crust (43%) and mineral ores were produced (Condie,
62 2000). Studies by Condie (2000) and Rino et al. (2004) suggest that crust production
63 took place episodically, forming predominantly granitoidal crust and secondary
64 volcanic and metamorphic rocks, some of which are extraordinarily well preserved.
65 The Amazonian Craton (AC) is one of the largest preserved Precambrian terrains in the
66 world ($4.6 \times 10^6 \text{ km}^2$) (Almeida et al., 1981). It occupies approximately half of the
67 Brazilian territory and it is the location of important mineral resources such as gold,
68 iron, copper, and tin, among others (e.g. Faraco et al., 1997; Bahia and Quadros, 2000;
69 Juliani, 2002; Klein et al., 2002, 2004; Reis et al., 2006; Klien and Carvalho, 2008;

1
2
3
4
5
6
7
8
9
10
11
12
13
14
15
16
17
18
19
20
21
22
23
24
25
26
27
28
29
30
31
32
33
34
35
36
37
38
39
40
41
42
43
44
45
46
47
48
49
50
51
52
53
54
55
56
57
58
59
60
61
62
63
64
65

70 Monteiro et al., 2008; Juliani et al., 2014, Dall’Agnol et al., 2017). Although the
71 geological investigation of the AC has recently seen a renewed interest of the national
72 and international scientific community, mainly because of the massive presence of ore
73 deposits, a general consensus related to the interpretation of its complex
74 Paleoproterozoic evolution is still missing. Ancient volcanic regions represent a
75 challenge for the understanding of emplacement dynamics especially when the
76 stratigraphic relationships are difficult to decipher or blurred by erosion or vegetation
77 cover. The present work constitutes the natural prosecution of previous investigations,
78 carried out by our research group (Juliani et al., 2005, 2010, 2014; Fernandes et al.,
79 2011; da Cruz et al., 2015; Roverato, 2016; Roverato et al., 2016, 2017), which are
80 devoted to characterize the dynamics of emplacement of Precambrian volcanic rocks
81 and their relationships to sedimentary facies. The study area comprises of the Tapajós
82 Mineral Province (TMP) and the São Felix do Xingú (SFX) region, Pará state, northern
83 Brazil. This contribution provides a means to interpret the volcanic processes active in
84 this region during the Precambrian, mainly based on field observation and detailed
85 lithofacies analyses. In addition, new geochemical and geochronological data are
86 provided. Our study demonstrates how powerful is the approach of rock structure and
87 texture characterization to the interpretation of the eruptive processes that governed the
88 emplacement of volcanic and volcanoclastic sequences. The detailed lithofacies
89 characterization and the stratigraphic reconstruction are important in this area and
90 constitute a powerful key-tool to appropriately interpret the evolution of Precambrian
91 volcano-sedimentary basins. Such an approach would turn to be useful when employed
92 to investigate ancient terrains associated both to the ancient Amazonian felsic
93 volcanism and Precambrian terrains in general.

94 95 2. Geological evolution of the southern portion of the Amazonian craton

96 The AC (Almeida et al., 1981) is located in the northern part of South America
97 and is divided into two Precambrian shields, the Central-Brazil (or Guaporé, southern
98 portion) and Guiana Shields (northern portion), which are separated by the
99 Phanerozoic Amazonian Sedimentary Basin (Fig. 1) (Almeida et al., 1981). The entire
100 craton has become tectonically stable before the end of the Precambrian (Dall’Agnol et
101 al., 1994).

102 It has also been considered (Amaral, 1974; Hasui et al., 1993; Costa and Hasui,
103 1997) as a large Archean platform that had been reworked and reactivated during the

104 ca. 2100 Ma Trans-Amazonian event. Alternative proposals based on geochronological
105 and isotopic data (Teixeira et al., 1989; Tassinari and Macambira, 1999; Santos et al.,
106 2000) divided the craton into several, predominantly NW-oriented, geochronological
107 provinces, which have been interpreted as successive continental accretionary events,
108 followed by granitic magmatism and tectonic reworking (Santos, 2003; Vasquez et al.,
109 2008).

110 In a recent review Teixeira et al. (2019) report that the AC is the host of four
111 LIP-scale (or SLIP) magmatic events discriminated by the Orocaima, Uatumã,
112 Avanavero and Rincón del Tigre events. The igneous rocks described in the present
113 manuscript are widely attributed to the Uatumã event (Dall'Agnol et al., 1999;
114 Lamarão et al., 1999). The studied region is located between TMP and SFX, which is
115 considered to be related to a continental arc, with a NE-SW arc migration as suggested
116 by Juliani and Fernandes (2010), Fernandes et al. (2011) and Roverato et al. (2017).
117 According to these authors a migration from the Serra do Cachimbo graben (in TMP
118 where the subduction trench is located) towards the SFX could be explained by a
119 change in the subducting angle of the oceanic plate beneath the continental plate. This
120 is in agreement with the flat-subduction plate settings proposed by previous authors in
121 other parts of the world (Ferrari et al., 2012; Gutscher et al., 2000; Kay et al., 2005;
122 Mori et al., 2007; Manea et al., 2012).

124 2.1. The TMP (Tapajós Mineral Province)

125 The TMP (Fig. 2a) is primarily situated in the Tapajós–Parima
126 geochronological/tectonic province (Santos et al., 2000) with the eastern part
127 belonging to the Amazonia Central geochronological/tectonic province (Fig. 1). Based
128 on Sm–Nd data and U–Pb ages (2100–1870 Ma), Santos et al. (2001, 2004) and
129 Vasquez et al. (2008), identified several different domains for the Tapajós–Parima
130 geochronological province and consider the TMP as a sequence of continental
131 magmatic arcs (Ferreira et al., 2000; Santos et al., 2000, 2004; Vasquez et al., 2000;
132 Klein et al., 2001; Lamarão et al., 1999, 2002). Late Paleoproterozoic volcanism of the
133 Tapajós domain is represented by the Vila Riozinho Formation, formed by ca. 2000–
134 1990 Ma intermediate to acid volcanic rocks (Lamarão et al., 2002), and by the Iriri
135 Group that can be divided into the Bom Jardim (Almeida et al., 2000), Salustiano
136 (1870 ± 0.008 Ma; Juliani et al., 2005) and Aruri (Pessoa et al., 1977) formations.

137 The Bom Jardim Formation (1898 ± 5 Ma, Santos et al., 2001) consists of

138 mafic to intermediate high-K to shoshonitic calc-alkaline rocks while the latter
139 formations are characterized by rhyolites, dacites and their pyroclastic and epiclastic
140 derivatives. Juliani et al. (2005) considered the Bom Jardim volcanism as a preliminary
141 step of the Iriri event representing pre-caldera volcanism followed by the Salustiano
142 and Aruri caldera-related felsic activity. Post-caldera volcanism is characterized by
143 ring-felsic volcanic structures that produced A-type (Vasquez and Dreher, 2011)
144 rhyolitic lavas and volcanoclastic deposits. Lamarão et al. (2002, 2005) described the
145 felsic A-type Moraes Almeida volcanic sequence (1890 ± 6 Ma rhyolite, 1875 ± 4 Ma
146 ignimbrite) represented by lavas and ignimbrites as part of the Iriri Group. Juliani et al.
147 (2014) consider these last A-type rocks as similar in composition and age to the Santa
148 Rosa Formation that crops out in the São Felix do Xingú region (SFX), which is
149 considered to have formed by the same fissural-type volcanism (Juliani and Fernandes,
150 2010; Fernandes et al., 2011; Roverato et al., 2016). Preliminary data indicate that
151 these rocks, for both TMP and SFX, display a very low grade of metamorphism, falling
152 into the prehnite-pumpellyite field (Echeverri-Misas, 2010; Lagler et al., 2011;
153 Fernandes et al., 2011).

154

155 2.2. The SFX (São Felix do Xingú region)

156 According to the work of Santos (2003) and Vasques et al. (2008) the SFX
157 region belongs to the Amazonia Central province (Fig. 1). The study area (Fig. 2b) is
158 located near to São Felix do Xingú city, which corresponds to the southern portion of
159 the Carajás Province. The Paleoproterozoic volcanic sequences in the SFX comprise
160 the basal Sobreiro and upper Santa Rosa formations (Macambira and Vale, 1997;
161 Juliani and Fernandes, 2010), which are crosscut by the Sn-bearing A-type granitoids of
162 the Velho Guilherme Suite (Teixeira et al., 2002). Antonio et al. (2017) published the
163 first U-Pb ages on zircons for the Santa Rosa Formation with 1877.4 ± 4.3 Ma for a
164 rhyolite and 1895 ± 11 Ma for a dike. Recent geochronological data on a felsic
165 porphyritic dike belonging to the Velho Guilherme suite yielded an age of 1857 ± 8.4
166 Ma (Shrimp U/Pb zircon analyses; Roverato, 2016). Other available geochronological
167 data yielded ca. 1880 ± 6 Ma (TIMS Pb–Pb in zircon) for the Sobreiro Formation and
168 ca. 1879 ± 2 Ma (TIMS Pb–Pb in zircon) for the Santa Rosa Formation (Fernandes et
169 al., 2011; Pinho et al., 2006; Teixeira et al., 2002). Despite their similar ages, their
170 geochemical compositions, geological features and eruption styles point to their non-
171 cogeneticity (Fernandes et al., 2011). The Sobreiro Formation (SF) comprises basaltic

172 andesite, andesite and less dacite massive lava flows and volcanoclastic rocks with
173 high-K calc-alkaline signature (Fernandes et al., 2011; Roverato et al., 2017).
174 According to da Cruz et al. (2015) late- to post-magmatic hydrothermal alteration in
175 these rocks is responsible for a secondary paragenesis characterized by epidote,
176 chlorite, carbonate, clinozoisite, sericite, quartz, albite, hematite and pyrite. The Santa
177 Rosa Formation (SRF) is described by Fernandes et al. (2011) as characterized by four
178 lithological facies with A-type signature: (i) rhyolitic lava flow and thick dikes of
179 banded rhyolite and ignimbrite; (ii) highly rheomorphic felsic ignimbrite associated
180 with un-welded ash tuff; (iii) felsic crystal tuff, lapilli-tuff and co-ignimbritic breccias;
181 (iv) granitic porphyry stocks and dikes and subordinate equigranular granitic
182 intrusions.

184 3. Lithofacies analyses

185 Lithofaciological analyses were carried out in the course of this study in order
186 to understand the geodynamic evolution of the study area. Here we report on the
187 lithofacies analysis of rocks recognized during our field campaigns (and after in
188 petrological thin section) at the TMP and SFX provinces. Within the study area (TMP
189 and SFX), massive to banded lava flows and rheomorphic ignimbrites (Fig. 3) as well
190 as felsic volcanoclastic rocks of various origin (Figs. 4-8, 11) are frequently found.
191 Reworked (secondary) volcanoclastic rocks (Fig. 9,10) and sedimentary alluvial/coastal
192 clastic deposits (epiclastic) are also widely distributed in both TMP and SFX areas.
193 Primary volcanoclastic rocks are here defined as those fragmental products formed
194 during a syn-eruptive explosion, which were deposited regardless of whether their
195 transport occurs through air, water, granular debris or a combination of them (McPhie
196 et al., 1993; White and Houghton, 2006, Manville et al., 2009; Roverato et al., 2017).
197 On the other hand, all the units deposited as a consequence of a reworking process of
198 pre-existing volcanic units are defined here as secondary volcanoclastic rocks. We also
199 introduce into this group all those epiclastic products that constitute sediments that had
200 been reworked before, independent of their source and composition. Table 1 shows a
201 description and interpretation of the volcanoclastic lithofacies, both primary and
202 secondary, for the deposits identified in the study areas.

204 4. Lava flows and rheo-ignimbrites

205 As already discussed by Roverato et al. (2016), the absence of unequivocal

1
2
3
4
5
6
7
8
9
10
11
12
13
14
15
16
17
18
19
20
21
22
23
24
25
26
27
28
29
30
31
32
33
34
35
36
37
38
39
40
41
42
43
44
45
46
47
48
49
50
51
52
53
54
55
56
57
58
59
60
61
62
63
64
65

206 vitroclastic textures complicates the distinction between volcanoclastic and layered lava
207 flows in general and, more in particular, for the ancient volcanic rocks investigated
208 here. Lava flows found in the TMP and SFX provinces have both massive and banded
209 structures (Fig. 3) while still maintaining, in some cases, glassy (obsidian) and
210 aphanitic to porphyritic texture. Their composition varies from trachytic to rhyolitic with
211 various content of alkalis (see section 8). The phenocryst assemblage consists mainly
212 of plagioclase, quartz, Fe–Ti oxides and accessory-amount of zircon and apatite.
213 Plagioclase and bipiramidal quartz crystals (Fig. 3a), with a maximum size of 3-4 mm,
214 range from euhedral to anhedral, showing moderate to intense resorption. Plagioclase
215 shows sieve texture indicating non-equilibrium conditions likely determined by
216 magmatic transport. K-feldspar is also present as anhedral crystals in the groundmass
217 often associated with sericite as alteration phase. Samples are generally affected by
218 variable intensity of hydrothermal alteration. Plagioclase phenocrysts, in particular,
219 present diffuse potassic and minor propylitic alterations. Abundant spherulites and
220 lithophysae of variable size, from millimetric to decimetric, were recognized in almost
221 every sample and are thus common in these rocks (Fig. 3b, c). The spherulites
222 (radiating fibers of K-feldspar and cristobalite), ranging from few millimeters to 2 cm,
223 are typically associated with perlitic fractures. Their content can vary from 10 vol% to
224 70% in the investigated rocks. A large amount of the spherulites developed into
225 lithophysae commonly reaching 10-12 cm as a consequence of cooling and degassing
226 processes. In the obsidian-type lavas (Fig. 3c), the groundmass is characterized by a
227 micro-granophiric-like devitrification texture characterized by crystallization of
228 amorphous quartz and alkali feldspar, a process that occurred after the emplacement of
229 lava bodies. Several rocks show textures that are not easy to be associated to either
230 lava flows or flows of fragmented material which underwent rheomorphism (Fig. 3d-
231 g). Both banded lavas and rheo-ignimbrites display folds (Fig. 3d-g, see also Fig. 11e)
232 and sub-parallel bands on mm- to dm-scale, planar to wavy (Fig. 3e, see also Fig. 6 and
233 7) (parataxitic fabric), that deform and flattened around lithic fragments and crystals
234 which alignment suggests the flow direction. In thin sections, the bands are
235 characterized by extremely flattened vitroclastic textures with the former glass
236 completely replaced by a mixture of quartz and feldspar (Roverato et al., 2016).

238 5. Primary volcanoclastic rocks

239 We consider primary volcanoclastic rocks those dense, scoriaceous and

240 pumiceous products of fragmental character emplaced by explosive processes. With
241 pyroclastic we refer to fragmental material generated by any kind of explosive volcanic
242 activity and transported as ash-fall and pyroclastic density currents (Manville et al.,
243 2009), which deposition occurs by suspension settling, from traction, by en masse
244 freezing, or any combination of these (White and Houghton, 2006). Depending on the
245 mechanism of transport and the eruptive style these clastic rocks were distinguished
246 into two different categories, i.e. massive and stratified; and they can vary from well
247 sorted, poorly sorted or unsorted. The rocks are predominantly rhyolitic in composition
248 (Fernandes et al., 2011, Roverato et al., 2016) and there is no significant geochemical
249 difference from the lava flows. Nine main lithofacies (Lf) have been recognized for the
250 volcanoclastic rocks: six of them are massive and three are stratified.

251

252 5.1. Massive

253 Six massive lithofacies (mAL, mLA, mLb, *l-gwLA*, *m-gwLA* and *h-gwLA*)
254 were recognized during our field campaign, three of them belong to the welded
255 ignimbrites sub-group (Table 1). By using the granulometric classification proposed by
256 Fisher (1961), ash is defined as any fragment with size <2 mm, lapilli are fragments
257 with size between 2 to 64 mm and blocks (or bombs) have sizes > 64 mm. Massive
258 lithofacies includes all those deposits that display a massive coherent structure.
259 Outcrops of such kind of lithofacies are constituted by a high percentage of ash up to
260 block-rich textures. Most of the observed samples appear to have been affected by
261 devitrification processes of the juvenile pyroclastic fragments and matrix. The presence
262 of juvenile material linked with other observed textures such as broken crystals (Best
263 and Christiansen, 1997) and eutaxitic fabric allows us to confirm that the rocks
264 belonging to lithofacies mAL, mLA, *l-gwLA*, *m-gwLA* and *h-gwLA* are fragmental
265 and pyroclastic in origin. We discuss the meaning of Lf mLb below in section 5.1.2.

266

267 5.1.1. Lf mAL; mLA (massive Ash to Lapilli; massive Lapilli *and* Ash)

268 Description: the ash to lapilli (mAL) and lapilli *and* ash (mLA) deposits (Fig.
269 4a-e, Fig.6) are heterolithologic, matrix supported, containing angular to sub-rounded
270 medium to coarse devitrified lapilli (displaying axiolitic fabric), banded fragments,
271 occasional (or absent) lithics and angular-shaped broken crystals of plagioclase,
272 bipiramidal quartz and rare oxides (Fig. 5). In mLA, clasts < 25 cm in size are
273 randomly immersed in the groundmass (Fig 4d and 4e, 11d). Some of them are altered

274 by carbonate minerals. Groundmass of mAL and mLA is formed by K-feldspar and
275 quartz crystals, devitrified ash fragments and sericite crystals as phase of alteration
276 (Fig. 5).

277 Interpretation: the general massive aspect and the poor sorting of mAL and
278 mLA point to a laminar granular flow transport regime and the fine content suggests
279 the deposition from a dilute fluid escape-dominated flow-boundary zone in which
280 turbulent shear-induced tractional segregation is suppressed (Branney and Kokelaar,
281 2002; Sulpizio et al., 2007, Roverato et al., 2017). These lithofacies are interpreted as
282 ash flow deposits suggesting the deposition from a pyroclastic density current (PDC)
283 (Lenhardt et al., 2011; Sulpizio et al., 2014; Roverato et al., 2017). The coarser
284 lithofacies mLA (fig. 4e) could be related to proximal co-ignimbritic breccias as result
285 of deposition by denser pyroclastic granular flows (Branney and Kokelaar, 2002). The
286 angular aspect of the clasts indicates short-period transport.

287

288 5.1.2. Lf mLB (massive Lapilli and Block)

289 Description: this lithofacies (fig. 4f, fig.7) represents monolithologic coarse-
290 grained rocks having high-clast content (clast:matrix ratios up to 3:1). Angular/sub-
291 angular coarse lapilli and blocks up to 50-60 cm of devitrified banded or massive lava
292 fragments are immersed in a devitrified fine lapilli and coarse ash matrix.

293 Interpretation: the blocky and monolithologic coarse-grained aspect of the
294 lithofacies mLB and its position underneath thick flow-deposits is attributed to the
295 basal auto-brecciation of lava flows and/or rheo-ignimbrite flows. Despite the
296 lithofacies is likely a consequence of an effusive volcanic activity (in the lava-flow
297 case) it is considered anyway as part of the volcanoclastic group due to its fragmental
298 character.

299

300 5.1.3. Lf *l-gwLA*; *m-gwLA*; *h-gwLA* (welded Ignimbrites)

301 Description: all massive deposits displaying welding characteristics have been
302 grouped in the “welded ignimbrites” group (Table 1), following the idea of “grade of
303 welding” (Walker, 1983) (i.e. the amount of welding and compaction exhibited by
304 deposits). The rocks are matrix-supported with sub-rounded to angular lapilli and ash
305 lithic clasts, euhedral, subhedral and broken crystals (plagioclase and less quartz) and
306 deformed devitrified juvenile fragments (*fiamme*). Slightly- (low-grade, *l-gwLA*),
307 medium- (medium-grade, *m-gwLA*), well-stretched (high-grade, *h-gwLA*) *fiamme*

308 (Fig. 6), as well as, devitrified shards define the eutaxitic fabric (Roverato et al., 2016).
309 These fragments varying from millimetric to 3–4 cm in size are immersed in a
310 homogeneous micro-granophiric-like devitrified groundmass (see Roverato et al., 2016
311 for details). Figure 6 shows a stratigraphic column representing a 35 m thick sequence
312 of ignimbrite deposits found in the TMP, displaying very low-grade to high-grade
313 welded fabric where the grade of welding increases toward the top of the succession.
314 The very top of the sequence is characterized by columnar jointing.

315 Interpretation: the massive aspect and the poor sorting of the lithofacies *l*-
316 *gw*LA, *m-gw*LA and *h-gw*LA point to a laminar granular flow transport regime,
317 interpreted to be deposited from a pyroclastic density current (PDC). The welded
318 character of these lithofacies is indicative of hot PDC emplacement and compaction
319 that result into the low- up to high-grade eutaxitic fabric. This process is favored by
320 loading-compaction, low-viscosity fragments, high temperature (i.e. > 900°C), cooling
321 of gas-permeable fragments (pumices) and dissolved water (Branney and Kokelaar,
322 2002; Roverato et al., 2016 and references therein).

323

324 5.2. Stratified

325 These lithofacies, although commonly associated with ignimbrites, are not very
326 spread in the studied areas. We also didn't find any alternation between massive and
327 stratified deposits even if this association is a common occurrence in PDC deposits
328 (Sulpizio et al., 2014; Roverato et al., 2017), alternating dilute (stratified deposits
329 resulting) and concentrated (massive deposits resulting) regimes during transport
330 (Sulpizio et al., 2014). Just one example has been found in TMP and is reported in the
331 stratigraphic reconstruction of fig.11.

332

333 5.2.1 Lf sA; xsA; dsAL (stratified Ash; cross-stratified Ash; diffusely stratified Ash to 334 lapilli)

335 Description: the stratified samples and outcrops analyzed comprise well sorted
336 very fine to fine ash organized in millimetric to sub-millimetric parallel (sA) or cross-
337 stratified (xsA) layers, with sharp or gradational changes in grain size (Fig. 8). The
338 fragments are represented by devitrified shards, crystals (plagioclase), and rare (or
339 absent) lithics (fig. 8d) immersed in a devitrified groundmass. Diffuse-stratified
340 lithofacies dsAL display a coarser character with coarse lithic and devitrified ash and
341 lapilli fragments forming well developed parallel continuous meter-long stratification

342 (or very-low angle cross-stratification) at centimeter scale (fig. 11b), with gradational
343 changes in grain-size. The sorting varies from well to moderate.

344 Interpretation: the fine parallel layering of shards material displayed by
345 lithofacies sA is interpreted here as being deposited under the product of sedimentation
346 by the upper and highly dilute ash-cloud that accompany a pyroclastic-density current.
347 We don't exclude the direct sedimentation from tephra fall-out activity. Cross-stratified
348 (Lf xsA) and diffuse-stratified (Lf dsAL) deposits indicate tractive processes usually
349 attribute to pyroclastic surge-type depositional condition from dilute currents (Cas and
350 Wright 1987; Lenhardt et al., 2011; Roverato et al., 2017). We interpreted these as
351 pyroclastic surge deposits although Lf dsAL could also be the product of coarse ash
352 fall-out processes. Pyroclastic surge deposits usually display small volume and rarely
353 reach more than 10 km from their source (Lenhardt et al., 2011). Conversely, fall-out
354 deposits could emplace tens of kilometers from their source.

355

356 6. Secondary volcanoclastic/epiclastic rocks

357 The nomenclature of Fisher et al. (1961) is applied also for the secondary
358 volcanoclastic rocks as follow: silt ($2 <> 64\mu\text{m}$), sand ($64\mu\text{m} <> 2\text{ mm}$), gravel ($2 <> 64$
359 mm), cobble ($64 <> 256\text{mm}$). These rocks are considered as the product of reworking
360 and erosive processes. The clasts belonging to this group show a wide range of
361 composition, size and shape variations. Based on their component, texture and fabric,
362 we recognized five massive, both matrix- and clast-supported, and four stratified
363 lithofacies (fig. 9).

364

365 6.1. Massive

366 6.1.1. Lf mS (massive Sand)

367 Description: this lithofacies consists of reddish moderately to well-sorted,
368 massive, fine- to medium grained sand forming parallel strata intercalated to clast-
369 supported conglomerate deposits (Lf csG) (fig. 9a). The sandstone strata extend tens of
370 meters and present thinness between 0.4-0.8 m. Lf mS is predominantly composed of
371 quartz, feldspar and minor rock fragments. Contacts between mS and csG are sharp
372 with rare slightly erosional surfaces. The tops of the sandstone are characterized by the
373 presence of centimeters ripples (fig. 9b).

374 Interpretation: the massive sand (mS) and the small ripples found at the top of
375 the strata indicate low energy under tractional currents in shallow water conditions

376 (Collison and Thompson, 1982; Lenhardt et al., 2011). The alternation of Lf csG and
377 mS indicates changes in energy conditions of sedimentation. We interpret these
378 oscillations as belonging to a subaqueous-subaerial fan-delta interface setting where
379 continental supply of material alternates to under-water sand accumulation (Lf mS).

380

381 6.1.2. Lf csG (clast supported Gravel)

382 Description: this lithofacies (Fig. 9a, c, d) is massive, clast to matrix supported,
383 with heterolithologic felsic rounded high-spherical coarse gravel with a sandy inter-
384 clast matrix. Clasts are mainly characterized by massive and banded medium- to
385 coarse-size felsic lava fragments (and rare quartz; size does not exceed 5 cm) and
386 present rounded with low- to high-sphericity. We found lithofacies csG also associated
387 to xsSG (see below section 6.2.2.) (Fig. 9c, 10b).

388 Interpretation: lithofacies csG is dominated by water flow processes where
389 matrix plays a secondary role. The clast-supported character and less matrix content
390 indicates that water removed the finer particles during transport and deposition. Lf csG
391 display rounded clasts and well-sorting indicative of good selection during transport
392 and emplacement. The rounded character of csG and the presence of matrix in the
393 deposits suggest a laminar debris-flow regime in medial reaches of stream-dominated
394 fluvial/alluvial fans (Mueller and Corcoran, 1998).

395

396 6.1.3. Lf csGS (clast supported Gravel to Sand)

397 Description: Lf csGS (Fig. 9e, 11c) is massive, moderately well-sorted and
398 clast-supported. Clasts (gravel to sand) present sub-rounded to sub-angular with
399 low/medium sphericity with maximum size of 2-3 cm. The rocks belonging to this
400 lithofacies are mainly formed by massive felsic lava fragments with different color and
401 crystallinity.

402 Interpretation: Lf csGS is dominated by water flow processes where matrix
403 plays a secondary role. The clast-supported character and less matrix content indicates
404 that water removed the finer particles during transport and deposition. This lithofacies
405 represents deposition within a debris-flow dominated fluvial/alluvial environment.
406 Poor sorting, clast-supported and sub-angular clasts point to deposition by localized
407 laminar hyperconcentrated-flows in volcanic fans fringing flanks of volcanic edifices.
408 Single cross-beds are usually ca. 1 cm thick

409

410 6.1.4. Lf csGC (clast supported Gravel and Cobble)

411 Description: Lithofacies csGC (Fig. 9f) is massive, low-sorted and clast-
412 supported. The clast population is characterized by sub-rounded, low/medium
413 sphericity, massive felsic porphyritic fragments with maximum size up to 20 cm. This
414 lithofacies has an interstitial matrix characterized by medium to coarse sand.

415 Interpretation: Lf csGC is dominated by water flow processes where matrix
416 plays a secondary role. The clast-supported character and less matrix content indicates
417 that water removed the finer particles during transport and deposition. This lithofacies
418 represents deposition within a debris-flow dominated alluvial environment. Poor
419 sorting, clast-supported and sub-angular clasts likely points to deposition by localized
420 non-cohesive debris-flows.

421

422 6.2. Stratified

423 6.2.1 Lf xsS (cross-stratified Sand)

424 Description: lithofacies cross-stratified Sand (Fig. 10a) consist of white to
425 brownish low-angle cross-stratified coarse quartzitic sandstone. The sandstones are
426 characterized by lobe to sheet-shaped bodies. Major bedsets are recognized ranging in
427 thickness from 0.5 to 1.5 m, composed of fine-grained sandstone dominated by
428 medium-angle cross strata (18-20°). Single cross-beds are usually 0.7-1cm thick. The
429 outcrops displaying this lithofacies extend tens of meters with sharp upper and lower
430 contact.

431 Interpretation: the cross-stratification of xsS is interpreted as formed in fluvial
432 channels attesting the deposition from crested dune bed-forms that formed under
433 condition of lower flow regime (Collinson, 1996; Miall, 1996; Capuzzo and Wetzel,
434 2004; Went, 2016). The deposition of medium-angle cross-bedding within large-scale
435 examples of beds indicates that these larger beds are likely a product of bar migration.
436 The beds are interpreted as channel-fill deposits (Lenhardt et al., 2017) related to a
437 fluvial environment likely associated to meandering or braided rivers. Shoreline
438 deposition developed around margins of immature marine basins is also considered.

439

440 6.2.2. Lf xsSG (cross-stratified Sand and Gravel)

441 Description: Lf xsSG (Fig. 10b) is characterized by crystal-lithic fine to coarse
442 sand and fine gravel (max 5-6 mm in size) organized in cross-bedded stratification.
443 Clasts display medium roundness and sphericity and are mostly composed by felsic

1
2
3
4
5
6
7
8
9
10
11
12
13
14
15
16
17
18
19
20
21
22
23
24
25
26
27
28
29
30
31
32
33
34
35
36
37
38
39
40
41
42
43
44 fragments. Stratification is defined by alternating of well to poorly sorted, fine to
445 coarse millimeters-thick strata. The finer black layers are formed by sub-millimetric
446 hematite sand.

447 Interpretation: Lf xsSG correspond to cross-stratified water reworked deposits.
448 The cross-stratified thicker fine gravelly strata, alternated with sandy layers laterally
449 discontinuous, were interpreted as different pulses as the result of rapid deposition
450 from hyperconcentrated flows (Zanchetta et al., 2004) in a stream-dominated
451 fluvial/alluvial setting. Alternation with csG (Fig. 9c) represents difference of energy
452 condition.

453 454 6.2.3. Lf dsSt (diffusely layered Silt)

455 Description: this lithofacies consists of parallel, lenticular, truncated, and
456 locally low-angle cross-stratified multicolor millimetric well-sorted fine- to very fine-
457 grained sand and silt strata (Fig. 10c). Within the sandy bedset, a thinning- and fining-
458 upward trend may be distinguished. Small and straight groove marks have been
459 detected and reduced tiny slump folding is also presence in some parts.

460 Interpretation: lithofacies dsSt displays diffuse fine stratification with tiny
461 ripples, suggesting transport and sedimentation in shallow water. The thin sheet-shaped
462 is interpreted as flood sediments (Lenhardt et al., 2011). These deposits are interpreted
463 to have been formed in low energy lacustrine environment or ponds (Collinson, 1996;
464 Roverato et al., 2017) characterized by small turbidities successions affected by
465 scouring and tiny deformations (slumps) of the sediments.

466 467 6.2.4. Lf bChS (bedded Chert and Sand)

468 Description: the bedded chert lithofacies (with sand) (bChS) (Fig. 10d) crops
469 out in both regions and it is characterized by outcrops that can be traced on strike for
470 hundreds of meters. The facies consist of thin laminated pinkish chert (layers < 1mm in
471 thickness) with darker laminae intercalated, formed predominantly by hematite
472 (Lenhardt et al., 2017). The layers are composed by microcrystalline quartz. In some
473 portions, these lithofacies are associated with fine to medium sand composed mainly
474 by quartz and less volcanic fragments.

475 Interpretation: this lithofacies is interpreted as inorganic precipitation of silica
476 in a closed lake basin mainly due to its association with volcanic rocks and fine
477 sandstone (Blatt et al., 1980; Eriksson et al., 1994). The picture in figure 10d shows

1
2
3
4
5
6
7
8
9
10
11
12
13
14
15
16
17
18
19
20
21
22
23
24
25
26
27
28
29
30
31
32
33
34
35
36
37
38
39
40
41
42
43
44
45
46
47
48
49
50
51
52
53
54
55
56
57
58
59
60
61
62
63
64
65

478 elongated ripped-up millimetric fragments of chert immersed in the sandstone eroded
479 by low-energy stream flow or local lacustrine turbidites. As suggests by Lenhardt et al.
480 (2017) the chert may have formed during repeated pulses of hydrothermal fluids that
481 circulated into the lake water during hiatuses in the volcanism (Van Kranendonk,
482 2006).

483 484 7. Analytical methods for geochemistry and geochronology

485 A total of 19 new samples (9 volcanoclastics and 10 lava flows) from the
486 Tapajós region (associated with the data published in Roverato et al., 2016; Table 2)
487 were analysed for bulk rock major and trace elements. Major element bulk rock
488 analyses were performed by X-ray fluorescence, using a wavelength dispersive Philips
489 PW 2400 spectrometry, using fused glass disks according to procedures described by
490 Mori et al. (1999). Accuracy was greater than 2%. Trace element analyses in selected
491 samples were performed by Inductively Coupled Plasma-Mass Spectrometry (ICP-MS)
492 using the procedure described by Navarro et al. (2008). Accuracy, determined with
493 respect to the reference standards BHVO-2 and BR, was 0.5–2%.

494 Zircon grains were examined with a FEI-QUANTA 250 scanning electron
495 microscope equipped with secondary-electron and cathodoluminescence (CL) detectors
496 at the Instituto de Geociências - Centro de Pesquisas Geocronológicas - Universidade
497 de São Paulo (IGc-CPGeo-USP); the most common conditions used in CL analysis
498 were 60 μ A of emission current, 15.0 kV of accelerating voltage, 7 μ m of beam
499 diameter, 200 μ s of acquisition time, and a resolution of 2048x1887 pixels and 345 dpi.
500 Selected samples were analyzed for U-Pb isotopes using a SHRIMP-IIe also at IGc-
501 CPGeo-USP, following the analytical procedures of Williams (1998) as reported by
502 Giovanardi et al. (2015). Correction for common Pb is based on the measured ^{204}Pb ,
503 and the typical error for the $^{206}\text{Pb}/^{238}\text{U}$ ratio is less than 2%; U abundance and U-Pb
504 ratios were calibrated against the TEMORA-II standard. The dataset consists of 56 new
505 U-Pb SHRIMP-II analyses and is reported in Table 3. Thirty-five analyses were
506 performed on zircon grains from the Tapajós region as follow: 11 analyses on sample
507 NP380-C, 11 analyses on sample NP183 and 13 analyses on sample NP396-B. Eleven
508 analyses were performed on zircon grains from Xingú sample XU08. For all samples,
509 $^{207}\text{Pb}/^{235}\text{U}$ and $^{206}\text{Pb}/^{238}\text{U}$ concordia ages (with 95% of confidence level and 2σ error)
510 are calculated using Isoplot 4.1 software (Ludwig, 2009).

511

512

513 8. Geochemistry of the TMP samples

514 Independently of their nature (lavas or volcanoclastic), the rocks of the TMP
515 follow a typical calc-alkaline trend (Fig. 12). They are mostly rhyolitic in composition
516 (Table 2), with four exceptions which fall in the trachytic field. In addition, their low
517 LOI values (0.32-3.51%) and the low FeO content (0.78 – 3.26%) together with the
518 negative correlation FeO vs SiO₂ appears to indicate that the investigated volcanic
519 rocks neither underwent significant alteration processes nor they belong to sedimentary
520 suites which commonly contain water rich clay minerals. TMP volcanoclastic and lava
521 flows show similar negative correlation between TiO₂, Al₂O₃, MgO, FeO, CaO, Na₂O
522 and P₂O₅ with SiO₂. A negative correlation between K₂O and SiO₂ also exists for the
523 volcanoclastic, but not for the lava flows. The similar trends observed suggest that both
524 these kind of rocks are originated by similar magmatic sources. Such a conclusion is
525 supported by similar variation paths, although with different values, of minor and trace
526 elements (Fig. 13). In particular, TMP lava flows show LREE enrichment
527 ((La/Yb)_N=10.68-21.45; normalization to Chondrite I from Anders & Ebihara, 1982)
528 and a negative Eu anomaly which increases from trachytes ((Eu/Eu*)_N=0.89-0.78) to
529 rhyolites ((Eu/Eu*)_N=0.69-0.31) (Fig. 13). The Eu negative anomaly, shown from all
530 the samples, is expression of feldspar fractionation. On the other hand, volcanoclastics
531 rocks show similar LREE enrichment ((La/Yb)_N=11.12-28.10) and negative Eu
532 anomaly ((Eu/Eu*)_N=0.97-0.37) (Fig. 13). In addition, volcanoclastics have higher
533 LREE abundances with respect to lavas (La between 35.5-91.3 ppm and between 40.5-
534 71.9 ppm, respectively) while they have similar MREE and HREE contents (Yb
535 between 1.56-3.43 ppm and between 1.83-4.11 ppm, respectively). Volcanoclastics
536 commonly show higher Rb (121-272.9 ppm) and Pb (4.5-137.1 ppm) with respect to
537 lavas (Rb=96.1-232 ppm and Pb=2.7-45.8 ppm). Volcanoclastics are enriched in LILE,
538 Th and U with respect to MORB (Fig. 13; normalization to MORB from Hoffman,
539 1988), with the exception of Sr, which commonly show a pronounced negative
540 anomaly ((Sr/Sr*)_N=0.55-0.05). The Sr negative anomaly is consistent with feldspar
541 fractionation. Negative anomalies are also present for Nb and Ta, while Ba and Pb are
542 commonly enriched (Fig. 13). Lavas show a similar trace pattern, but higher values
543 dispersion (Fig. 13). The Ba enrichment is less pronounced with respect to
544 volcanoclastics (Ba between 75-1965 ppm and 310-2245 ppm, respectively) and the
545 Nb/Ta ratio show higher dispersion (3.29-14.63 and 6.73-13.9, respectively), indicating

1
2
3
4
5
6
7
8
9
10
11
12
13
14
15
16
17
18
19
20
21
22
23
24
25
26
27
28
29
30
31
32
33
34
35
36
37
38
39
40
41
42
43
44
45
46
47
48
49
50
51
52
53
54
55
56
57
58
59
60
61
62
63
64
65

546 more limited fractionation of feldspar. Geochemical affinity of Tapajós volcanics
547 and lava flows suggests that the magmatism occurred in active continental setting (Fig.
548 14). Using the tectonic discriminant diagrams of $Zr+Nb+Ce+Y$ (ppm) vs FeO_{tot}/MgO
549 (wt.%), Yb vs Ta and $Th-Ta-Hf/3$ (Wahlen et al., 1987; Pearce et al., 1984; Wood,
550 1980), the magmatism in the Tapajós region appears related to a syn- to post-
551 collisional setting with few samples falling into the intraplate field (Fig. 14).
552 According to the refined diagram $Nb+Y$ vs Rb of Pearce (1996), all the Tapajós
553 volcanics, together with the majority of volcanic rocks from the Sobreiro formation
554 (Fernandes et al., 2011) are consistent with a late- to post-collisional setting (Fig. 14).

555 556 9. U-Pb zircon Geochronology

557 Zircons from Tapajós samples are colorless, sometimes fractured and euhedral
558 to sub-euhedral. They can contain inclusions of apatite or spinel and display commonly
559 low emission in Cathodoluminescence (CL). All crystals show magmatic oscillatory
560 zoning and commonly a dark core which, in most cases, appears to be homogenous.
561 Nonetheless, in few cases an inner core with discordant and partially reabsorbed
562 domains is recognized. Some of the zircons also show a bright CL rim with
563 transgressive or sub-concordant contacts with the inner oscillatory zoning. Zircons
564 from sample XU08 from the Xingu region are colourless, rarely fractured and sub-
565 euhedral. Inclusions of apatite or spinel are also observed sometimes. Crystals are
566 medium in CL emissions and commonly show a homogeneous core and a concordant
567 magmatic oscillatory zoning. Few zircons show a core with discordant zoning. No
568 transgressive bright CL rims were recognized. Analyses were carried out on zircons
569 that do not show transgressive or resorption features and discordant inner cores.
570 Zircons from sample NP183 (Ignimbrite) provide 4 discordant and 7 concordant
571 analyses that provide an upper intercept at 1984 ± 8.5 Ma (95% confident decay-const.
572 errs included, MSWD 1.09) and a concordia age at 1986 ± 8.2 Ma (2σ , decay-const.
573 errs included, MSWD 1.08, Probability of concordance = 0.30; Fig. 15). Single spot
574 $^{206}Pb/^{207}Pb$ ages range between 2010 ± 17 Ma and 1909 ± 53 Ma with an average age of
575 1985 ± 11 Ma (95% confident decay-const. errs included, MSWD 1.6, Probability of
576 concordance = 0.15; Fig. 15). Zircons from sample NP380 (Ignimbrite) show slightly
577 older single spot $^{206}Pb/^{207}Pb$ ages between 2023 ± 31 Ma and 1981 ± 24 Ma with an
578 average age of 1998 ± 5.9 Ma (95% confident decay-const. errs included, MSWD 0.74,

1
2
3
4
5
6
7
8
9
10
11
12
13
14
15
16
17
18
19
20
21
22
23
24
25
26
27
28
29
30
31
32
33
34
35
36
37
38
39
40
41
42
43
44
45
46
47
48
49
50
51
52
53
54
55
56
57
58
59
60
61
62
63
64
65

579 Probability of concordance = 0.68; Fig. 15). Analyses are slightly discordant (up to
580 4%) providing an upper intercept at 1998 ± 7.7 Ma (95% confident decay-const. errs
581 included, MSWD 0.74). Zircons from sample NP396 (Banded lava) provide 5
582 discordant ages and 8 concordant analyses, which provide an upper intercept at 1994
583 ± 8.2 Ma (95% confident decay-const. errs included, MSWD 1.40) and a concordia age
584 at 1997 ± 7.0 Ma (2σ , decay-const. errs included, MSWD 5.70, Probability of
585 concordance = 0.02; Fig. 15). Single spot $^{206}\text{Pb}/^{207}\text{Pb}$ ages range between 2014 ± 14 Ma
586 and 1973 ± 8 Ma with an average age of 1994 ± 8.7 Ma (95% confident decay-const.
587 errs included, MSWD 1.6, Probability of concordance = 0.12; Fig. 15). Pooling
588 together the analyses of the Tapajós samples provides an average age of 1991 ± 12 Ma
589 (2σ , MSWD 1.50, Probability of concordance = 0.06). Zircons from sample XU08
590 (Lava flow) provide a concordia age at 1882 ± 6.4 Ma (2σ , decay-const. errs included,
591 MSWD 2.70, Probability of concordance = 0.10; Fig. 16). Single spot $^{206}\text{Pb}/^{207}\text{Pb}$ ages
592 range between 1899 ± 10 Ma and 1875 ± 13 Ma, with an average at 1884 ± 5.2 Ma (95%
593 confident decay-const. errs included, MSWD 0.60, Probability of concordance = 0.82).

594

595 10. Discussion

596 10.1. Subduction-related to extensional setting

597 The geochemistry of the TMP samples presented in this work display a high-K
598 calc-alkaline signature (Fig. 12); they mainly fall into the A-type intra-plate granite
599 field and tectonic discriminant diagrams suggest a late- to post-collisional setting for
600 the TMP volcanism (Fig. 14). This interpretation is also supported by enrichment in
601 LILE, Th, U and LREE of our samples, which suggest a strong crustal component in
602 the parent melt consistent with a subduction/post orogenic geodynamic setting (Figs.
603 12, 13, 14), and the high HSFE which shifted the TMP volcanics composition in the A-
604 type granites showing however FeO/MgO which are low and comparable with I- and
605 S-types granites (Fig. 14). Similar features are reported in previous works (Lamarão et
606 al., 1999; Lamarão et al., 2002) for volcanics in the Tapajós region, which are grouped
607 into the Vila Riozinho (VR) and Maraes Aldeida (MA) formations, respectively. The
608 VR rocks are intermediate to felsic in composition (Lamarão et al., 2002) with a calc-
609 alkaline signature, while the rhyolites and ignimbrites of MA are slightly enriched in
610 silica compared to the rhyolites of VR and are geochemically similar to evolved A-type
611 granites (Lamarão et al., 2002). Our results show similarities with these data,

1
2
3
4
5
6
7
8
9
10
11
12
13
14
15
16
17
18
19
20
21
22
23
24
25
26
27
28
29
30
31
32
33
34
35
36
37
38
39
40
41
42
43
44
45
46
47
48
49
50
51
52
53
54
55
612 suggesting that our specimens could be part of the VR and/or MA formations. The
613 identification of two volcanic series has important implications for the understanding
614 of the magmatic evolution of the Amazonian craton in late Paleoproterozoic. A model
615 for the evolution of the TMP involves a first stage of subduction-related magmatism
616 followed by an intracontinental magmatism related to a distensional event (Lamarão et
617 al., 2002). Geochronological analyses by Lamarão et al. (2002) yielded ages of ca. 2
618 Ga for the VR and ca. 1.88-1.87 Ga for the MA volcanisms. The three new U-Pb
619 geochronological analyses reported in this study yielded ages of ca. 2000 Ma (fig. 15)
620 are concordant with the ages presented by Lamarão et al. (2002) for the VR
621 magmatism, thus suggesting that the TMP rocks could be part of the VR volcanic
622 sequence. However, TMP rocks are geochemically more evolved with respect to VR in
623 terms of SiO₂ (63.8-76.6 wt.% and 54.4-71.8 wt.%, respectively), K₂O (2.3-7.1 wt.%
624 and 2.1-5.8 wt.%, respectively) and REE abundances and are more similar to MA
625 rocks (Figs. 11, 12 and 13). In particular, REE patterns of the TMP samples are
626 comparable with the rocks of the MA formation (Fig. 12) while they are more enriched
627 in REE with respect to VR rocks. Conversely, TMP rocks are enriched in Ba (Fig. 12),
628 while MA are depleted, and have compositions for Rb/Zr ratio and Nb, considered as a
629 proxy for arc maturity (Brown et al., 1984), similar to VR and different from MA
630 (Rb/Zr between 0.3-1.1 in TMP, 0.2-0.7 in VR and 0.2-1.7 in MA; Lamarão et al.,
631 2002). Thus, according to geochronological and petrological data, we proposed that the
632 TMP rocks in this study must be ascribed to the VR formation. Geochemical
633 differences in our rocks and VR volcanics could be explained by a more evolved
634 character of the TMP rocks. The evidences of plagioclase fractionation from the parent
635 melts of the TMP (negative Eu and Sr anomalies, Fig. 12) and their absence in less
636 evolved VR rocks reinforce this interpretation, and suggest fractional crystallization as
637 the prominent process controlling the VR magmatism evolution. However, we want to
638 point out that due to the large area covered by the presented investigation (Fig. 2),
639 together with the VR area, the geochemical variations between our rocks (TMP) and
640 VR could be the result of local/regional heterogeneities in the magmatism. This
641 hypothesis is supported by the intermediate characteristics of the TMP samples with
642 respect to the VR and MA volcanoclastic material (Figs 11, 12 and 13).

643 Recently, new authors (Juliani et al., 2014) suggest the geochemical and
644 geochronological signature of the MA formation could be correlated to the felsic Santa
645 Rosa formation (SRF) cropping out in the SFX region. Our new U-Pb geochronological

1
2
3
4
5
6
7
8
9
10
11
12
13
14
15
16
17
18
19
20
21
22
23
24
25
26
27
28
29
30
31
32
33
34
35
36
37
38
39
40
41
42
43
44
45
46
47
48
49
50
51
52
53
54
55
56
57
58
59
60
61
62
63
64
65

646 analyses on one rock sample from the SRF yielded an average age of 1884 ± 5.2 Ma
647 (Fig. 16) that is consistent with previous Pb-Pb ages on other locations. Juliani and
648 Fernandes (2010) published two Pb-Pb ages on zircons of 1879 ± 2 Ma and 1884 ± 1.7
649 for a rhyolite and an ash tuff, respectively. Recently Antonio et al. (2017) publishes the
650 first U-Pb ages on zircons for the Santa Rosa Formation with 1877.4 ± 4.3 Ma for a
651 rhyolite and 1895 ± 11 Ma for a dike. All geochronological results support a ca. 1880
652 Ma age for the emplacement of these rocks.

653 The southern Amazonian craton, as well as other Precambrian terrains
654 worldwide (Condie, 2002; Hoffman, 1988; Zhao et al., 2002), are considered to be
655 characterized by a series of orogenic to post-orogenic events from 2.0 up to 1.88 Ga.
656 The amalgamation of cratonic blocks worldwide established connections between
657 South America and West Africa and other cratonic terrains such as Western Australia
658 and South Africa, Laurentia and Baltica, Siberia and Laurentia, Laurentia and Central
659 Australia, etc (Zhao et al., 2002). These late-Paleoproterozoic collisional processes
660 likely formed the controversial supercontinent Columbia (Zhao et al., 2004). This
661 period also coincides with a major peak in orogenic gold resources (Goldfarb et al.,
662 2001; Juliani et al., 2014) and understanding the geodynamic of this period is crucial
663 for economic interests. Antonio et al. (2017) highlight that for the period 1.88 Ga,
664 many cratonic terrains have been characterized by extensive magmatism. These
665 authors report as examples the 1880 Ma NE-trending Ghost dike swarm and the 1880
666 Ma Circum-Superior LIP in the Canadian shield (Minifie et al., 2013), the 1880 Ma
667 Southern Bastar- Cuddapah LIP in India (French et al., 2008), the Mashonaland sills
668 and the Post-Waterberg dolerites in Kalahari craton (Hanson et al., 2004), an extensive
669 A-type magmatism in Baltica and in Siberia. The A-type affinity of the 1.88 Ga rocks
670 is widely described by other authors in different regions into the Amazonian craton
671 (Ferron et al., 2010; Pierosan et al., 2011; Fernandes et al., 2011; Klein et al., 2012;
672 Barreto et al., 2014; Teixeira et al., 2018). Currently, the significance of the 1.88 Ga A-
673 type magmatism in the AC is still matter of debate, also due to the extremely large
674 aerial cover which interested several different domains with different basements and
675 geologic evolutions. For example, studies on the Carajas region suggest that the 1.88
676 Ga anorogenic magmatism in this domain was provoked by delamination and fusion of
677 the Archean basement by a mantle plume which originated an extensional setting
678 (Dell'Agnol et al., 2005; Silva et al., 2016; Teixeira et al., 2018; Teixeira et al., 2019).

679 Conversely, the geochemical features of the TMP and SFX magmatism

1
2
3
4
5
6
7
8
9
10
11
12
13
14
15
16
17
18
19
20
21
22
23
24
25
26
27
28
29
30
31
32
33
34
35
36
37
38
39
40
41
42
43
44
45
46
47
48
49
50
51
52
53
54
55
56
57
58
59
60
61
62
63
64
65

680 presented in this work and in literature (Lamarão et al., 2002, 2005; Fernandes et al.,
681 2011) mainly support an extensional regime of these regions related to a late- to post-
682 collisional event, being possibly related to the end of the subduction process. The
683 transition from convergent (late-/post-orogenic) to extensional tectonic setting could
684 register the beginning of the taphrogenesis that marked the Amazonian Craton
685 throughout the Mesoproterozoic (Brito Neves, 1999; Lamarão et al., 2002). The ca.
686 1.88 Ga felsic magmatism in different provinces of the Amazonian craton could
687 represent the oldest magmatism related to this event.

688 It should be mentioned that in term of textural features, the products emitted
689 during the transition between the late-/post-collisional to extensive events don't display
690 substantial variations. In other words, the lithofaciological signature of the volcanic
691 and volcanoclastic rocks that characterized the 2 Ga VR event (subduction related) is
692 similar for those products erupted during the 1.88-1.87 Ga extensional volcanism that
693 characterized the MA and SRF events. Moreover, the post-orogenic to extensional
694 setting emphasizes the continental setting where the studied volcanic products have
695 been emitted. Following the idea of Roverato et al. (2017) for the Late-
696 Paleoproterozoic andesitic Sobreiro Formation, we stress the lack of any evidences in
697 favour of subaqueous eruptions for the emitted felsic products such as pillow lavas as
698 well as hyaloclastites. This suggests the subaerial character of the volcanism and its
699 emitted products acted in both regions.

700

701 10.2. Eruptive style and emplacement

702 The study areas are widely characterized by volcanic deposits whose eruptive
703 style is hard to differentiate. Distinguishing between banded lavas and high grade
704 ignimbrites is, sometime, extremely challenging (Henry and Wolff, 1992; Manley,
705 1995). This is made even more complicated when the investigated deposits are ancient
706 and the outcrops intensely eroded, such as those Precambrian terrains investigated here
707 (Lenhardt et al., 2012; Roverato et al., 2016; Lenhardt et al., 2017). Evidences in the
708 field show that a great volume of the volcanic activity is represented by the emission of
709 lava flows and/or high-grade to rheomorphic ignimbrites, although an important
710 amount of other fragmental products of different type (Lf mAL, mL, l-g/m-g/h-
711 gwAL) are also well represented in both regions. High-grade welded and rheomorphic
712 (up to lava-like) ignimbrites share similar features with lavas, displaying banding and

1
2
3
4
5
6
7
8
9
10
11
12
13
14
15
16
17
18
19
20
21
22
23
24
25
26
27
28
29
30
31
32
33
34
35
36
37
38
39
40
41
42
43
44
45
46
47
48
49
50
51
52
53
54
55
56
57
58
59
60
61
62
63
64
65

713 ductile folds formed by the elongation of fiamme and vesicles (Schmincke and
714 Swanson, 1967; Chapin and Lowell, 1979; Wolff and Wright, 1981; Branney et al.,
715 1992; Sumner and Branney, 2002; Pioli and Rosi, 2005; Andrews and Branney, 2011;
716 Brown and Bell, 2013). Although the ignimbrites investigated here have a fragmental
717 derivation their origin largely differ from those characteristic of fallout deposits that
718 form by a sustained column explosive-driven eruption. High-grade welded and
719 rheomorphic ignimbrites are correlated with highly explosive plinian-type eruptions
720 which produce, during their column collapse stage, large PDC. In addition, high-grade
721 rheomorphism of silicic products, either deriving from an explosive or effusive
722 eruption, are favored by high temperature low-viscosity emplacement conditions and
723 the presence of some residual water. The high temperatures condition of our deposits is
724 also confirmed by the pervasive presence of spherulites and lithophysae formed during
725 the slow-cooling regimes of large silica-rich lavas and welded ignimbrites (Lofgren,
726 1971; Breitzkreuz, 2013). The eruptive scenario showed in figure 17 giving origin to the
727 frequent eruption of large volume and high discharge rate lava flows and ignimbrites
728 was likely characterized by fissure-fed and caldera collapses systems as those
729 described by previous authors (Legros et al., 2000; Aguirre et al., 2003; Cas et al.,
730 2011; Lesti et al., 2011; Lenhardt et al., 2012; Willcock et al., 2013). Eruptions fed by
731 extensive fissures of large size, in fact, appear to be the most favourable volcanic
732 systems to minimize cooling during emplacement and produce an alternance of low-
733 height sustained column eruptions feeding PDC and eruptions characterized by the
734 effusion of low viscosity lava flows, coulees and domes, while maintaining high
735 discharge rates (e.g. Bachmann et al., 2000; Aguirrez-Diaz & Labarthe-Hernandez,
736 2003; Polo et al., 2018a, b; Simões et al., 2017). The sustained fountaining and
737 entrainment of air in the eruptive jet is strongly influenced by the geometry of the
738 conduit (Legros et a., 2000) as well as the transition from sustained to collapsing
739 eruptive column. A wide-geometry conduit would impede much air entrainment into
740 the pyroclastic fountain and, at the same time, would favors magmatic escape of
741 volcanic gases, favoring the low fountaining and promoting a “boil-over” style
742 eruption (Branney and Kokelaar, 1992, 2002; Lenhardt et al., 2017) with high
743 discharge rate. Moreover, the low air injection would inhibit the dilution of the
744 eruptive material making it thermodynamically isolated from the surrounding
745 environment (Lesti et al., 2011), preserving the high temperatures and enhancing the
746 agglutination of fragments (welding) (Quane and Russell, 2004; Russell and Quane

1
2
3
4
5
6
7
8
9
10
11
12
13
14
15
16
17
18
19
20
21
22
23
24
25
26
27
28
29
30
31
32
33
34
35
36
37
38
39
40
41
42
43
44
45
46
47
48
49
50
51
52
53
54
55
56
57
58
59
60
61
62
63
64
65

747 2005; Giordano et al., 2005). When the low-altitude pyroclastic fountaining or the
748 emission of high temperature lavas would be maintained for long time the high flow-
749 mobility is ensured (Sulpizio et al., 2014). If the material supply from the vent
750 continues for long time and with high discharge rate, the mobility could be maintained
751 even on very low slope angles (Sulpizio et al., 2014; Giordano et al., 2017; Kolzenburg
752 et al., 2017), and flowing various kilometers up to hundreds of kilometers far from the
753 vent (Aguirre-Diaz et al., 2008; Cas et al., 2011; Giordano et al., 2017). This could
754 explain the presence of large silicic volcanic areas characteristic of the ancient
755 Amazonian volcanism (Roverato et al., 2016). Although, volcanoclastic rocks seem to
756 be volumetrically less important in the study areas than the lava flows and/or
757 rheomorphic ignimbrites the recognition of fragmental rocks during our field
758 campaigns is important to understand their significance into our paleogeographic
759 reconstruction (Fig. 17). An idealized deposit sequence of a caldera forming eruption
760 displays an air-fall deposit overlain by an ignimbrite (Druitt and Sparks, 1984) and the
761 transition from the sustained column phase to the pyroclastic flow phase is often
762 accompanied by a strong increase in the discharge rate (Bursik and Woods, 1996). The
763 stratigraphic sequence of figure 11 shows this association of a possible air-fall deposit
764 (Lf dsAL) linked with pyroclastic flow-dominated deposits (Lf mAL and *m-gwLA*). In
765 some cases, pyroclastic eruptions commonly precede lava emplacement (Fink 1983;
766 Heiken and Wohletz 1987). The sequence presented in figure 7 shows a low-grade
767 welded ignimbrite deposit (Lf *l-gwAL*) overlaid by a thick banded body that we are
768 interpreting here as a lava flow. At the base of the banded lava is a breccia (Lf mLB)
769 consisting of clasts of a mix of lava textural types, including massive, vesicular, flow
770 banded and flow-folded, glassy, pumiceous and devitrified. Autobrecciation in lavas or
771 rheomorphic ignimbrites occurs when more rigid layers and the external parts are
772 broken in response to the applied shear stress locally exceeding the tensile strength
773 (Fink and Manley; 1987). Some polymictic breccia deposits (Lf mL) are
774 characterized by lithic angular clasts and devitrified fragments that could point to co-
775 ignimbritic breccias with short transport of the emitted material. These deposits could
776 be also related to collapse-caldera-breccias falling down into the caldera ring during
777 the roof subsidence. Air-fall (sA) and dilute pyroclastic flow (xsA) deposits (surge
778 type) crop out in both regions. These, linked with the glassy and lithic pyroclastic
779 material described above, are evidence of intense explosive phases from more
780 sustained column eruptions of smaller intra-caldera volcanic centers and/or associated

781 to events of caldera collapse (Fig. 17).

782

783 10.2.1 The sedimentary response

784 Sets of small basins intra-calderas and probable relatively immature shallow
785 marine deposits are interpreted as forming part of a tectonically unstable setting of a
786 young extensional environment that characterized the southern Amazonian craton
787 during the Paleoproterozoic. Reworked sediments can accumulate into volcano-
788 tectonic depressions created by the eruption, which often collects an intra-caldera lake
789 (Heiken et al., 2000 Németh et al., 2009, Manville et al., 2009). The sedimentation into
790 intra-volcano shallow-water lacustrine basins would have be facilitated (Fig. 17). The
791 alternation of subaerial to shallow-water sedimentation displayed by the alternation of
792 Lf mS and csG is indicative of this volcano-tectonic depressions, which could be also
793 interpreted as immature marine depressions. Subaerial and subaqueous talus coarse-
794 grained up to finer grained turbidites (dsSt) and suspension deposits formed during
795 quiescent periods into lakes or pounds is also inferred (Bacon et al., 2002). Silica-rich
796 accumulations into shallow water basins (Chipera et al., 2008; Manville et al., 2009)
797 deriving from hydrothermal activity in a dynamic volcanic context is also thought to be
798 responsible for the formation of chert accumulation (Lf bChS). Post caldera uplifting
799 (Fig. 17), resurgence or central volcanism could also contribute to produce new
800 sediments to be reworked and transported. Fluvial erosion and reworking of primary
801 deposits produced wide range of different sediments from localized cross-bedded,
802 well-sorted sand (Lf xsS) and gravel (Lf xsSG) beds to massive clast-supported sand
803 and gravel (Lf csGS, csG) and cobble (Lf csGC) deposits. Fluvial deposits occur
804 throughout all successions, representing periods of stream and river reworking and re-
805 establishment after an eruptive phase (Zernack et al., 2011; Roverato et al., 2017).
806 Debris-flows, hyperconcentrated flows, sheet-floods and active sandy braided river
807 systems existed and the absence of vegetation during the Precambrian (Oberholzer and
808 Eriksson, 2000; Roverato et al., 2017) permitted that copious rainfalls easily reworked
809 the available sediments.

810

811 11. Conclusion

812 This study is the result of the lithofaciological analysis carried out during the
813 2013, 2014 and 2015 field campaigns in the Amazon Craton in the TMP and SFX
814 regions and the successive geochemical and geochronological analysis of samples

1
2
3
4
5
6
7
8
9
10
11
12
13
14
15
16
17
18
19
20
21
22
23
24
25
26
27
28
29
30
31
32
33
34
35
36
37
38
39
40
41
42
43
44
45
46
47
48
49
50
51
52
53
54
55
56
57
58
59
60
61
62
63
64
65

815 collected in the field. This work constitutes a further step ahead toward the
816 comprehension of significance, chronostratigraphic distribution and the dynamic of
817 eruption and emplacement of felsic volcanic products in the region. Our results
818 complete previous studies and confirm that products present in the Amazonia Craton
819 could be related either to caldera-type systems (e.g. Lamarão et al., 2002; Juliani et al.,
820 2005; Lamarão et al., 2005; Pierosan et al., 2011) and to fissure-fed eruptive
821 environment following the model proposed by Aguirre-Diaz and Labarthe-Hernandez
822 (2003) for the “Sierra Madre Occidental” formation and by Juliani and Fernandes
823 (2010) for the Xingu region. The two models are in fact very similar only differing for
824 the size of the hypothesized magma chambers and the shape of the fissural vents. The
825 described volcano-sedimentary sequences that were characterized by the emission of
826 large volcanic felsic products were likely formed in a late-/post-orogenic (~ 2 Ga) to
827 extensional regimes (~ 1.88 Ga).

828
829

830 Acknowledgments

831 This work was supported by the project CAPES/CNPq 402564/2012-0 (Programa
832 Ciências sem Fronteiras) to Caetano Juliani and Matteo Roverato. M. Roverato
833 acknowledges the grant of the Brazilian CAPES/ CNPq Programa Ciências Sem
834 Fronteiras, Atração de Jovem Talento 402564/2012-0. We acknowledge the CNPq/CT-
835 Mineral (Proc. 550.342/ 2011-7) and the INCT-Geociam (573733/2008-2) —
836 (CNPq/MCT/ FAPESPA/PETROBRAS). Furthermore, the first author would like to
837 thank Jeovaci Jr. Martins da Rocha, Diego Felipe Gomez Gutierrez, Lucas Villela
838 Cassini for the help in the field and Carlos Marcelo Diaz Fernandez for the help and
839 very useful discussions. Dr. Giordano acknowledges the financial support for this
840 research from the CAPES project (proposal 302827) of the Ciências Sem Fronteiras
841 program (Brazil) and the local research funds (2012, 2013, 2014) of the University of
842 Turin (Ex60-2015). We are indebted to Nils Lenhardt and Roberto Dall’Agnol for the
843 dedication in reviewing this manuscript and important comments and reviews, which
844 improved considerably this work.

845
846

847 References

848
849 Aguirre-Diaz, G.J., Labarthe-Hernández, G., 2003. Fissure ignimbrites: fissure-source

850 origin for voluminous ignimbrites of the Sierra Madre Occidental and its
 851 relationship with Basin and Range faulting. *Geology* 31, 773-776.
 852 Aguirre-Diaz, G.J., Labarthe-Hernández, G., Tristán-González, M., Nieto-Obregón, J.,
 853 Isaac Gutiérrez-Palomares, I., 2008. The ignimbrite flare-up and graben calderas
 854 of the Sierra Madre Occidental, Mexico. In: Martí, J., Gottsman, J. (Eds.), *Caldera*
 855 *Volcanism: Analysis, Modelling and Response. Developments in Volcanology* 10,
 856 143-180.
 857 Almeida, F.F.M., Hasui, Y., Brito Neves, B.B., Fuck, R.A., 1981. Brazilian structural
 858 provinces: an introduction. *Earth Science Reviews* 17, 1-29.
 859 Almeida, M.E., Brito, M.F.L., Ferreira, A.L., Monteiro, M.A.S., 2000. Projeto Especial
 860 Província Mineral do Tapajós. *Geologia e recursos minerais da Folha Vila Mamãe*
 861 *Anã (SB.21-V-D). Estados do Pará e Amazonas. CPRM, Brasília. [CD-ROM].*
 862 Amaral, G., 1974. *Geologia Pré-Cambriana da Região Amazônica. Tese de Livre*
 863 *Docência, IG/USP (212 pp.).*
 864 Anders, E., Ebihara, M., 1982. Solar system abundances of the elements. *Geochim.*
 865 *Cosmochim. Ac.* 46, 2363-2380.
 866 Andrews, G.D.M., Branney, M.J., 2011. Emplacement and rheomorphic deformation
 867 of a large, lava-like rhyolitic ignimbrite: Grey's Landing, southern Idaho.
 868 *Geological Society of America Bulletin* 123, 725-743.
 869 Antonio, P., D'Agrella-Filho, M.S., Trindade, R.I.F., Nédélec, A., de Oliveira, D.C., da
 870 Silva, F.F., Roverato M., Lana, C., 2017. Turmoil before the boring billion:
 871 Paleomagnetism of the 1880–1860 Ma Uatumã event in the Amazonian craton.
 872 *Gondwana Research* 49, 106-129.
 873 Araújo, O.J.B., Maia, R.G.N., Jorge, João, X.S., Costa, J.B.S., 1988. A
 874 megaestruturação arqueana da folha Serra dos Carajás. In: SBG (Ed.), *Congresso*
 875 *Latinoamericano de Geologia, seventh ed. Belém. 324-333.*
 876 Bacon, C.R., Gardner, J.V., Mayer, L.A., Buktenica, M.W., Dartnell, P., Ramsey,
 877 D.W., Robinson, J.E., 2002. Morphology, volcanism, and mass wasting in Crater
 878 Lake, Oregon. *Geological Society of America bulletin* 114, 675-692.
 879 Bahia, R.B.C., Quadros, M.L.E.S., 2000. *Geologia e recursos minerais da Folha*
 880 *Caracol SB.21-X-C. Estados do Pará e Amazonas. Escala 1:250.000. Brasília:*
 881 *CPRM, 2000. 1 CD ROM.*
 882 Barreto, C.J.S., Lafonb, J.M., da Rosa Costac L.T., Fernandes-Limad, E., 2014.
 883 Palaeoproterozoic (~1.89 Ga) felsic volcanism of the Iricoumé Group, Guyana

1
2
3
4
5
6
7
8
9
10
11
12
13
14
15
16
17
18
19
20
21
22
23
24
25
26
27
28
29
30
31
32
33
34
35
36
37
38
39
40
41
42
43
44
45
46
47
48
49
50
51
52
53
54
55
56
57
58
59
60
61
62
63
64
65

884 Shield, South America: geochemical and Sm-Nd isotopic constraints on sources
885 and tectonic environment. *International Geology Review*, 2014.
886 <http://dx.doi.org/10.1080/00206814.2014.930800>
887 Best, M.G., Christiansen, E.H., 1997. Origin of broken phenocrysts in ash-flow tuffs.
888 *GSA Bulletin*, 109 (1), 63-73.
889 Blatt, H., Middleton, G., Murray, R., 1980. *Origin of Sedimentary Rocks*. Prentice-
890 Hall, Englewood Cliffs, 634.
891 Branney, M.J., Kokelaar, B.P., 1992. A reappraisal of ignimbrite emplacement:
892 progressive aggradation and changes from particulate to non-particulate flow
893 during emplacement of high-grade ignimbrite. *Bull. Volcanol.* 54, 504-520.
894 Breikreuz, C., 2013. Spherulites and lithophysae—200 years of investigation on high
895 temperature crystallization domains in silica-rich volcanic rocks. *Bull. Volcanol.*
896 75:705.
897 Brito-Neves, B.B., 2011. The Paleoproterozoic in the South-American continent:
898 Diversity in the geologic time. *Journal of South American Earth Sciences* 32, 270-
899 286.
900 Brown, D.J., Bell, B.R., 2013. The emplacement of a large, chemically zoned,
901 rheomorphic, lava-like ignimbrite: the Sgurr of Eigg Pitchstone, NW Scotland.
902 *Journal of the Geological Society* 170, 753-767.
903 Brown, G.C., Thorpe, R.S., Webb, P.C., 1984. The geochemical characteristics of
904 granitoids in contrasting arcs and comments on magma sources. *Journal of the*
905 *Geological society* 141, 413-426.
906 Bursik, M.I., Woods, A.W., 1996. The dynamics and thermodynamics of large ash
907 flows. *Bull. Volcanol.* 58, 175-193.
908 Capuzzo, N., Wetzel, A., 2004. Facies and basin architectural of the Late
909 Carboniferous Salvan-Dorénaz continental basin (Western Alps,
910 Switzerland/France). *Sedimentology* 51, 675-697.
911 Cas, R.A.F., Wright, J.V., 1987. *Volcanic Successions, Modern and Ancient*. Unwin
912 Hyman, Boston. 528.
913 Cas, R.A.F., Wright, H.M.N., Folkes, C.B., Lesti, C., Porreca, M., Giordano, G.,
914 Viramonte, J.G., 2011. The flow dynamics of an extremely large volume
915 pyroclastic flow, the 2.08-Ma Cerro Galán Ignimbrite, NW Argentina, and
916 comparison with other flow types. *Bull. Volcanol.* 73, 1583-1609.

- 1
2
3
4
5
6
7
8
9
10
11
12
13
14
15
16
17
18
19
20
21
22
23
24
25
26
27
28
29
30
31
32
33
34
35
36
37
38
39
40
41
42
43
44
45
46
47
48
49
50
51
52
53
54
55
56
57
58
59
60
61
62
63
64
65
- 917 Chipera, S.J., Goff, F., Goff, C.J., Fittipaldo, M., 2008. Zeolitization of intracaldera
918 sediments and rhyolitic rocks in the 1.25 Ma lake of Valles caldera, New Mexico,
919 USA. *Journal of Volcanology and Geothermal Research* 178, 317-330.
- 920 Collinson, J.D., 1966. Antidune bedding in the Namurian of Derbyshire, England:
921 *Geologie en Mijnbouw* 45, 262-264.
- 922 Collinson, J.D., Thompson, D.B., 1982 *Sedimentary structures*: London, Allen and
923 Unwin, 194.
- 924 Condie, K.C., 2000. Episodic continental growth models: after thoughts and
925 extensions. *Tectonophysics* 322, 153-162.
- 926 Condie, K.C., 2002. Continental growth during a 1.9-Ga superplume event. *Journal of*
927 *Geodynamics* 34, 249-264.
- 928 Costa, J.B.S., Hasui, Y. 1997. Evolução geológica da Amazônia. In: M.L. Costa &
929 R.S. Angélica (Ed.), *Contribuições à geologia da Amazônia*, 16-90.
- 930 Da Cruz, R.S., Fernandes, C.M.D., Villas, R.N.N., Juliani, C., Monteiro, L.V.S.,
931 Almeida, T.I.R., Lagler, B., Carneiro, C.C., Misas, C.M.E., 2015. A study of the
932 hydrothermal alteration in Paleoproterozoic volcanic centers, São Felix do Xingu
933 region, Amazonian Craton, Brazil, using short-wave infrared spectroscopy. *J.*
934 *Volc. Geoth. Res.* 304, 324-335.
- 935 Dall'Agnol, R., Lafon, J.M., Macambira, M.J.B., 1994. Proterozoic anorogenic
936 magmatism in the Central Amazonian Craton: geochronological and geochemical
937 aspects. *Mineral. Petrol.* 50, 113-138.
- 938 Dall'Agnol, R., Costi, H.T., Leite, A.A.S., Magalhães, M.S., Teixeira, N.P., 1999.
939 Rapakivi granites from Brazil and adjacent areas. *Precambrian Research* 95, 9-39.
- 940 Dall'Agnol, R., Teixeira, N.P., Rämö, O.T., Moura, C.A.V., Macambira, M.J.B.,
941 Oliveira, D.C., 2005. Petrogenesis of the paleoproterozoic, rapakivi, A-type granites
942 of the Archean Carajás metallogenic province, Brazil. *Lithos* 80, 101-129.
- 943 Dall'Agnol, R., da Cunha, I.R.V., Guimarães, F.V., de Oliveira, D.C., Teixeira,
944 M.F.B., Feio, G.R.L., Lamarão, C.N., 2017. Mineralogy, geochemistry, and
945 petrology of Neoproterozoic ferroan to magnesian granites of Carajás province,
946 Amazonian Craton: The origin of hydrated granites associated with charnockites.
947 *Lithos* 277, 3-32.
- 948 Druitt, T.H., Sparks, R.S.J., 1984. On the formation of calderas during ignimbrite
949 eruptions. *Nature* 310, 679-681.
- 950 Echeverri-Misas, C.M., 2010. Geologia e gênese do depósito de Au-(Cu) do Palito,

- 1
2
3
4
5
6
7
8
9
10
11
12
13
14
15
16
17
18
19
20
21
22
23
24
25
26
27
28
29
30
31
32
33
34
35
36
37
38
39
40
41
42
43
44
45
46
47
48
49
50
51
52
53
54
55
56
57
58
59
60
61
62
63
64
65
- 951 Província Aurífera do Tapajós. Dissertação de Mestrado, IG/USP.
- 952 Eriksson, P.G., Engelbrecht, J.P., Res, M., Harmer, R.E., 1994. The Bushy Bend lavas,
953 a new volcanic member of the Pretoria Group, Transvaal Sequence. S. Afr. J.
954 Geol. 97, 1-7.
- 955 Faraco, M.T.L., Carvalho, J.M.A., Klein, E.L., 1997. Carta metalogenética da
956 Província Auréfera do Tapajós, in: Costa, M.L.C., Ange´lica, R.S. (Eds.),
957 Contribuic,ões a` Geologia da Amazônia. Sociedade Brasileira de Geologia,
958 Belém, Brazil 1, 423-437.
- 959 Fernandes, C.M.D., Juliani, C., Monteiro, L.V.S., Lagler, B., Misas, C.M.E., 2011.
960 High-K calc-alkaline to A-type fissure-controlled volcano-plutonism of the São
961 Félix do Xingu region, Amazonian craton, Brazil: Exclusively crustal sources or
962 only mixed Nd model ages? Journal of South America Earth Science 32 (4), 351-
963 368.
- 964 Ferrari, L., Orozco-Esquivel, T., Manea, V.C., Manea, M., 2012. The dynamic history
965 of the Trans-Mexican Volcanic Belt and the Mexico subduction zone.
966 Tectonophysics 522-523, 122-149.
- 967 Ferreira, A.L., Almeida, M.E., Brito, M.F.L., Monteiro, M.A.S., 2000. Projeto Especial
968 Província Mineral do Tapajós. Geologia e recursos minerais da Folha
969 Jacareacanga (SB.21-Y-B). Estados do Pará e Amazonas. Escala 1:250.000. Nota
970 explicativa e mapas, CPRM, Brasília. [CD ROM].
- 971 Ferron, J.M.T.M., Bastos-Neto, A.C., Lima, E.F., Nardi, L.V.S., Costi, H.T., Pierosan,
972 R., Prado, M., 2010. Petrology, geochemistry, and geochronology of
973 Paleoproterozoic volcanic and granitic rocks (1.89–1.88 Ga) of the Pitinga
974 Province, Amazonian Craton, Brazil. Journal of South American Earth Sciences
975 29, 483-497.
- 976 Fink, J., 1983. Structure and emplacement of a rhyolitic obsidian flow: little Glass
977 Mountain, Medicine Highland, northern California. GSA Bull. 94, 362-380.
- 978 Fink, J.H., Manley, C.R., 1987. Origin of pumiceous and glassy textures in rhyolite
979 flows and domes: Geological Society of America Special Paper 212, 77-88.
- 980 Fisher, R.V., 1961. Proposed classification of volcanoclastic sediments and rocks.
981 Geological Society of America Bulletin 72, 1409-1414.
- 982 French, J.E., Heaman, L.M., Chacko, T., Srivastava, R.K., 2008. 1891–1883 Ma
983 Southern Bastar–Cuddapah mafic igneous events, India: a newly recognized large
984 igneous province. Precambrian Research 160, 308-322.

- 985 Giordano, D., La Felice, S., Arzilli, F., De Cristofaro, S.P., Masotta, M., Polo L.
 986 (2017). Il vulcanismo effusivo acido del Monte Amiata: stima delle condizioni
 987 pre- e sin-eruttive ed implicazioni vulcanologiche. Effusive acidic volcanism of
 988 Monte Amiata: estimates of pre- and syn-eruptive conditions and volcanological
 989 implications. *Monografia Il Vulcano di Monte Amiata*, ISBN 978-88-99742-32-4,
 990 171-193.
- 991 Giordano, D., Nichols, A.R.L., Dingwell, D.B., 2005. Glass transition temperatures of
 992 natural hydrous melts: a relationship with shear viscosity and implications for the
 993 welding process. *Jour. Volc Geoth. Res.* 142, 105-118.
- 994 Giovanardi, T., Girardi, V.A.V., Correia, C.T., Sinigoi, S., Tassinari, C.C.G.,
 995 Mazzucchelli, M., 2015. U-Pb zircons SHRIMP data from the Cana Brava
 996 Layered Complex: New constraints for the mafic-ultramafic intrusions of Northern
 997 Goiás, Brazil. *Open Geosci* 7, 197-206.
- 998 Goldfarb, R., Groves, D., Gardoll, S., 2001. Rotund versus skinny orogens: well-
 999 nourished or malnourished gold? *Geology* 29, 539-542.
- 1000 Gutscher, M.A., Maury, R., Eissen, J.P., Bourdon, E., 2000. Can slab melting be
 1001 caused by flat subduction? *Geology* 28, 535-538.
- 1002 Hanson, R.E., Gose, W.A., Crowley, J.L., Ramezani, J., Bowring, S.A., Bullen, D.S.,
 1003 Hall, R.P., Pancake, J.A., Mukwakwami, J., 2004. Paleoproterozoic intraplate
 1004 magmatism and basin development on the Kaapvaal Craton: age, paleomagnetism
 1005 and geochemistry of ~1.93 to ~1.87 Ga post-Waterberg dolerites. *South African
 1006 Journal of Geology* 107, 233-254.
- 1007 Hasui, Y., Haraly, N.L.E., Schobbenhaus, C., 1993. Megaestruturação Pré-Cambriana
 1008 do território brasileiro baseada em dados geofísicos e geológicos. *Geociências* 12,
 1009 7-31.
- 1010 Heiken, G., Wohletz, K., 1987. Tephra deposits associated with silicic domes and lava
 1011 flows. *GSA Special Paper* 212.
- 1012 Heiken, G., Krier, D., McCormick, T., Snow, M.G., 2000. Intracaldera volcanism and
 1013 sedimentation — Creede caldera, Colorado. In: Bethke, P.M., Hay, R.L. (Eds.),
 1014 *Ancient Lake Creede: Its volcano-tectonic setting, history of sedimentation, and
 1015 relation to mineralization in the Creede Mining District*. Geological Society of
 1016 America Special Paper, 346. Boulder, Colorado, 127-157.
- 1017 Hofmann, A.W., 1988. Chemical differentiation of the Earth: The relationship between
 1018 mantle, continental crust and oceanic crust. *EPSL* 90, 297-314.

- 1019 Hollocher, K., Robinson, P., Walsh, E., Roberts, D., 2012. Geochemistry of
1020 amphibolite-facies volcanics and gabbros of the Støren Nappe in extensions west
1021 and southwest of Trondheim, Western Gneiss Region, Norway: a key to
1022 correlations and paleotectonic settings. *American Journal of Science* 312, 357-
1023 416.
- 1024 Juliani, C., 2002. Alteração hidrotermal e metalogênese em sistemas vulcano-
1025 plutônicos paleoproterozóicos na Província Aurífera do Tapaj, Cráton Sul
1026 Amazônico, Pará. Tese de Livre-Docência, IG/USP.
- 1027 Juliani, C., Vasquez, M.L., Klein, E.L., Villas, R.N., Echeverri-Misas, C.M., Santiago,
1028 E.S.B., Monteiro, L.V.S., Carneiro, C.C., Fernandes, C.M.D., Usero, G., 2014.
1029 Metalogenia da Província Tapajós. In: Silva M.G.; Jost H.; Kuyumajian R.M.
1030 (Org.). *Metalogênese das Províncias Tectônicas Brasileiras*. 1 ed. : CPRM —
1031 Serviço Geológico do Brasil 1, 51-90.
- 1032 Juliani, C., Rye, R.O., Nunes, C.M.D., Snee, L.W., Correa Silva, R.H., Monteiro,
1033 L.V.S., Bettencourt, J.S., Neumann, R., Neto, A.A., 2005. Paleoproterozoic high
1034 sulphidation mineralization in the Tapajós gold province, Amazonian Craton,
1035 Brazil: geology, mineralogy, alunite argon age, and stable-isotope constraints.
1036 *Chemical Geology* 215, 95-125.
- 1037 Juliani, C., Fernandez C.M.D., 2010. Well-preserved Late Paleoproterozoic volcanic
1038 centers in the São Félix do Xingu region, Amazonian Craton, Brazil. *Journal of*
1039 *Volcanology and Geothermal Research* 191, 167-179.
- 1040 Kay, S.M., Godoy, E., Kurtz, A., 2005. Episodic arc migration, crustal thickening,
1041 subduction erosion, and magmatism in the south_central Andes. *Geological*
1042 *Society of America Bulletin* 117, 67-88.
- 1043 Klein, E.L., Almeida, M.E., and Costa, L.T.R., 2012. The 1.89-1.87 Ga Uatumã Silicic
1044 Large Igneous Province, northern South America: Large Igneous Provinces
1045 Commission: <http://www.largeigneousprovinces.org/12nov> (accessed 12 January
1046 2012).
- 1047 Klein, E.L., Santos, R.A., Fuzikawa, K., Angélica, R.S., 2001. Hydrothermal fluid
1048 evolution and structural control of the brittle-style Guarim lode-gold
1049 mineralisation, Tapajós Province, Amazonian Craton, Brazil. *Miner. Depos.* 36,
1050 149-164.
- 1051 Klein, E.L., Vasquez, M.L., Rosa-Costa, L.T., Carvalho, J.M.A., 2002. Geology of
1052 Paleoproterozoic gneiss- and granitoid-hosted gold mineralization in Southern

- 1053 Tapajós Gold Province, Amazonian Craton, Brazil. *Intern. Geol. Rev.*, 44, 544-
1054 558.
- 1055 Klein, E.L., Rosa-Costa, L.T., Carvalho, J.M.A., 2004. Estudo de inclusões fluidas em
1056 veio de quartzo aurífero do prospecto Patinhas, Província Aurífera do Tapajós,
1057 Cráton Amazônico. *RBG* 34, 59-66.
- 1058 Lagler, B., Juliani, C., Pessoa, F.F., Fernandes, C.M.D., 2011. Petrografia e
1059 geoquímica das sequências vulcânicas Paleoproterozóicas na região de Vila
1060 Tancredo, São Félix do Xingu (PA). In: SBGq, Congr. Bras. Geoquí., 13, e Simp.
1061 Países do Mercosul, 3, Gramado, RS. Anais, [CD-ROM].
- 1062 Lamarão, C.N., Dall'Agnol, R., Lafon, J.M., Lima, E.F., 1999. As associações
1063 vulcânicas e plutônicas de Vila Riozinho e Morais Almeida, Província Aurífera do
1064 Tapajós, SW do estado do Pará. In: Simpósio sobre Vulcanismo e Ambientes
1065 Associados. 1, Gramado*/RS, Boletim de resumos, 93 (in Portuguese).
- 1066 Lamarão, C.N., Dall'agnol, R., Lafon, J.M., Lima, E.F., 2002. Geology, geochemistry,
1067 and Pb-Pb zircon geochronology of the Paleoproterozoic magmatism of Vila
1068 Riozinho, Tapajós Gold Province, Amazonian craton, Brazil. *Prec. Res.* 119, 189-
1069 223.
- 1070 Lamarão, C.N., Dall'agnol, R., Pimentel, M.M., 2005. Nd isotopic composition of
1071 Paleoproterozoic volcanic rocks of Vila Riozinho: Implications for the crustal
1072 evolution of the Tapajós gold province, Amazon craton. *J. South Am. Earth Sci.*
1073 18, 277-292.
- 1074 Legros, F., Kelfoun, K., 2000. On the ability of pyroclastic flows to scale topographic
1075 obstacles. *J. Volcanol. Geotherm. Res.* 98, 235-241.
- 1076 Lenhardt, N., Hornung, J., Hinderer, M., Böhnell, H., Torres-Alvarado, I.S., Trauth, N.,
1077 2011. Build-up and depositional dynamics of an arc front volcanoclastic complex:
1078 the Miocene Tepoztlan Formation (Transmexican Volcanic Belt, Central Mexico).
1079 *Sedimentology* 58, 785-823.
- 1080 Lenhardt, N., Eriksson, P., Catuneanu, O., Bumby, A.J., 2012. Nature of and controls
1081 on volcanism in the ca. 2.32-2.06 Ga Pretoria Group, Transvaal Supergroup,
1082 Kaapvaal Craton, South Africa. *Precambrian Research* 214-215, 106-123.
- 1083 Lenhardt, N., Masango S.M., Jolayemi, O.O., Lenhardt, S.Z., Peeters, G.J., Eriksson,
1084 P.G., 2017. The Palaeoproterozoic (~2.06 Ga) Rooiberg Group, South Africa:
1085 Dominated by extremely high-grade lava-like and rheomorphic ignimbrites? New
1086 observations and lithofacies analysis. *Journal of African Earth Sciences* 131, 213-

- 1087 232.
- 1088 Lesti, C., Porreca, M., Giordano, G., Mattei, M., Cas, R.A.F., Wright, H.M.N., Folkes,
1089 C.B., Viramonte, J., 2011. High-temperature emplacement of the Cerro Galán and
1090 Toconquis Group ignimbrites (Puna plateau, NW Argentina) determined by TRM
1091 analyses. *Bull. Volcanol.* 73, 1535-1565.
- 1092 Lofgren, G., 1971. Spherulite textures in glassy and crystalline rocks. *J. Geophys. Res.*
1093 76, 5635-5648.
- 1094 Ludwig, K.R., 2009. Isoplot 4.1. A geochronological toolkit for Microsoft Excel.
1095 Berkeley Geochronology Center special publication 4, 76.
- 1096 Macambira, E.M.B., 1997. Geologia e aspectos metalogenéticos dos elementos do
1097 grupo de platina no complexo máfico-ultramáfico da serra da Onça – sul do Pará.
1098 Tese de Mestrado, UFPA, Belém, Pará, Brasil.
- 1099 Macambira, E.M.B., Vale, A.G., 1997. Programa Levantamentos Geológicos Básicos
1100 do Brasil. São Félix do Xingu. Folha SB-22-Y-B. Estado do Pará, CPRM, Brasília
1101 (in Portuguese).
- 1102 Manea, V.C., Pérez-Gussinyé, M., Manea, M., 2012. Chilean flat-slab subduction
1103 controlled by overriding plate thickness and trench rollback. *Geology* 40 (1), 35-
1104 38.
- 1105 Manville, V., Németh, K., Kano, K., 2009. Source to sink: A review of three decades
1106 of progress in the understanding of volcanoclastic processes, deposits, and
1107 hazards. *Sedimentary Geology* 220, 136-161.
- 1108 McPhie, J., Doyle, M., Allen, S.R., 1993. *Volcanic textures: A guide to the*
1109 *interpretation of textures in volcanic rocks*, Centre for Ore Deposit and
1110 *Exploration Studies*. University of Tasmania, 198.
- 1111 Miall, A.D., 1996. *The Geology of Fluvial Deposits: Sedimentary Facies, Basin*
1112 *Analysis, and Petroleum Geology*. Springer-Verlag, New York. 582.
- 1113 Minifie, M.J., Kerr, A.C., Ernst, R.E., Hastie, A.R., Ciborowski, T.J.R., Desharnais,
1114 G., Millar, I.L., 2013. The northern and southern sections of the western ca. 1880
1115 Ma Circum-Superior Large Igneous Province, North America: the Pickle Crow
1116 dyke connection? *Lithos* 174, 217-235.
- 1117 Monteiro, L.V.S., Xavier, R.P., de Carvalho, E.R., Hitzman, M.W., Johnson, C.A., de
1118 Souza Filho, C.R., Torresi, I., 2008. Spatial and temporal zoning of hydrothermal
1119 alteration and mineralization in the Sossego iron oxide-copper-gold deposit,
1120 Carajás Mineral Province, Brazil: paragenesis and stable isotope constraints.

- 1121 Miner Deposita 43, 129-159.
- 1 1122 Mori, L., Gómez-Tuena, A., Cai, Y., Goldstein, S., 2007. Effects of prolonged flat
2 subduction on the Miocene magmatic record of the central Trans-Mexican
3
4 1123
5 1124 Volcanic Belt. *Chemical Geology* 244, 452-473.
- 6
7 1125 Mori, P.E., Reeves, S., Correia, C.T., Haukka, M., 1999. Development of a fused glass
8
9 1126 disc XRF facility and comparison with the pressed powder pellet technique at
10
11 1127 Instituto de Geociências. *Rev. Bras. Geociências*, 29, 441-446.
- 12 1128 Mueller, W.U., Concoran, P.L., 1998. Late-orogenic basins in the Archaean Superior
13
14 1129 Province, Canada: characteristics and inferences. *Sedimentary Geology* 120, 177-
15
16 1130 203.
- 17
18 1131 Mueller, W.U., Chown, E.H., Thurston, P.C., 2000a. Processes in physical
19
20 1132 volcanology and volcanoclastic sedimentation: modern and ancient. *Precambrian*
21
22 1133 *Research* 101, 81-85.
- 23 1134 Navarro, M.S., Andrade, S., Ulbrich, H.H.G.J., Gomes, C.B., Girardi, V.A.V., 2008.
24
25 1135 The analysis of rare earth elements with ICP-MS in basaltic and related rocks:
26
27 1136 testing the efficiency of sample decomposition procedures. *Geostand. Geoanal.*
28
29 1137 *Res.* 32(2),167-180.
- 30
31 1138 Németh, K., Cronin, S.J., Stewart, R.B., Charley, D., 2009. Intra- and extra- caldera
32
33 1139 volcanoclastic facies architecture of a frequently active mafic island-arc volcano,
34
35 1140 Ambryn Island, Vanuatu. *Sedimentary Geology* 220, 256-270.
- 36 1141 Oberholzer, J.D., Eriksson, P.G., 2000. Subaerial volcanism in the Palaeoproterozoic
37
38 1142 Heekpoort Formation (Transvaal Supergroup), Kaapvaal craton. *Precambrian*
39
40 1143 *Research* 101, 193-210.
- 41
42 1144 Pearce, J.A., Harris, N.B.W., and Tindle, A.G., 1984. Trace element discrimination
43
44 1145 diagrams for the tectonic interpretation of granitic rocks. *Journal of Petrology* 25,
45
46 1146 956-983.
- 47 1147 Pearce, J.A., 1996. Sources and settings of granitic rocks. *Episodes* 19 (4), 120-125.
- 48 1148 Pessoa M.R., Santiago A.F., Andrade A.F., Barreto E.L., Nascimento J.O., Santos
49
50 1149 J.O.S., Oliveira J.R., Lopes R.C., Prazeres W.V. 1977. Projeto Jamaxim.
51
52 1150 CPRM/DNPM, 1-3, 614.
- 53
54 1151 Pierosan, R., Lima, E.F., Nardi, L.V.S., Bastos Neto, A.C., Campos, C.P., Jarvis, K.,
55
56 1152 Ferron, J.M.T.M., Prado, M., 2011. Geochemistry of Palaeoproterozoic volcanic
57
58 1153 rocks of the Iricoumé Group, Pitinga Mining District, Amazonian craton, Brazil:
59
60 1154 *International Geology Review* 53, 946-979.

- 1155 Pinho, S.C.C., Fernandes, C.M.D., Teixeira, N.P., Paiva Jr., A.L., Cruz, V.L.,
1156 Lamarão, C.N., Moura, C.A.V., 2006. O magmatismo paleoproterozóico da região
1157 de São Félix do Xingu, Província Estanífera do Sul do Pará: Petrografia e
1158 geocronologia. *Revista Brasileira de Geociências* 36, 793-802.
- 1159 Pioli, L., Rosi, M., 2005. Rheomorphic structures in a high-grade ignimbrite: the
1160 Nuraxi tuff, Sulcis volcanic district (SW Sardinia, Italy). *Journal of Volcanology
1161 and Geothermal Research* 142, 11-28.
- 1162 Polo, L.A., Giordano, D., Janasi, V., Freitas-Guimaraes, L., 2017(a). Effusive silicic
1163 volcanism in the Paraná Magmatic Province, South Brazil: Physico-chemical
1164 conditions of storage and eruption and considerations on the rheological behaviour
1165 during emplacement. *J. Volcanol. Geoth. Res.* 355, 115-135.
- 1166 Polo L.A., Janasi V., Giordano D., Lima E.F., Cañon-Tapia E., Roverato M., 2017(b).
1167 Effusive silicic volcanism in the Paraná Magmatic Province, South Brazil:
1168 Evidence for locally-fed lava flows and domes from detailed field work. *J.
1169 Volcanol. Geoth. Res.* 355, 204-218.
- 1170 Quane, S. L., Russell, J. K., 2005. Welding: Insights from high-temperature analogue
1171 experiments. *Journal of Volcanology and Geothermal Research* 142 (1-2), 67-87.
- 1172 Reis, N.R., Almeida, M.E., Ferreira, A.L., Riker, S.R., 2006. *Geologia e Recursos
1173 Minerais do Estado do Amazonas. Sistema de Informações Geográficas
1174 1:1.000.000. CPRM, Manaus, 144.*
- 1175 Rino, S., Tsuyoshi, K., Windley, B.F., Katayama, I., Motoki, A., Hirata, T., 2004.
1176 Major episodic increases of continental crustal growth determined from zircon
1177 ages of river sands; implications for mantle overturns in the Early Precambrian.
1178 *Physics of the Earth and Planetary Interiors* 146, 369-394.
- 1179 Roverato, M., Capra, L., Sulpizio, R., Norini, G., 2011. Stratigraphic reconstruction of
1180 two debris avalanche deposits at Colima Volcano (Mexico): insights into pre-
1181 failure conditions and climate influence. *J. Volc. Geoth. Res.* 207 (1), 33-46.
- 1182 Roverato, M., Cronin, S., Procter, J., Capra, L., 2014. Textural features as indicators of
1183 debris avalanche transport and emplacement, Taranaki volcano. *Geol. Soc. Am.
1184 Bull.* B30946-1
- 1185 Roverato, M., 2016. The Montesbelos mass-flow (southern Amazonian craton, Brazil):
1186 a Paleoproterozoic volcanic debris avalanche deposit? *Bull. Volcanol.* 78, 49.
- 1187 Roverato, M., Giordano, D., Echeverri-Misas, CM., Juliani, C., 2016.
1188 Paleoproterozoic felsic volcanism of the Tapajós Mineral Province, Southern

- 1189 Amazon Craton, Brazil. *Journal of Volcanology and Geothermal Research* 310,
1190 98-106.
- 1191 Roverato, M., Juliani, C., Marcelo Dias-Fernandes, C., Capra, L., 2017.
- 1192 Paleoproterozoic andesitic volcanism in the southern Amazonian craton, the
1193 Sobreiro Formation: new insights from lithofacies analysis of the volcanoclastic
1194 sequences. *Precambrian Research* 289, 18-30.
- 1195 Russell, J. K., Quane, S. L., 2005. Rheology of welding: Inversion of field constraints.
1196 *Journal of Volcanology and Geothermal Research* 142 (1-2), 173-191.
- 1197 Santos, J.O.S., Hartmann, L.A., Gaudette, H.E., Groves, D.I., McNaughton, N.J.,
1198 Fletcher, I.R., 2000. A new understanding of the provinces of the Amazon craton
1199 based on integration of field mapping and U-Pb and Sm-Nd geochronology.
1200 *Gondwana Research* 3, 453-488.
- 1201 Santos, J.O.S., Groves D.I., Hartmann L.A., Moura M.A., McNaughton, N.J. 2001.
1202 Gold deposits of the Tapajós and Alta Floresta Domains, Tapajós-Parima orogenic
1203 belt, Amazon Craton, Brazil. *Mineralium Deposita* 36, 278-299.
- 1204 Santos, J.O.S., 2003. Geotectônica dos Escudos da Guiana e Brasil Central. In: L.A.
1205 Bizzi, C. Schobbenhaus, R.M. Vidotti, J.H. Gonçalves (Eds.). *Geologia, tectônica
1206 e recursos minerais do Brasil. Texto, mapas e SIG. CPRM - Serviço Geológico do
1207 Brasil, Brasília* 169-226.
- 1208 Santos, J.O.S., Van Breemen, O.B., Groves, D.I., Hartmann, L.A., Almeida, M.E.,
1209 McNaughton, N.J., Fletcher, I.R., 2004. Timing and evolution of multiple
1210 Paleoproterozoic magmatic arcs in the Tapajós Domain, Amazon Craton:
1211 constraints from SHRIMP and TIMS zircon, baddeleyite and titanite U-Pb
1212 geochronology. *Prec. Res.* 13, 73-109.
- 1213 Silva, F.S., Oliveira, D.C., Antonio, P.Y., D'Agrella-Filho, M., Lamarão, C.N., 2016.
1214 Bimodal magmatism of the Tucuma area, Carajás Province: U-Pb geochronology,
1215 classification and processes. *J. S. Am. Earth Sci.* 72, 95-114.
- 1216 Simões, M.S., Lima, E.F., Sommer, C.A., Rossetti, L.M.M., 2017. Structures and
1217 lithofacies of inferred silicic conduits in the Paraná-Etendeka LIP, southernmost
1218 Brazil. *Journal of Volcanology and Geothermal Research* 355, 319-336.
- 1219 Sulpizio, R., Mele, D., Dellino, P., La Volpe, L., 2007. Deposits and physical
1220 properties of pyroclastic density currents during complex Subplinian eruptions: the
1221 AD 472 (Pollena) eruption of Somma-Vesuvius, Italy. *Sedimentology* 54, 607-
1222 635.

- 1223 Sumner, J.M., Branney, M.J. 2002. The emplacement history of a remarkable
1224 heterogeneous, chemically zoned, rheomorphic and locally lava-like ignimbrite:
1225 'TL' on Gran Canaria. *Journal of Volcanology and Geothermal Research* 115,
1226 109-138.
- 1227 Tassinari, C.C.G., Macambira, M.J.B., 1999. Geochronological provinces of the
1228 Amazonian craton. *Episodes* 22, 174-182.
- 1229 Teixeira, M.F.B., Dall'Agnol, R., Santos, J.O.S., Oliveira, D.C., Lamarão, C.N.,
1230 McNaughton, N.J., 2018. Crystallization ages of Paleoproterozoic A-type granites
1231 of Carajás province, Amazon craton: Constraints from U-Pb geochronology of
1232 zircon and titanite. *J. of South American Earth Sciences* 88, 312-331.
- 1233 Teixeira, N.P., Bettencourt, J.S., Moura, C.A.V., Dall'Agnol, R., Macambira, E.M.B.,
1234 2002. Archean crustal sources for Paleoproterozoic tin-mineralized granites in the
1235 Carajas Province, SSE Para, Brazil: Pb-Pb geochronology and Nd isotope
1236 geochemistry. *Precambrian Research* 119, 257-275.
- 1237 Teixeira, W., Tassinari, C.C.G., Cordani, U.G., Kawashita, K., 1989. A review of the
1238 geochronology of the Amazonian craton: tectonic implications. *Precambrian Res.*
1239 42, 213-227.
- 1240 Teixeira, W., Nelson, J.R., Bettencourt, J.S., Klein, E.L., Oliveira, D.C., 2019.
1241 Intraplate Proterozoic magmatism in the Amazonian Craton reviewed:
1242 geochronology, crustal tectonics and global matches. In book: *Dyke Swarms of the*
1243 *World: A Modern Perspective*. DOI:10.1007/978-981-13-1666-1_4
- 1244 Van Kranendonk, M.J., 2006. Volcanic degassing, hydrothermal circulation and the
1245 flourishing of early life on Earth: a review of the evidence from c. 3490-3240 Ma
1246 rocks of the Pilbara Supergroup, Pilbara Craton, Western Australia. *Earth Science*
1247 *Rev.* 74, 197-240.
- 1248 Vasquez, M.L, Klein, E.L, Macambira, M.J.B., Santos, A., Bahia, R.B.C., Ricci, P.,
1249 dos, S.F., Quadros, M.L.E.S., 2000. Geochronology of granitoids, mafic intrusions
1250 and mineralizations of the Tapajós Gold Province - Amazonian Craton - Brazil. In:
1251 *Inter. Geol. Congr. 31, Abstracts, [CD-ROM]*.
- 1252 Vasquez, M.L., Sousa, C.S., Carvalho, J.M.A., 2008. Mapa Geológico e de Recursos
1253 Minerais do Estado do Pará, escala 1:1.000.000. Programa Geologia do Brasil,
1254 Belém, CPRM.
- 1255 Vasquez, M.L., Dreher, A.M. 2011. Uma avaliação da estratigrafia dos eventos
1256 magmáticos de 1900-1860 Ma do Cráton Amazônico. In: *SBG, Simp. Geol.*

- 1257 Amaz. 12, Bol. Res. [CD ROM].
- 1258 Walker, G.P.L., 1983. Ignimbrite types and ignimbrite problems. *J. Volcanol.*
- 1259 *Geotherm. Res.* 17, 65-88.
- 1260 Went, D.J., 2016 Alluvial fan, braided river and shallow-marine turbidity current
- 1261 deposits in the Port Lazo and Roche Jagu formations, Northern Brittany:
- 1262 relationships to andesite emplacements and implications for age of the Plourivo-
- 1263 Plouézec Group. *Geol. Mag.* 1-24, Cambridge University Press 2016.
- 1264 White, J.D.L., Houghton, B.F., 2006. Primary volcanoclastic rocks. *Geological Society*
- 1265 *of America Bulletin* 34, 677-680.
- 1266 Willcock, M.A.W., Cas, R.A.F., Giordano, G., Morelli, C., 2013. The eruption,
- 1267 pyroclastic flow behaviour, and caldera in-filling processes of the extremely large
- 1268 volume (N1290 km³), intra- to extra-caldera, Permian Ora (Ignimbrite) Formation,
- 1269 Southern Alps, Italy. *J. Volcanol. Geotherm. Res.* 265, 102-126.
- 1270 Williams, I.S., 1998. U-Th-Pb geochronology by ion microprobe. In: McKibben, M.A.,
- 1271 Shanks, W.C.P., Ridley, W.I. (eds) *Applications of Microanalytical Techniques to*
- 1272 *Understanding Mineralizing Processes*, *Rev Econ Geol* vol 7. Soc. Econ. Geol,
- 1273 Littleton, 1-35.
- 1274 Wolff, J.A., Wright, J.V., 1981. Rheomorphism of welded tuffs. *Journal of*
- 1275 *Volcanology and Geothermal Research* 10, 13-34.
- 1276 Zanchetta, G., Sulpizio, R., Di Vito, M.A., 2004. The role of volcanic activity and
- 1277 climate in alluvial fan growth at volcanic areas: an example from southern
- 1278 Campania (Italy). *Sedimentary Geology* 168, 249-280.
- 1279 Zernack, A.V., Cronin, S.J., Neall, V.E., Procter, J.N., 2011. A medial to distal
- 1280 volcanoclastic record of an andesitic stratovolcano: detailed stratigraphy of the
- 1281 ring-plain succession of south-west Taranaki, New Zealand: *International Journal*
- 1282 *of Earth Sciences* 100, 1937-1966.
- 1283 Zhao, G., Cawood, P.A., Wilde, S.A., Sun, M., 2002. Review of global 2.1–1.8 Ga
- 1284 orogens: implications for a pre-Rodinia supercontinent. *Earth-Science Reviews* 59,
- 1285 125-162.
- 1286 Zhao, G., Sun, M., Wilde, S.A., Li, S., 2004. A Paleo-Mesoproterozoic supercontinent:
- 1287 assembly, growth and breakup. *Earth-Science Reviews* 67, 91-123.
- 1288
- 1289
- 1290

1291 Figure Captions

1292

1293 Figure 1: location map of the northern South America and the Amazonian Craton

1294 divided into several geochronological provinces and other domains according to Santos
1295 et al. (2000); TMP = Tapajós Mineral Province, SFX = São Felix do Xingú Region.

1296

1297 Figure 2: distribution map of the outcrops analyzed during the field campaigns in both

1298 regions a) Tapajós Mineral Province (TMP) and b) São Felix do Xingú region (SFX);

1299 PW=distribution of the Santa Rosa formation inferred during the present work;

1300 F=distribution of the Santa Rosa formation inferred by Fernandes et al. (2011);

1301 BIF=Banded Iron Formation; red and white dot refers to primary andesitic deposits

1302 analyzed in Roverato et al. (2017). In both figures are reported the outcrops described

1303 in the paper.

1304

1305 Figure 3: massive and banded lavas and rheo-ignimbrite (?) deposits. a) Np173

1306 (7°33'52.31" S, 55°10'58.80" W), b) Xu23 (6°41'08.65" S, 52°25'55.67" W), c) Xu101

1307 (6°52'12.82" S, 52°09'16.12" W), d) Xu52 (6°28'19.32" S, 51°50'08.90" W), e), f), g)

1308 Np396 (6°32'41.06" S, 55°23'59.37" W); see Fig. 2 for the outcrops location. For the

1309 lithofacies description and more details see the text.

1310

1311 Figure 4: massive primary volcanoclastic rocks with different proportion of ash, lapilli

1312 and blocks. All the deposits are interpreted to be emplaced from pyroclastic density

1313 currents except (f) that is interpreted as a basal-breccia of a lava body. a) Xu104

1314 (6°52'22.96" S, 52°08'15.91" W), b) Np183 (7°32'04.13" S, 55°08'50.02" W), c) Np93

1315 (6°44'16.60" S, 55°27'12.96" W), d) Xu29 (6°41'42.51" S, 52°01'23.06" W), e) Xu07

1316 (6°41'56.36" S, 52°08'42.27" W) f) Xu192 (6°31'31.92" S, 53°02'36.60" W); see Fig.

1317 2 for the outcrops location. For the lithofacies description see the text and Table 1.

1318

1319 Figure 5: microphotographs of different massive ash and lapilli ignimbrite deposits in

1320 thin section: a) broken crystals suggesting the fragmental character of the rock; b)

1321 detail of a devitrified juvenile fragment displaying axiolitic fabric; c) banded sub-

1322 millimetric to millimetric lithic fragments immersed in a devitrified groundmass.

1323

1324 Figure 6: reconstructed schematic stratigraphic column and associated photographs

1325 representing the evolution of ignimbrite deposits cropping out in the TMP (Np183;
1326 7°32'04.13" S, 55°08'50.02" W); note the increase of welding from the base to the top.
1327
1328 Figure 7: schematic stratigraphic column and relative photographs of a >150 m thick
1329 felsic banded lava(s) cropping out in SFX (Xu192; 6°31'31.92" S, 53°02'36.60" W)
1330 overlying a basal breccia (Lf mLB) and an ignimbrite deposit characterized by a low
1331 grade of welding (Lf *l-gw*LA).
1332
1333 Figure 8: stratified primary volcanoclastic rocks, a) related to sedimentation by highly
1334 dilute ash-cloud (Np130; 6°54'16.09" S, 55°10'59.38" W) and, b) attribute to
1335 pyroclastic surge-type depositional condition from dilute currents (XU162;
1336 6°32'28.39" S, 52°25'26.07" W); see Fig. 2 for the outcrops location. Relative thin
1337 section microphotographs (c/d) showing micrometric shards. For the lithofacies
1338 description see the text and Table 1.
1339
1340 Figure 9: massive sedimentary rocks. a) The alternation of lithofacies *csG* and *mS*
1341 indicates changes in energy conditions of sedimentation belonging to a subaqueous-
1342 subaerial fan-delta interface (Np146; 6°42'58.24" S, 55°28'53.49" W); b) detail of
1343 centimeters ripples of Lf *mS* (Np89; 6°54'39.36" S, 55°26'12.28 W); c) Lf *csG* is also
1344 associated to Lf *xsSG* (see stratified rocks in section 6.2) (Np27; 8°08'18.43" S,
1345 54°54'37.33" W). d) Np27, e) Xu209 (6°13'55.26" S, 52°42'29.25" W), f) Np158
1346 (7°03'33.79" S, 55°24'11.84" W); the rounded and clast supported character of these
1347 lithofacies is linked with fluvial/alluvial deposition by debris-flow dominated
1348 processes; see Fig. 2 for the outcrops location. For a more detailed lithofacies
1349 description see the text and Table 1.
1350
1351 Figure 10: stratified sedimentary rocks. a) The quartzitic sandy cross-bedded
1352 lithofacies is interpreted as formed in fluvial channel or around margins of immature
1353 marine basins (?) (Xu 201; 6°16'12.95" S, 52°52'18.84" W); b) the cross-stratified
1354 water reworked lithofacies is linked with stream-dominated fluvial/alluvial settings
1355 (Np82; 8°03'40.79" S, 54°50'43.52" W); c) the silty sedimentation likely belong to a
1356 lacustrine environment characterized by small turbidities (Np158; 7°03'33.79" S,
1357 55°24'11.84" W); d) the top of the photographs shows the Lf *bChs* interpreted as
1358 inorganic precipitation of silica (chert) in a closed lake basin; white arrows show

1359 fragments of the chert deposit eroded by low-energy sandy stream flows or local
1360 lacustrine turbidites (Np90; 6°49'50.20" S, 55°28'15.47" W); see Fig. 2 for the
1361 outcrops location. For a more detailed lithofacies description see the text and Table 1.

1362

1363

1364 Figure 11: sketch of a wide (300 x 80 m) outcrop in the TMP (Np407; 6°40'35.21" S,
1365 55°21'14.63" W). The stratigraphic sequence is tilted showing sub-vertical contacts of
1366 the different deposits. The sequence is interpreted displaying at the base banded (or
1367 rheo-ignimbrite) and massive lava flows passing to fragmental deposits to the top. a)
1368 ignimbrite medium-grade welded; b) the diffuse-stratified lithofacies indicates tractive
1369 processes usually attribute to pyroclastic surge-type depositional condition from dilute
1370 currents; c) sedimentary clast-supported deposit ; d) non-welded lapilli to ash
1371 ignimbrite; e) banded lava o highly reomorphic ignimbrite (lava-like). For a more
1372 detailed lithofacies description see the text and Table 1.

1373

1374 Figure 12: classification diagrams for the Tapajos volcanics (TMP-V) and lava flow
1375 (TMP-LF). TAS diagram with limits of alkaline series from Kuno (1968), dashed line,
1376 and Irvine and Baragar (1971), solid line. AFM diagram with alkaline field from Irvine
1377 and Baragard (1971). SiO₂ vs K₂O classification diagram (Ewart, 1982). Literature
1378 values are from: VR (a) Vila Rozinho and MA (a) Moraes Almeida volcanic sequences
1379 from Lamarão et al. (2002); SF (b) Sobreiro Formation and SRF (b) Santa Rosa
1380 Formation from Fernandes et al. (2011).

1381

1382 Figure 13: REE and spider-diagrams of volcanics and lava flow rocks from the Tapajos
1383 region (TMP-V and TMP-LF). REE data are normalized to Chondrite I (CI; values
1384 from Ander and Ebihara, 1982) and trace elements are normalized to Mid Ocean Ridge
1385 Basalt (MORB; values from Hoffman, 1988). Literature values are from: VR (a) Vila
1386 Rozinho and MA (a) Moraes Almeida volcanic sequences are average values from
1387 Lamarão et al. (2002); SRF (b) Santa Rosa Formation from Fernandes et al. (2011)
1388 divided in -V volcanoclastics and -LF lava flow. Due to the lack of literature data,
1389 comparison of VR (a) and MA (a) is reported only for REE diagram.

1390

1391 Figure 14: tectonic affinity discriminant diagrams for the Tapajos volcanics (TMP-V)
1392 and lava flow (TMP-LF). Zr+Nb+Ce+Y (ppm) vs FeO_{tot}/MgO (wt.%) diagram. Yb vs

1393 Ta diagram. La/Yb vs Nb/La diagram. Th-Ta-Hf/3 diagram. Literature values are from:
1394 VR (a) Vila Rozinho and MA (a) Moraes Almeida volcanic sequences from Lamarão
1395 et al. (2002); SF (b) Sobreiro Formation and SRF (b) Santa Rosa Formation from
1396 Fernandes et al. (2011).

1397

1398 Figure 15: geochronological U-Pb data from Tapajos zircons. Average $^{206}\text{Pb}/^{207}\text{Pb}$ age
1399 (errors are calculated as 2σ) of the three samples. Probability density plot of $^{206}\text{Pb}/^{207}\text{Pb}$
1400 ages. Calculated concordia age for sample NP396 (lava flow) and NP183 (ignimbrite).

1401

1402 Figure 16: geochronological U-Pb data from Xingu zircons. Calculated concordia age
1403 for ignimbrite sample XU-08. Probability density plot of $^{206}\text{Pb}/^{207}\text{Pb}$ ages.

1404

1405 Figure 17: peoleogeographic reconstruction of the fissural and calderic volcanic activity
1406 during the Late-Paleoproterozoic in the southern part of the Amazonian craton. In the
1407 foreground is shown a section of a caldera and a post-caldera ignimbrite uplift that
1408 could facilitate the production of new sediments to be reworked and transported. The
1409 rising magma could form sporadic intra-caldera domes and volcanic centers as also
1410 shown in the background calderas. Reworked sediments can accumulate into volcano-
1411 tectonic depressions, which often collects intra-caldera lakes. In the background a
1412 fissure-fed volcanism is the responsible of the emission of lava flows and/or high-
1413 grade to rheomorphic ignimbrites. Fluvial deposits that occur throughout all
1414 successions represent periods of stream and river reworking. The area in punctuated by
1415 little scoria cones and maars that contribute to the amount of the fragmental products
1416 well represented in the study regions.

1417

1418

1419

1420

1421 Tables

1422

1423 Table 1: Summary of the main characteristics of volcanoclastic lithofacies of the
1424 primary and secondary products analyzed and their interpretation.

1425

1
2
3
4
5
6
7
8
9
10
11
12
13
14
15
16
17
18
19
20
21
22
23
24
25
26
27
28
29
30
31
32
33
34
35
36
37
38
39
40
41
42
43
44
45
46
47
48
49
50
51
52
53
54
55
56
57
58
59
60
61
62
63
64
65

1426 Table 2: Major and trace element bulk rock composition of Tapajos samples. Class
1427 identify the lithological features of the rocks: VC: volcanoclastic; I: ignimbrite; R:
1428 rhyolite; Type identify the geochemical affinity according to the granite classification
1429 (Zr+Nb+Ce+Y (ppm) vs FeO_{tot}/MgO (wt.%) diagram, Fig. 14): I is for I-type granites
1430 and A is for A-type granites; b.d.l. is below detection limits; Mg# is calculated as Mg^{2+}
1431 / ($Fe^{2+}_t + Mg^{2+}$); (*) major elements analyses already published in Roverato et. (2016).
1432
1433
1434
1435
1436
1437

Figure 1
[Click here to download high resolution image](#)

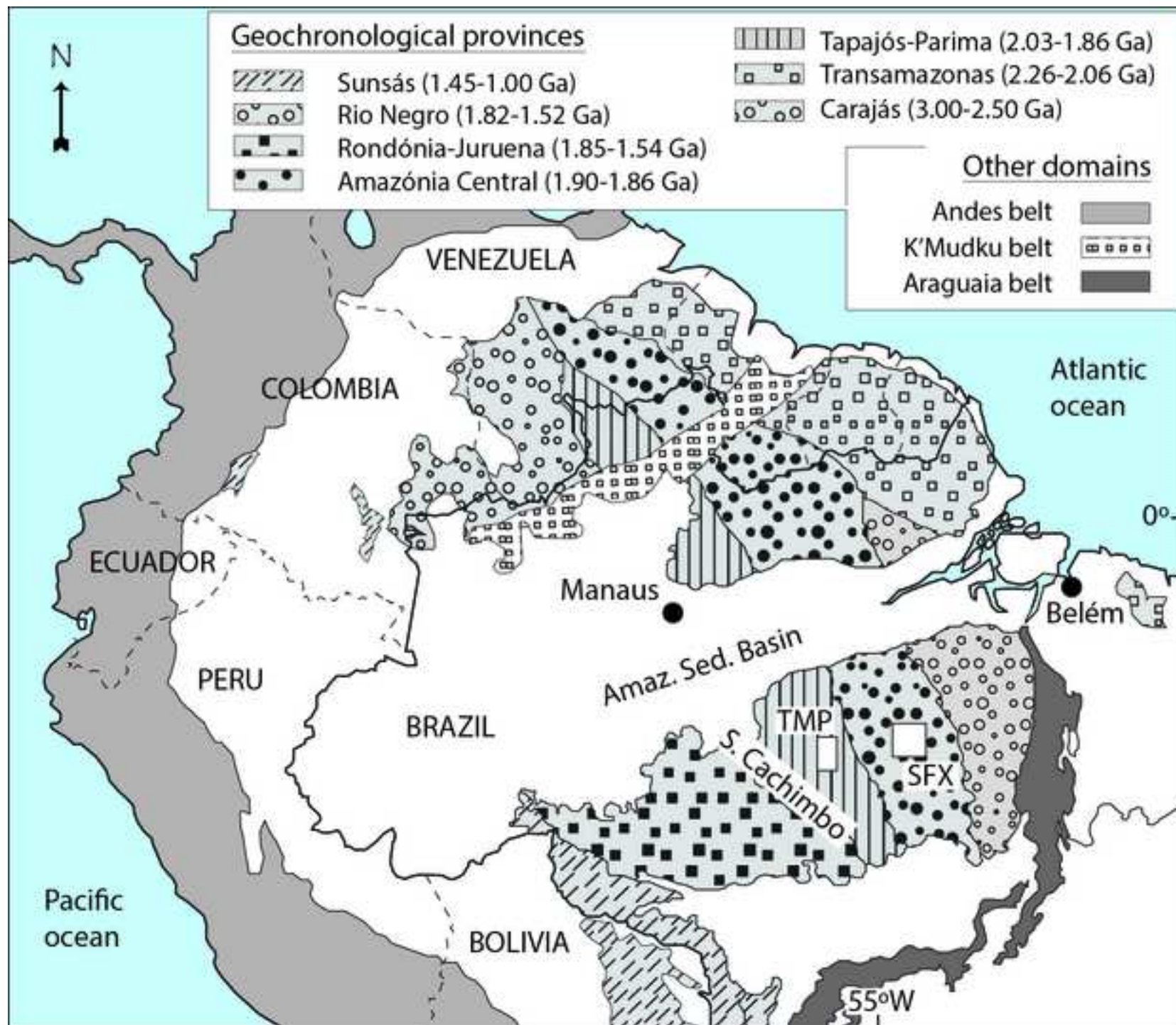


Figure 2

[Click here to download high resolution image](#)

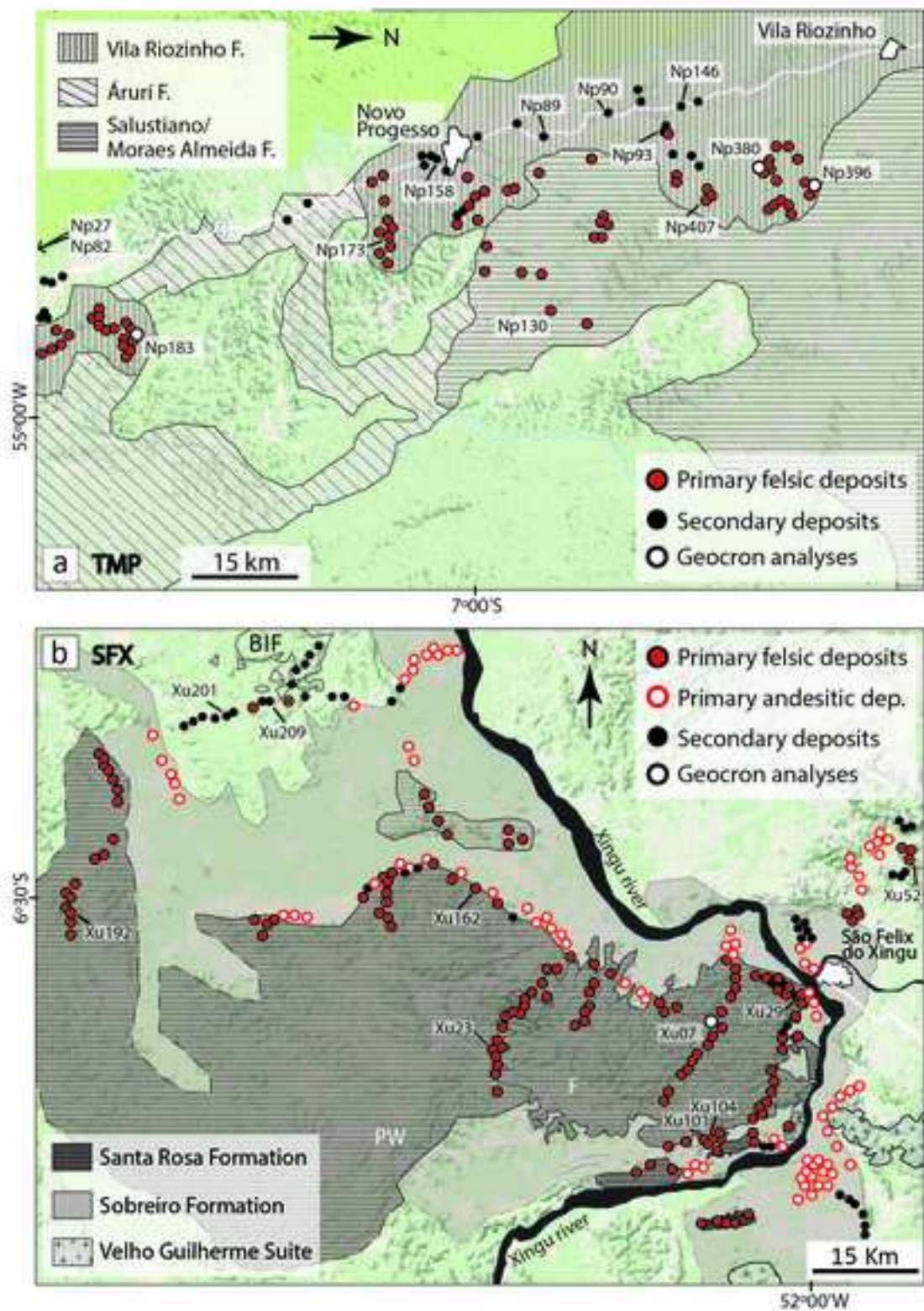


Figure 3
[Click here to download high resolution image](#)



Figure 4
[Click here to download high resolution image](#)

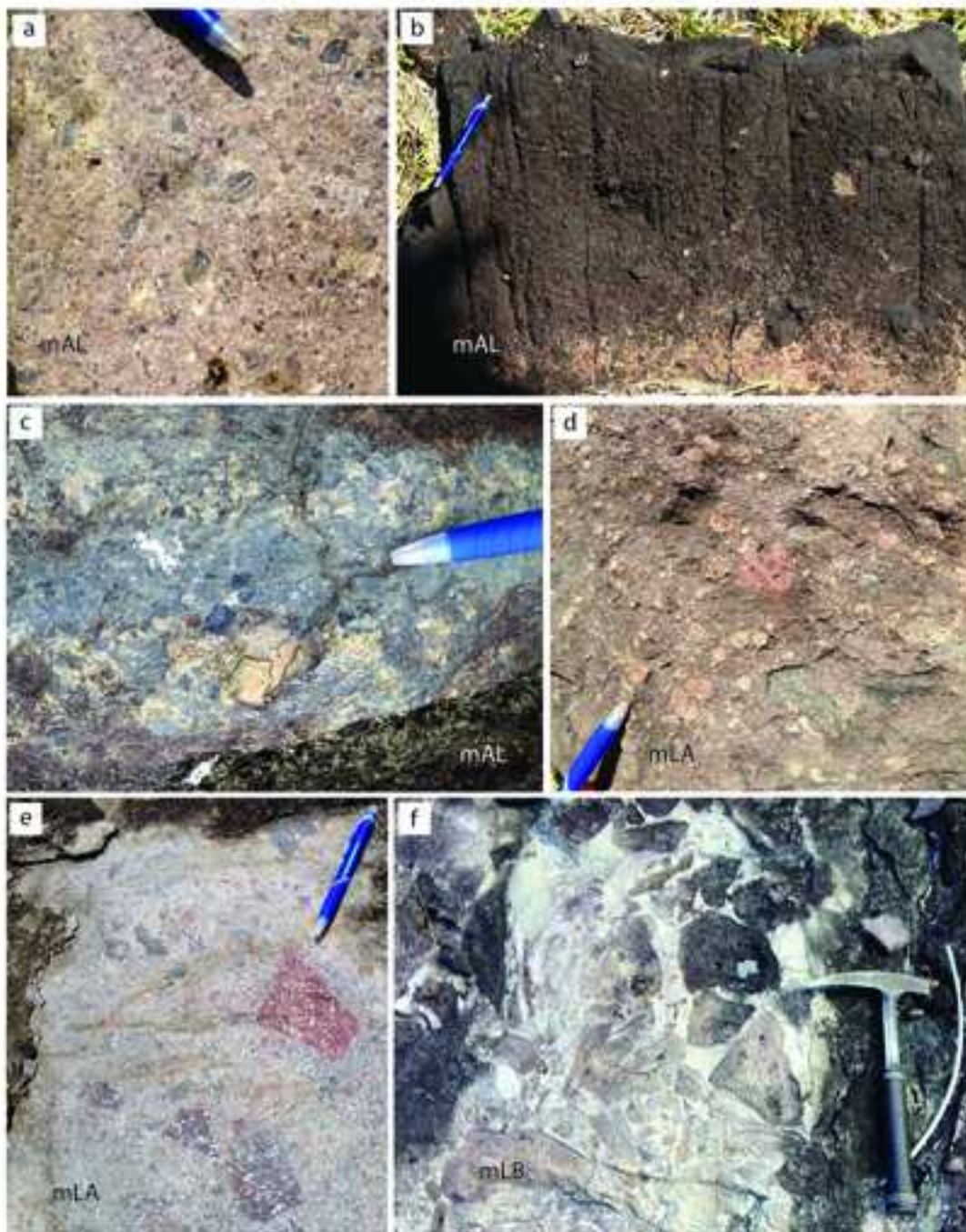


Figure 5
[Click here to download high resolution image](#)

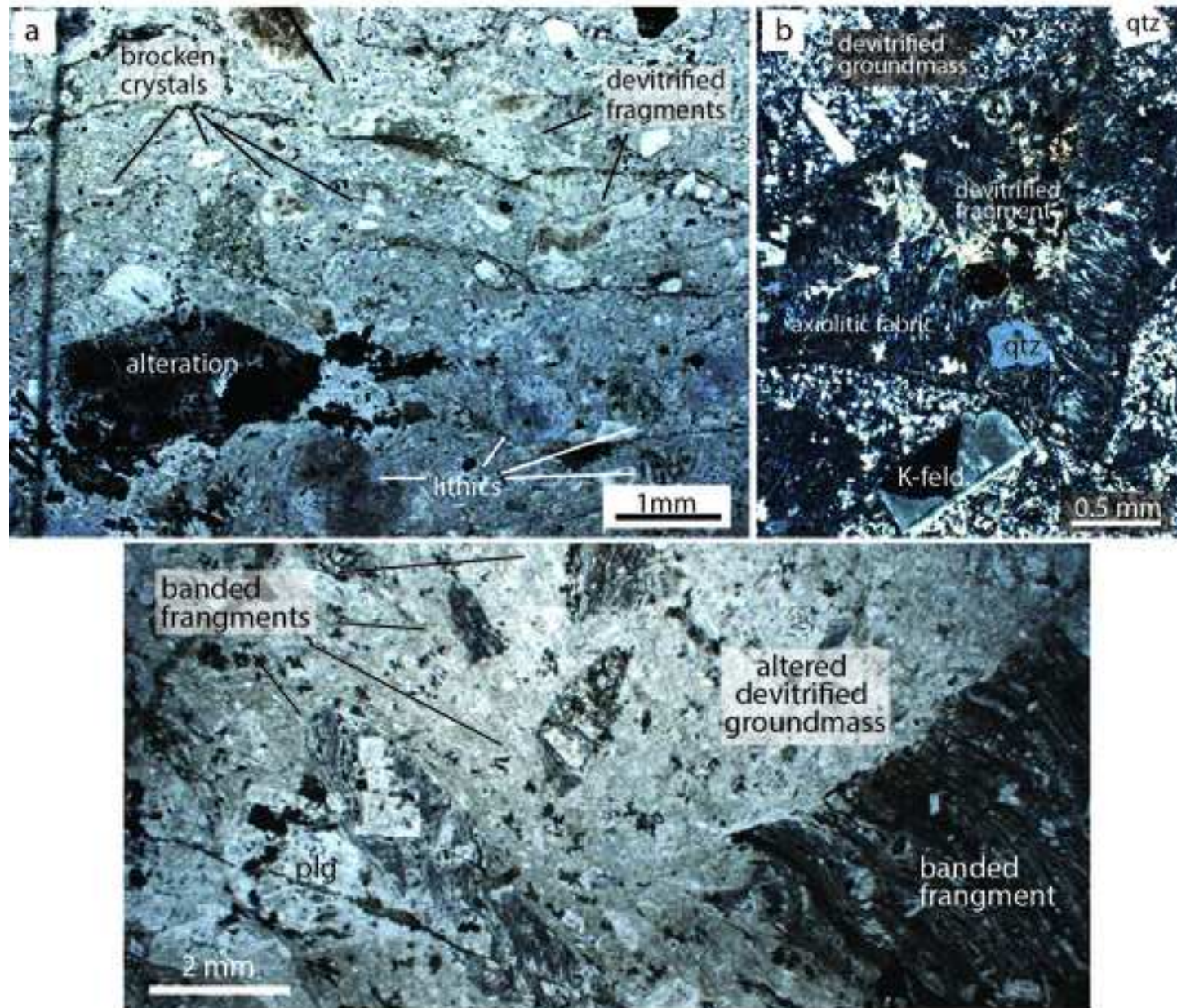


Figure 6
[Click here to download high resolution image](#)

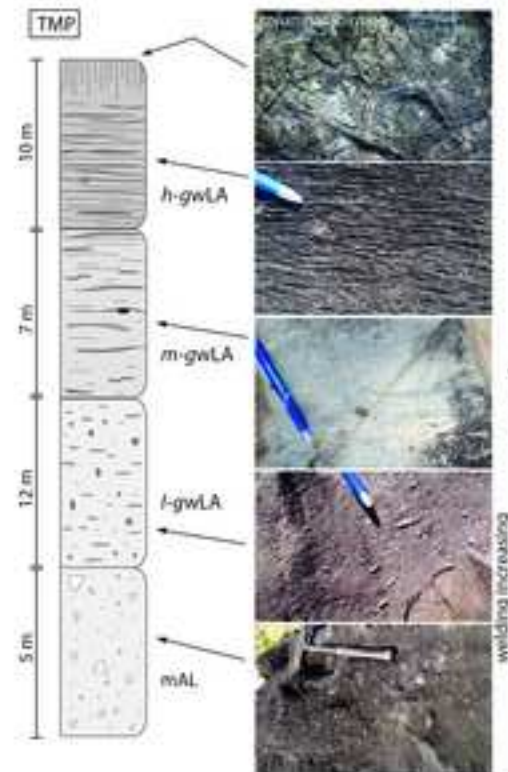


Figure 7

[Click here to download high resolution image](#)

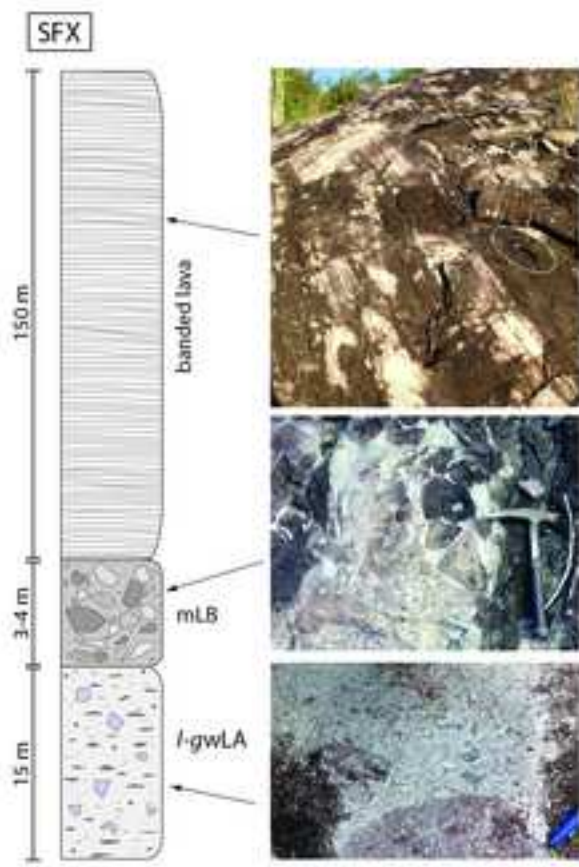


Figure 8
[Click here to download high resolution image](#)

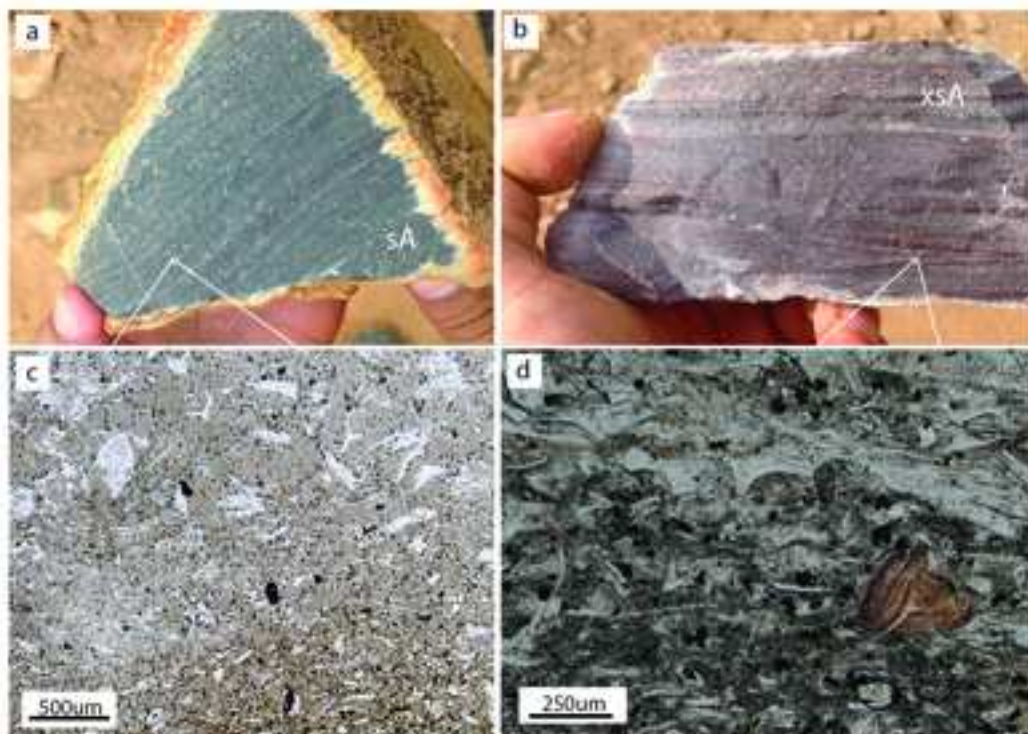


Figure 9

[Click here to download high resolution image](#)

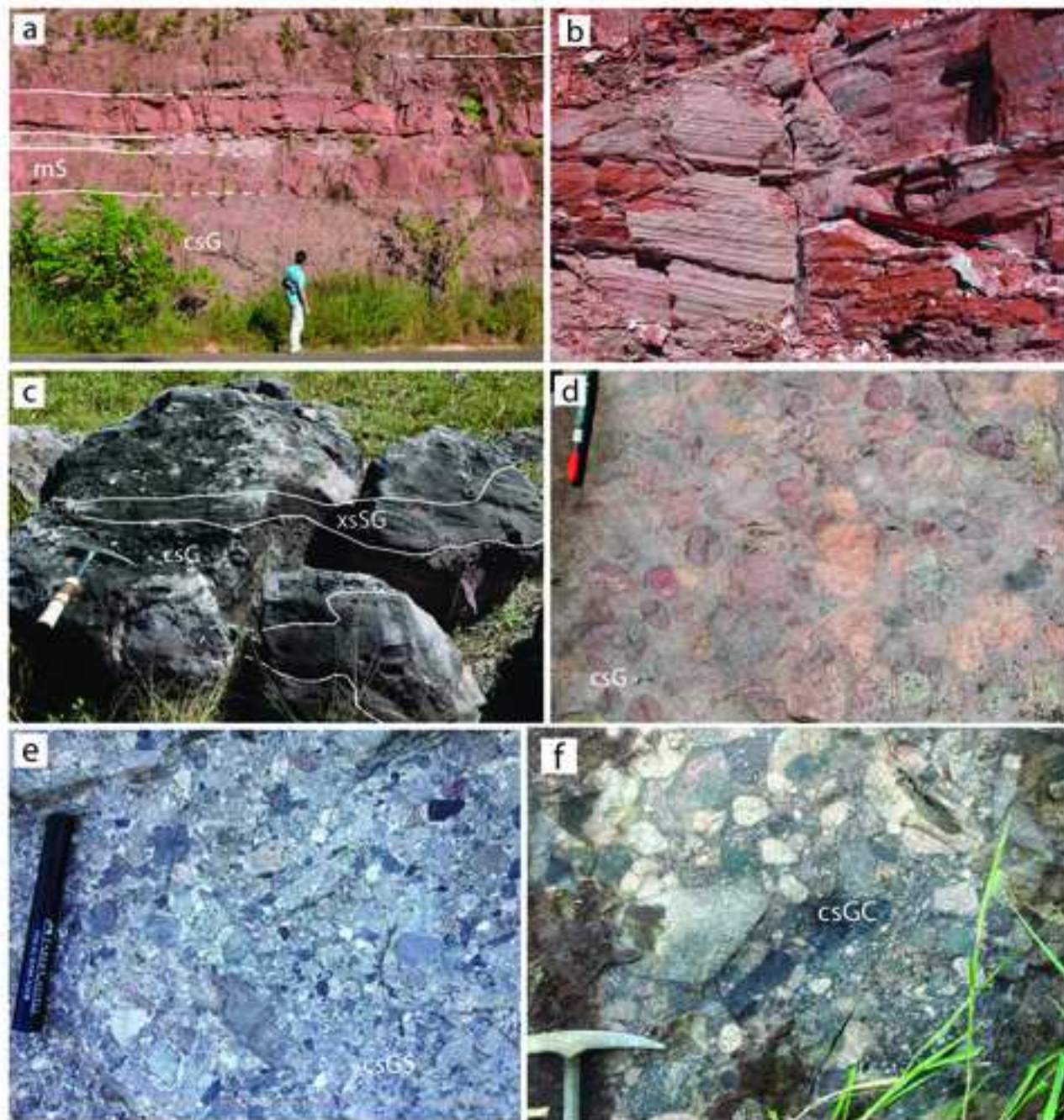


Figure 10
[Click here to download high resolution image](#)

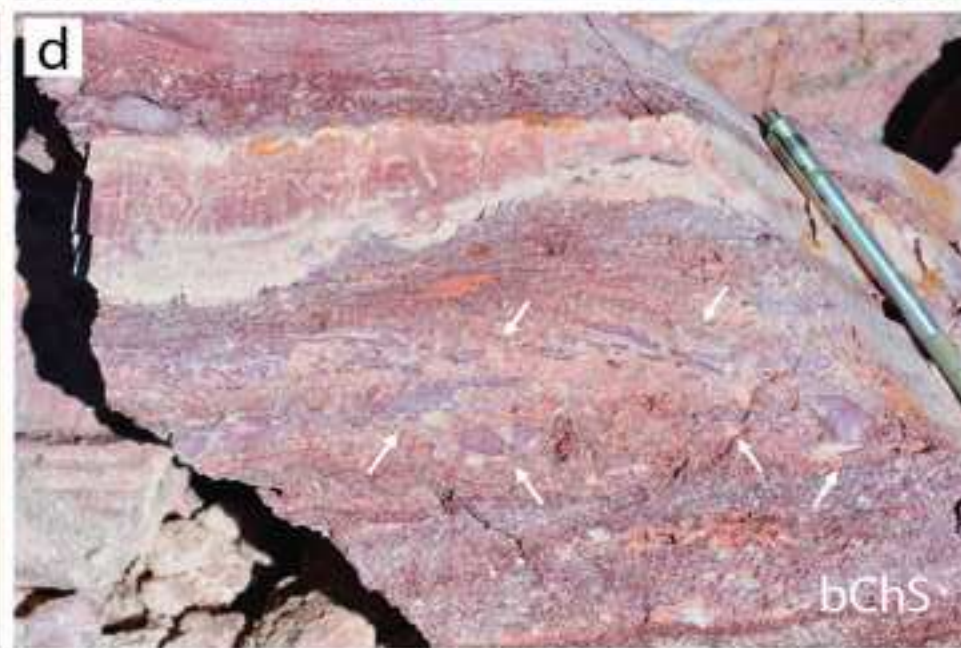
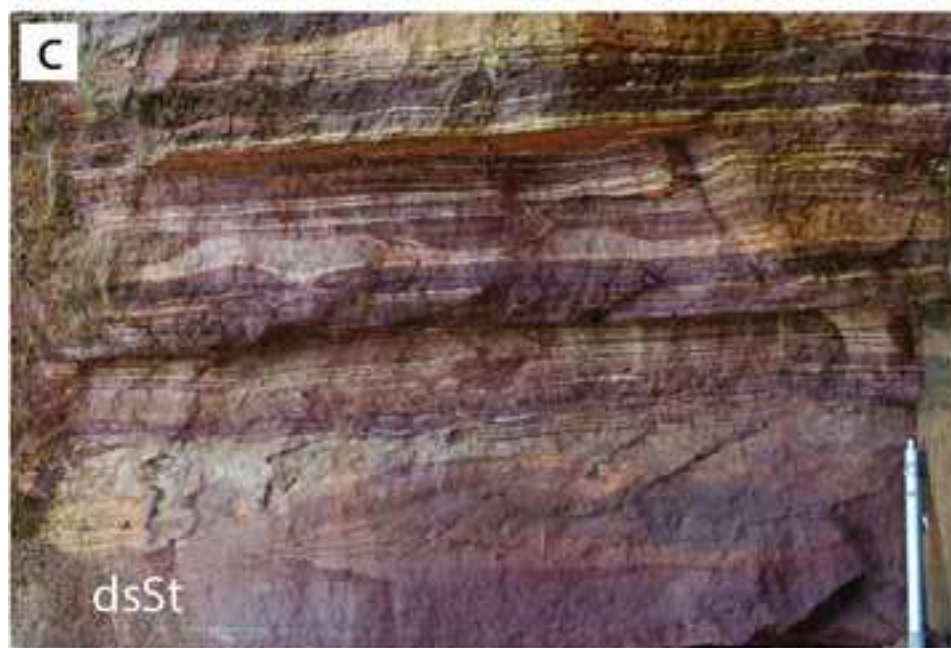


Figure 11

[Click here to download high resolution image](#)

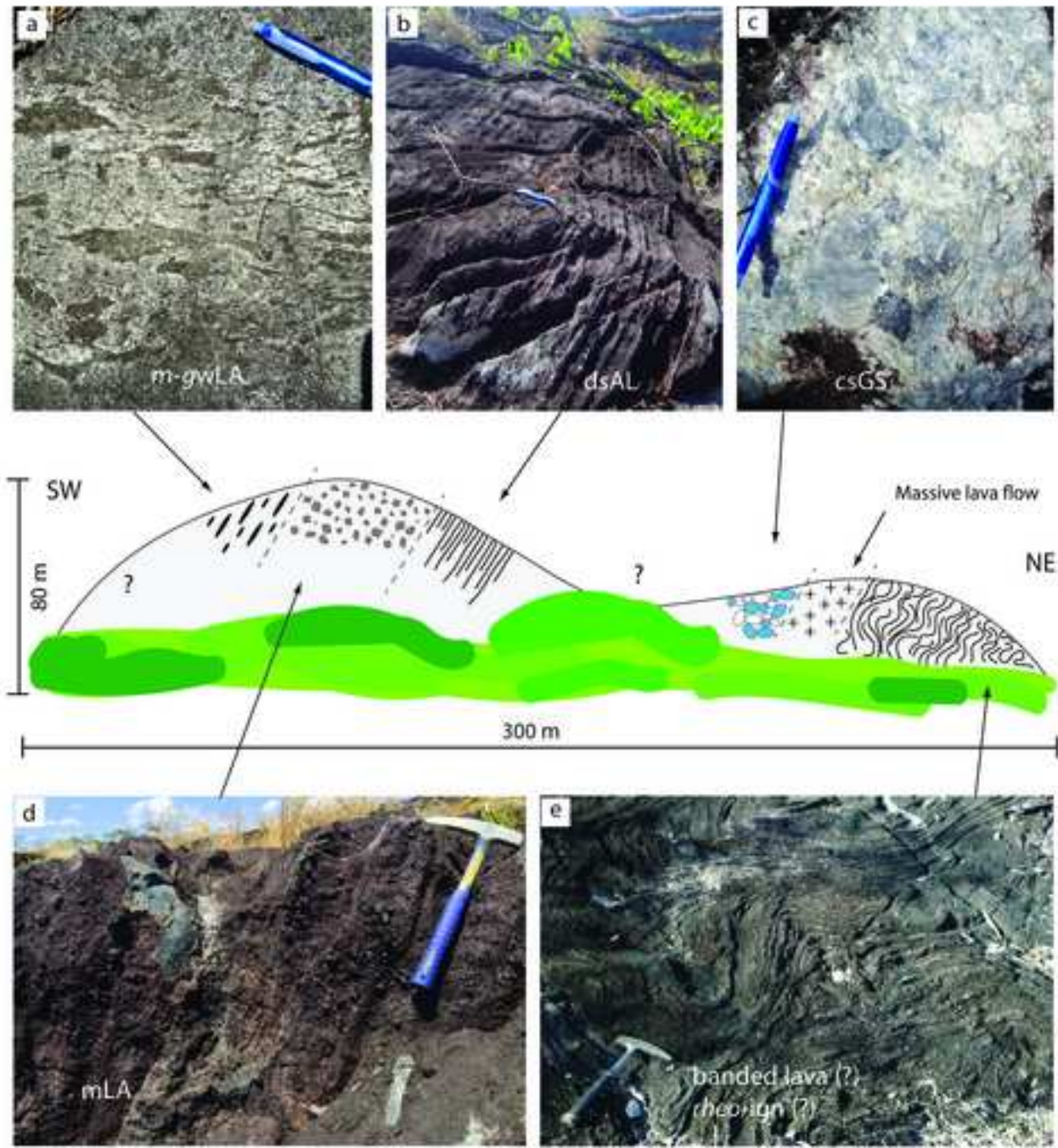


Figure 12

[Click here to download high resolution image](#)

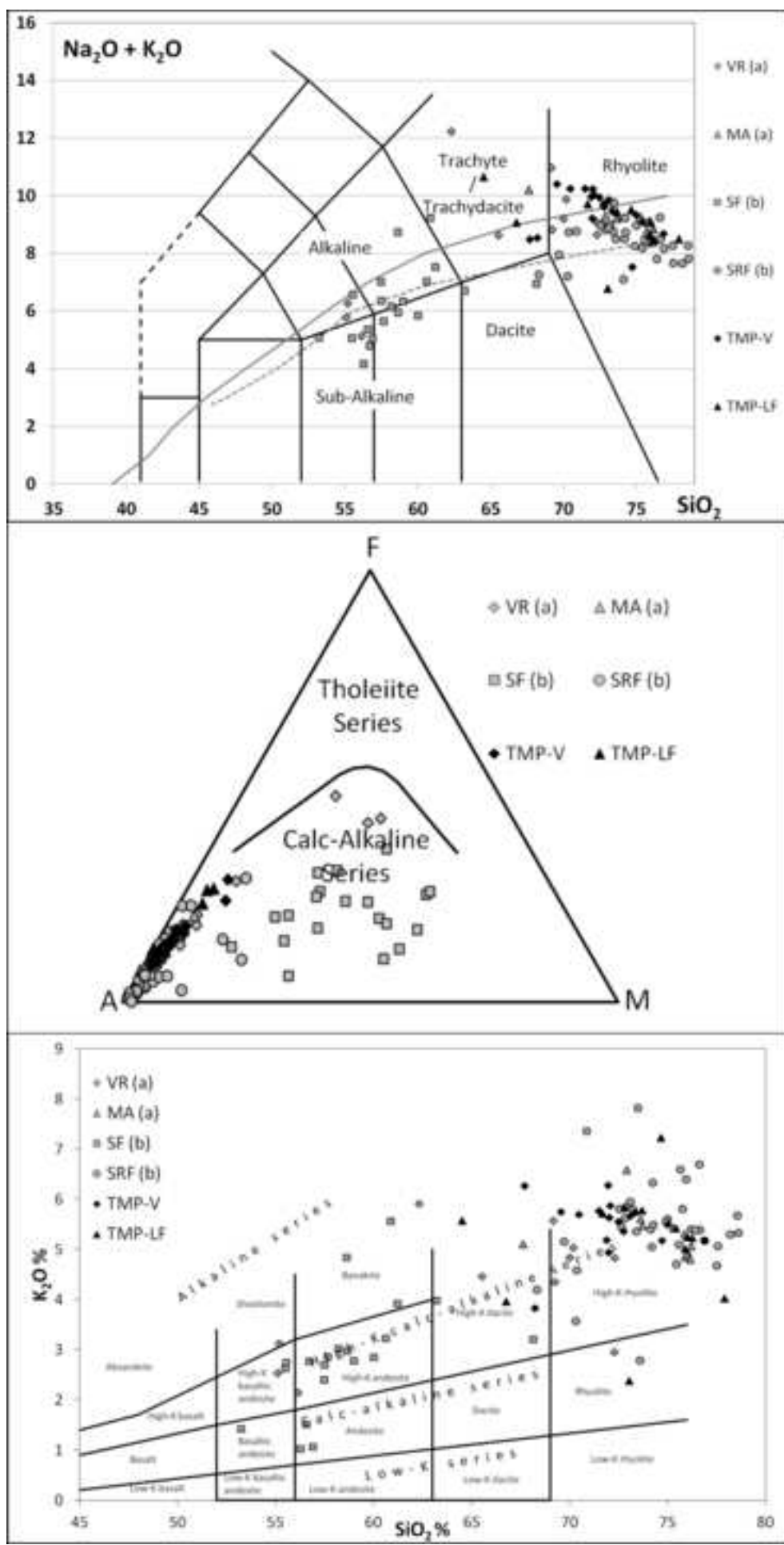


Figure 13

[Click here to download high resolution image](#)

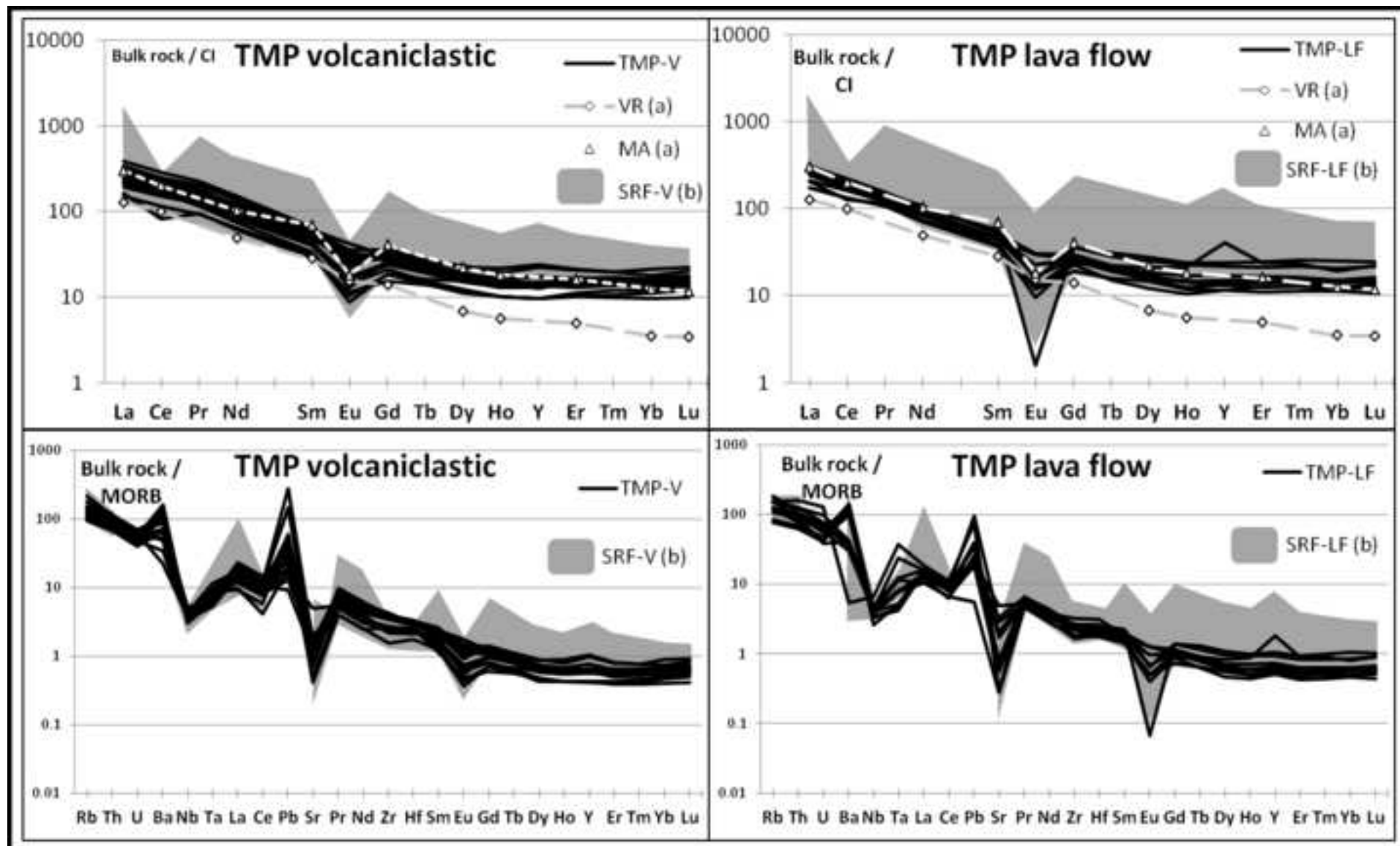


Figure 14
[Click here to download high resolution image](#)

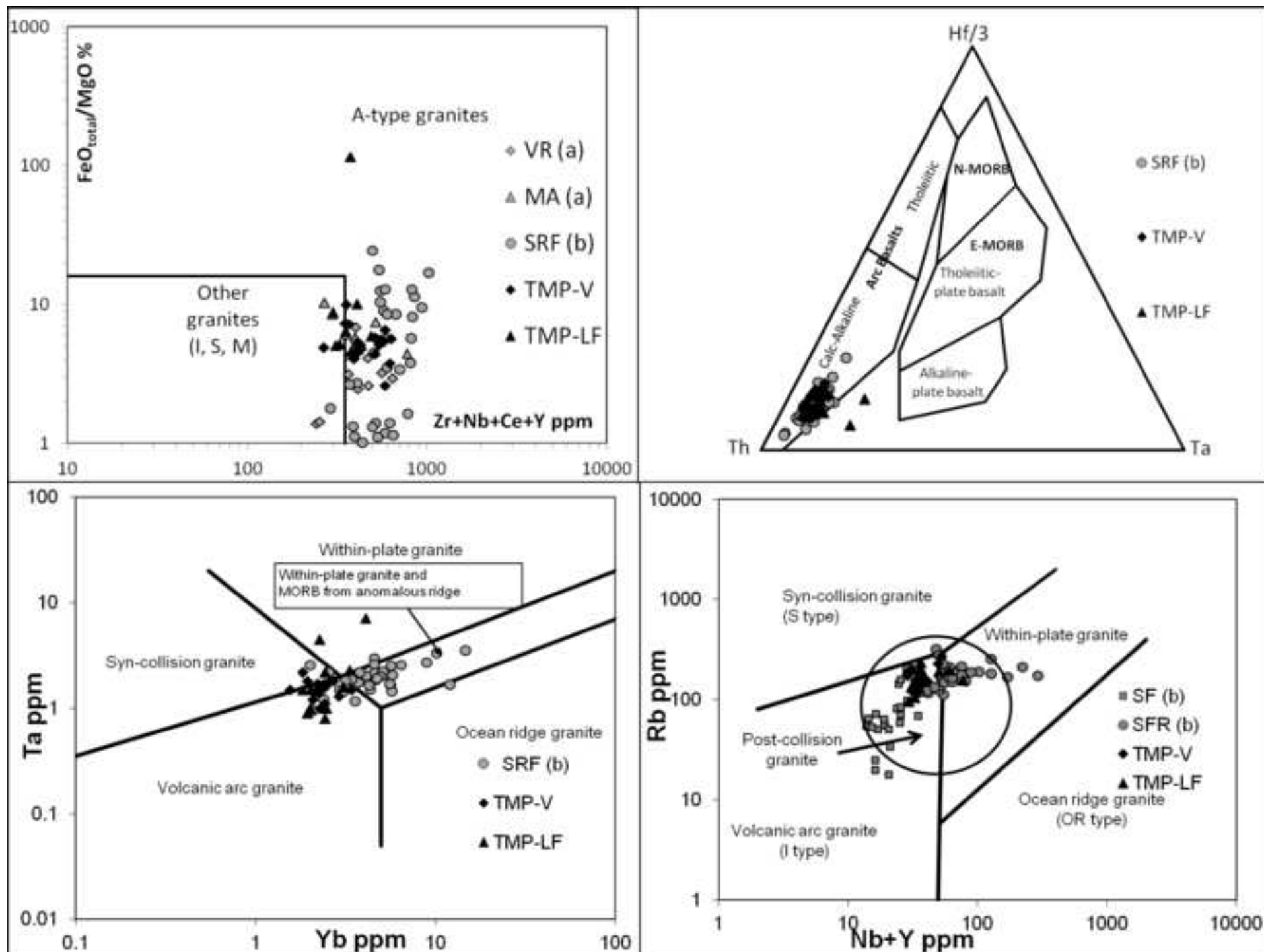


Figure 15

[Click here to download high resolution image](#)

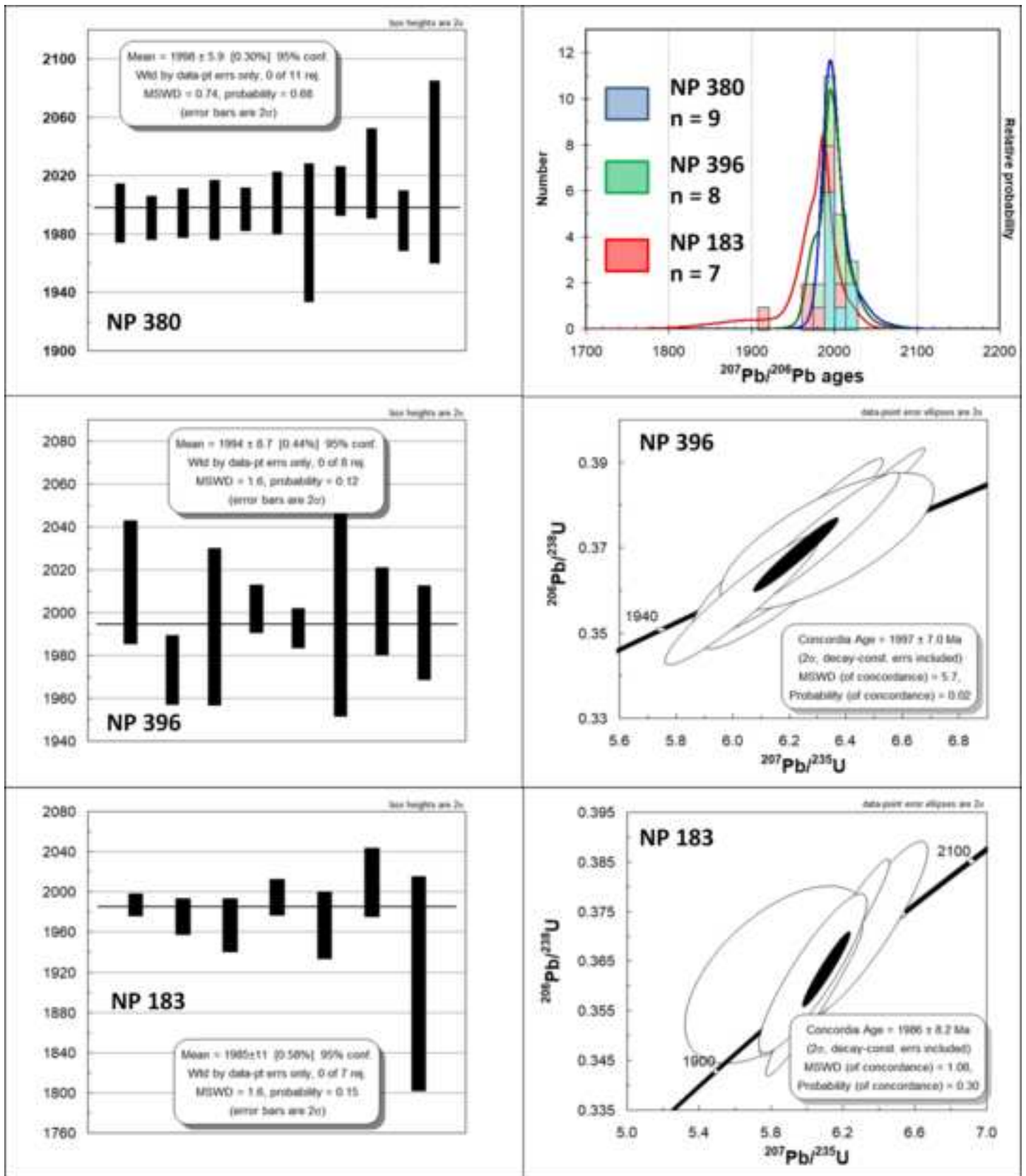


Figure 16

[Click here to download high resolution image](#)

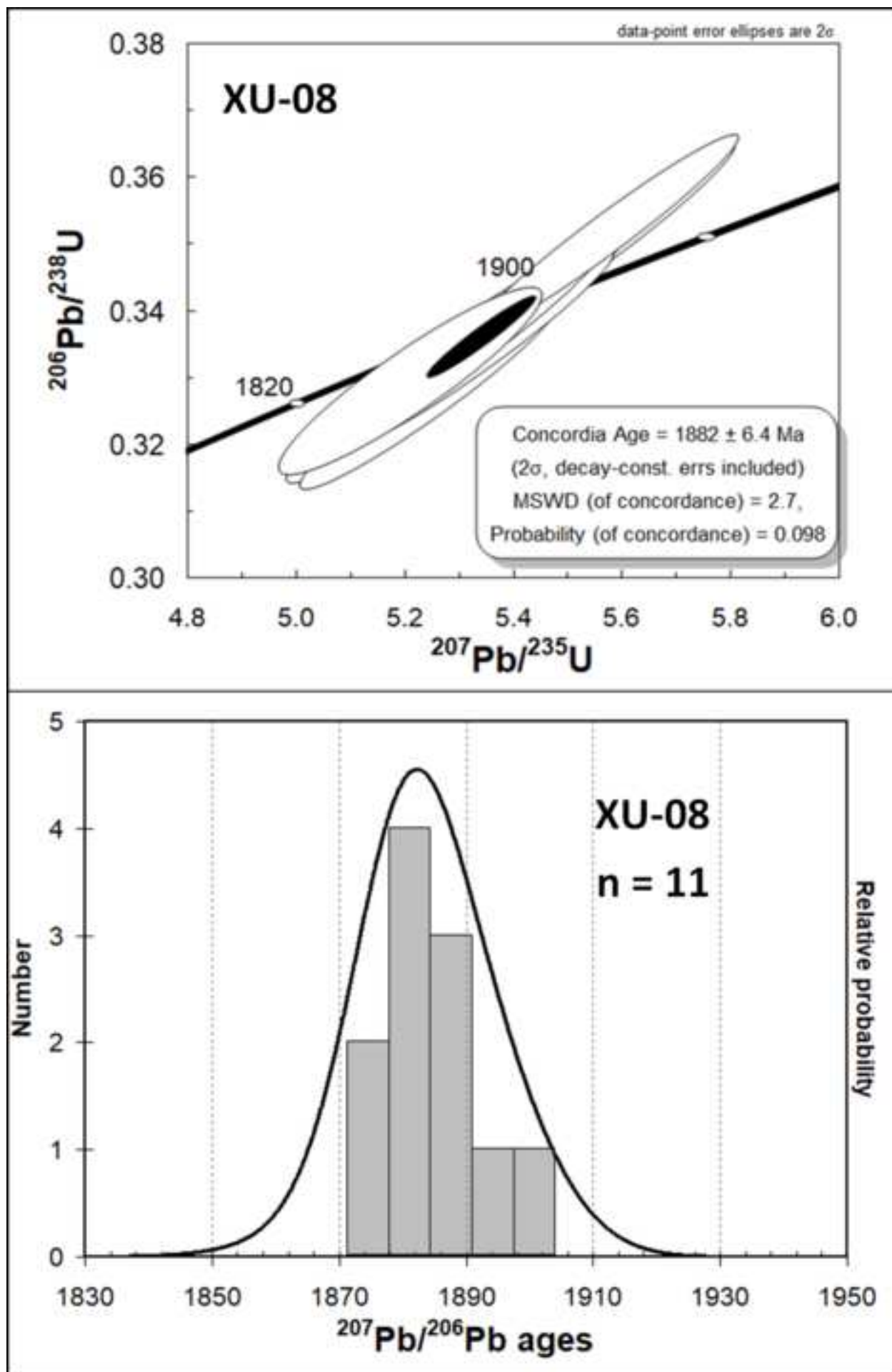


Figure 17

[Click here to download high resolution image](#)

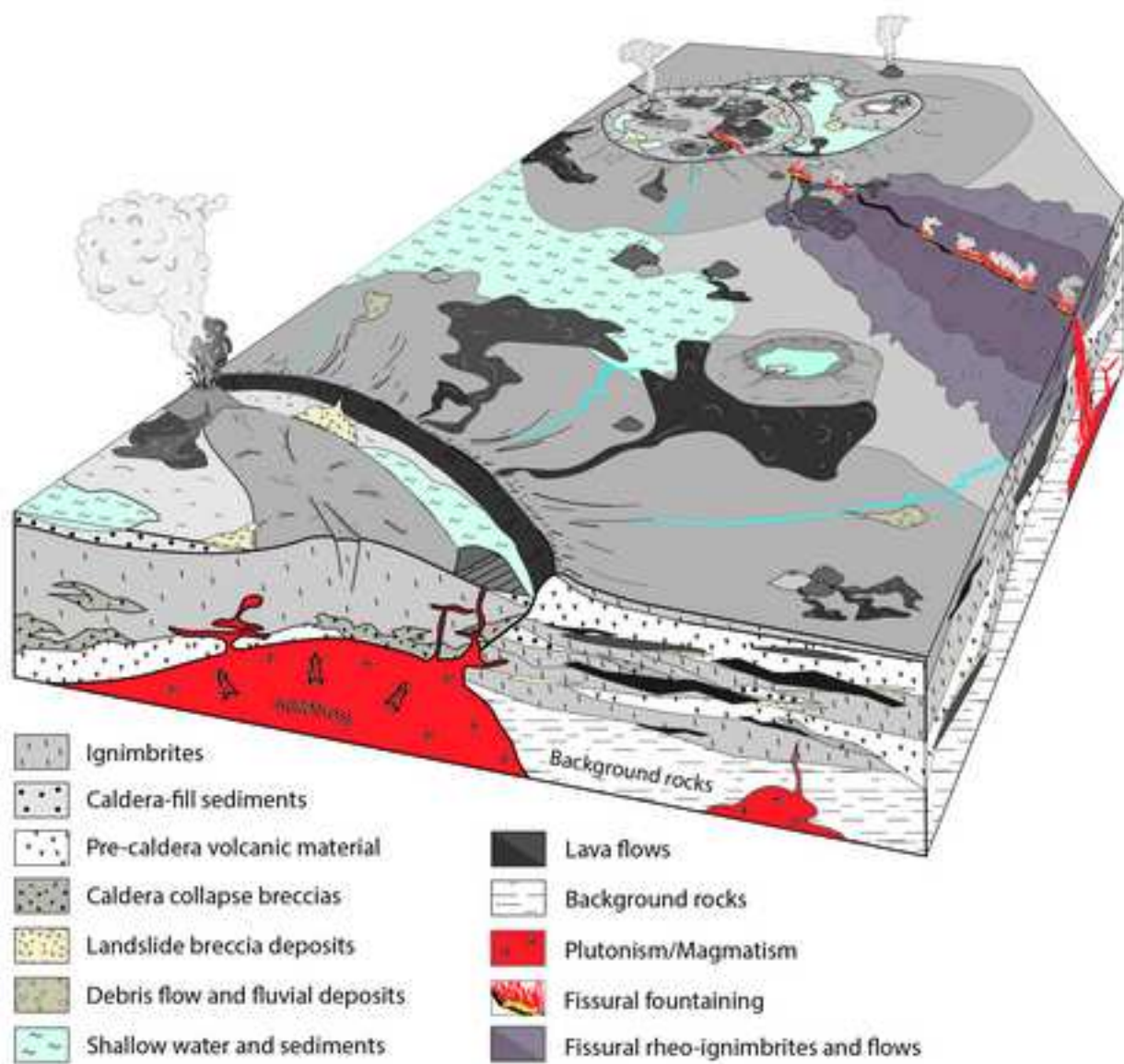


Table 1

		Lithofacies	Description	Interpretation	
Primary volcaniclastic rocks	Massive	mAL Massive Ash to Lapilli	Massive fine and coarse ash and variable fine to coarse lithic lapilli content. Devitrified fragments immersed. Brocken crystal (plg/prx) content. Moderate to bed sorting.	The massive fine aspect suggests deposition from a dilute pyroclastic density current (PDC). Brocken crystals confirm the fragmental character. Granular flow regime.	
		mLA Massive Lapilli and Ash	Massive, fine, fine to coarse and coarse devitrified lapilli immerse in ash matrix, less blocks immersed, maximum size 20-25 cm. Moderate sorting.	The massive aspect suggests deposition from a dilute PDC. The coarser character could be also related to proximal co-ignimbritic breccias as result of deposition by denser pyroclastic granular flows.	
		mLB, Massive Lapilli and Block	Massive, monolithologic, angular coarse lapilli and blocks (50-60 cm) immersed in lapilli matrix. Moderate sorting.	Basal auto-brecciation of lava flows and/or rheo-ignimbrite flows	
	Banded	Welded ignimbrites	l-gwLA, m-gwLA, h-gwLA low-, medium-, high-grade welded Lapilli and Ash	Massive, fine to coarse, moderately to strongly flattened devitrified lapilli (<i>fiamme</i>) varying from millimetric to 3–4 cm in size and lithic lapilli and ash. Crystal content. Clasts are immersed in a homogeneous ashy matrix. Low- to high-grade welded deposits. Eutaxitic texture. Moderate sorting.	The massive aspect suggests deposition from a pyroclastic density current. Welding is the result of post-depositional loading and are favored by low-viscosity pyroclasts that are promoted by high emplacement temperature, porosity and dissolved water.
			rheo-ign Rheoignimbrite (lava -like)	Layering of thin, dark and light bands and boudinaged <i>fiamme</i> . Parataxitic fabric displays subhorizontal bands and intricate small-scale intrafolial folds are present. The bands are deformed and flattened around lithic fragments and crystals.	The vitric fragments immersed in the welded ignimbrite distort and stretch up to the volcaniclastic flow becomes banded and starts to flow viscously.
	Stratified		sA Stratified Ash	Stratification of millimetric fine, devitrified, angular, sharply ash fragments.	The stratification is due to the bedding of shards fragments from a fall-out activity or from a dilute ignimbrite cloud.
			dsAL Diffusely stratified Ash to Lapilli	Diffusely stratified lithic and devitrified coarse ash and lapilli. Thickness of individual bedding surfaces ranges between few to several centimeters. Moderate sorting.	The diffuse stratification could indicate a flow boundary which is influenced by traction processes such as for pyroclastic density currents. Fall-out deposit (?).

Secondary volcaniclastic/epiclastic rocks		<p>xsA Cross-stratified Ash</p>	<p>Cross-stratified fine ash formed by angular and sharply devitrified fragments (shards). Cross stratification is discontinuous over decimeters in macro-scale and as well as over millimeters in microscopic scale. Well to moderate sorted.</p>	<p>The internal cross-stratification indicates a grain by grain deposition process from a turbulent current with a flow boundary zone dominated by traction mechanism. Pyroclastic density currents (surge).</p>
	Massive	<p>mS Massive Sand</p>	<p>Massive quartzitic sand, good sorting. No internal structures. centimeter ripples at the top of the strata.</p>	<p>Continental supply in a shallow, low energy, water sedimentary setting. Subaerial to sub-aqueous transition.</p>
		<p>csG Clast supported Gravel</p>	<p>Clast supported polymictic gravel with rounded clasts, good sphericity and sorting. Clasts are mainly characterized by massive and banded felsic lava fragments.</p>	<p>Clast-supported with minor matrix content is indicative of water flow. Shallow water to subaerial. Laminar debris-flow regime in a medial reaches of stream-dominated fluvial/alluvial fans.</p>
		<p>csGS Clast supported Gravel to Sand</p>	<p>Clast supported polymictic, gravel to coarse sand with sub-rounded/sub-angular fragments, low-medium shericity.</p>	<p>Clast-supported with minor matrix content is indicative of water flow. Deposition within a debris-flow dominated fluvial/alluvial environment.</p>
		<p>csGC Clast supported Gravel and Cobble</p>	<p>Clast supported polymictic, gravel and cobble with sub-rounded fragments (<20 cm), low-medium shericity, low-sorted.</p>	<p>Water removed the finer particles during transport and deposition. Deposition within a debris-flow dominated alluvial environment.</p>
	Stratified	<p>xsS Cross-stratified Sand</p>	<p>Low angle cross-stratified quartzitic sand, good sorting. Layers ranges between millimeters to centimeters.</p>	<p>Wave-induce structure in a coastal sub-aqueous marine-basin environment or fluvial channels environment in low energy regime.</p>
		<p>xsSG Cross-stratified Sand and Gravel</p>	<p>Fine to coarse sand and fine crystal-lithic gravel, poor sorting, layers ranges between millimeters to centimeters.</p>	<p>Low to medium energy processes. Hyperconcentrated flood in stream reworking setting.</p>
		<p>dsSt Diffusely layered Silt</p>	<p>Diffusely millimetric layered silt. Presence of ripples and low energy wave structures, good sorting.</p>	<p>Shallow water basin, sedimentation in lacustrine basin and/or ponds. Some turbidite sedimentation.</p>
		<p>bChS Bedded Chert (and Sand)</p>	<p>Bedded chert with local sand contribution. Thinly multicolor laminated deposit with < 1 mm microcrystalline quartz-dominate layers.</p>	<p>Precipitation of silica particles in closed lake basins in association with volcanic rocks and sandstone.</p>

Table 1

Table 2

Region	Tapajos										
Sample	NP – 079*	NP269a	Np380b	Np411c	NP-CO67*	NP - 080C	NP – 084A*	NP – 101*	NP - 123	NP - 156B*	NP - 159B
Class	VC	I	I	I	I	I	I	I	I	I	I
Type	A	A	A	A	A	A	A	A	A	A	A
XRF(%)											
SiO ₂	71.80	68.78	72.20	66.36	70.81	70.80	68.15	72.22	72.80	71.59	65.48
TiO ₂	0.34	0.32	0.35	0.72	0.40	0.40	0.48	0.32	0.31	0.36	0.58
Al ₂ O ₃	14.16	15.37	14.24	15.57	14.76	14.52	15.43	14.28	13.59	14.27	18.22
Cr ₂ O ₃	b.d.l.	b.d.l.	b.d.l.	b.d.l.	b.d.l.	b.d.l.	b.d.l.	b.d.l.	b.d.l.	b.d.l.	b.d.l.
FeOt	1.41	1.81	1.48	3.64	1.53	1.59	2.02	1.34	1.64	1.39	2.86
MnO	0.04	0.02	0.05	0.07	0.09	0.07	0.09	0.04	0.06	0.04	0.04
MgO	0.32	0.25	0.29	0.90	0.35	0.31	0.54	0.25	0.37	0.19	1.10
CaO	1.04	0.15	0.94	1.49	0.91	0.63	0.98	0.59	1.29	0.50	0.14
Na ₂ O	3.75	2.80	4.31	4.57	4.42	4.07	4.56	4.12	2.28	3.63	2.14
K ₂ O	5.73	6.00	5.32	3.73	5.71	5.77	5.63	5.60	5.04	5.60	6.06
P ₂ O ₅	0.04	0.06	0.05	0.22	0.07	0.06	0.09	0.04	0.06	0.04	0.10
LOI	0.99	3.51	0.32	1.30	1.03	1.48	1.34	0.82	2.59	1.28	3.42
Tot	99.62	99.07	99.55	98.57	100.08	99.70	99.31	99.62	100.03	98.89	100.14
Mg#	0.29	0.20	0.26	0.31	0.29	0.26	0.32	0.25	0.29	0.20	0.41
ppm											
V	20	11	11	34	14	17	29	13	28	10	38
Co	34	38	2	15	17	31	29	43	25	32	12
Ni	1.20	2.50	0.50	0.50	0.40	0.70	0.90	0.80	0.60	0.60	2.80
Zn	28	33	45	71	55	50	55	36	33	27	55
Rb	185	194	179	121	155	144	122	191	230	174	273
Sr	221	188	209	557	141	124	187	174	172	148	127
Y	15	15	22	23	21	22	21	22	37	15	35
Zr	267	241	277	245	361	371	440	276	224	272	401
Nb	13	15	14	12	12	13	11	14	13	14	18
Cs	2.10	1.20	2.30	3.0	2.70	2.10	2.80	2.60	15	2.10	7.1
Ba	673	945	1425	1536	2185	1813	2245	1365	898	1362	1202
La	53	67	56	57	64	72	79	51	70	38	72
Ce	100	98	111	110	117	136	149	99	126	50	129
Pr	10	12	11	11	13	16	18	11	13	8.4	16
Nd	34	40	39	42	47	53	63	37	45	28	54
Sm	4.9	5.8	6.4	6.9	7.3	7.9	9.0	6.0	8.0	4.3	8.2
Eu	0.58	0.80	0.98	1.52	1.83	1.58	2.36	0.90	1.23	0.64	1.67
Gd	3.6	4.1	5.0	5.4	5.4	5.4	6.1	4.8	7.2	3.0	6.7
Tb	0.52	0.56	0.73	0.76	0.73	0.78	0.76	0.69	0.99	0.50	0.97
Dy	2.69	3.0	3.9	4.1	3.8	4.0	3.9	3.6	5.4	2.92	5.6
Ho	0.57	0.57	0.74	0.76	0.78	0.75	0.77	0.73	1.21	0.57	1.06
Er	1.61	1.65	2.19	2.17	2.08	2.33	2.19	2.21	3.3	1.77	3.3
Tm	0.24	0.26	0.35	0.36	0.33	0.34	0.34	0.36	0.48	0.29	0.48
Yb	1.56	1.83	2.38	2.22	2.30	2.12	2.08	2.41	3.43	1.95	2.90
Lu	0.24	0.29	0.38	0.35	0.36	0.36	0.34	0.36	0.54	0.33	0.49
Hf	7.7	7.0	7.3	6.4	8.4	8.5	8.9	7.2	6.3	7.6	9.8
Ta	1.50	2.20	1.00	1.50	1.00	1.40	1.20	1.70	1.50	1.80	1.30
Pb	23	6.3	13	7.3	24	73	20	10	26	9.2	4.5
Th	21	21	19	13	15	17	14	20	22	20	21
U	4.9	3.4	5.0	2.90	3.3	3.6	2.90	4.0	2.90	4.6	4.8

Table 2: continued

Region	Tapajos										
Sample	NP - 175A	NP - 176*	NP - 178B*	NP - 179*	NP - 180*	NP - 183A*	NP - 184*	NP - 093	NP - 094	Np272a	Np393A
Class	I	I	I	I	I	I	I	VC	VC	R	R
Type	A	I	A	A	A	A	A	A	A	A	A
XRF (%)											
SiO ₂	73.86	75.93	70.86	72.53	69.73	71.25	70.99	60.36	62.46	71.13	76.57
TiO ₂	0.24	0.20	0.39	0.37	0.44	0.41	0.37	0.81	0.89	0.49	0.09
Al ₂ O ₃	13.40	12.71	14.62	14.44	15.20	14.65	14.54	15.42	16.36	14.44	11.93
Cr ₂ O ₃	b.d.l.	b.d.l.	b.d.l.	b.d.l.	0.01	b.d.l.	b.d.l.	0.01	b.d.l.	b.d.l.	b.d.l.
FeOt	1.10	0.78	1.57	1.67	2.03	1.57	1.75	5.70	4.97	2.52	1.16
MnO	0.07	0.06	0.07	0.09	0.09	0.09	0.08	0.11	0.09	0.06	0.03
MgO	0.11	0.16	0.29	0.30	0.36	0.24	0.30	3.24	1.68	0.51	0.01
CaO	0.50	0.34	0.88	0.65	0.88	0.56	0.68	4.59	3.03	1.57	0.14
Na ₂ O	3.78	3.46	4.70	4.38	4.49	4.54	4.97	2.79	3.11	4.27	4.39
K ₂ O	5.41	5.11	5.11	5.56	5.64	5.57	4.87	4.67	5.86	2.32	3.95
P ₂ O ₅	0.02	0.01	0.06	0.06	0.07	0.05	0.06	0.35	0.39	0.06	b.d.l.
LOI	1.15	0.88	1.28	0.85	1.00	0.81	1.07	1.37	0.64	1.38	0.58
Tot	99.64	99.64	99.83	100.90	99.94	99.74	99.68	99.43	99.48	98.75	98.85
Mg#	0.15	0.27	0.25	0.24	0.24	0.21	0.23	0.50	0.38	0.27	0.02
ppm											
V	b.d.l.	b.d.l.	14	b.d.l.	17	b.d.l.	10	112	59	11	b.d.l.
Co	36	34	32	40	28	37	38	27	24	2.60	63
Ni	0.50	0.50	0.80	2.30	3.4	1.50	0.60	19	0.50	0.60	1.10
Zn	20	32	45	51	46	52	60	55	73	55	33
Rb	156	158	136	153	136	133	127	116	169	105	196
Sr	54	46	179	120	115	78	103	614	620	321	33
Y	27	20	23	27	22	23	20	16	23	21	37
Zr	223	162	397	370	423	402	360	174	257	279	181
Nb	13	13	13	14	11	12	12	7.3	11	12	23
Cs	3.2	3.9	2.10	3.10	2.60	1.80	0.70	4.2	6.2	1.70	1.60
Ba	477	310	2021	998	880	746	2243	1362	2063	1363	75
La	45	36	75	76	91	80	64	35	53	59	72
Ce	92	70	140	138	174	151	122	70	106	108	133
Pr	11	8.3	15	15	20	18	14	8.5	13	11	14
Nd	39	29	57	52	69	64	52	31	48	38	45
Sm	6.7	4.7	8.9	8.1	10	9.4	7.9	5.2	7.6	6.5	8.1
Eu	0.72	0.49	1.98	1.36	1.63	1.51	1.84	1.35	1.71	1.27	0.09
Gd	5.3	3.7	6.9	6.9	6.6	6.6	5.7	4.3	5.5	4.9	7.0
Tb	0.81	0.59	0.76	0.87	0.92	0.91	0.78	0.57	0.81	0.70	1.14
Dy	4.7	3.7	4.5	4.3	4.4	4.6	4.0	3.0	4.3	3.7	6.8
Ho	0.90	0.72	0.86	0.91	0.80	0.83	0.82	0.56	0.82	0.69	1.31
Er	2.63	2.25	2.73	2.57	2.23	2.31	2.51	1.52	2.32	1.99	3.9
Tm	0.41	0.35	0.39	0.36	0.36	0.37	0.36	0.23	0.32	0.31	0.62
Yb	2.61	2.21	2.44	2.71	2.25	2.43	2.32	1.43	2.08	1.95	4.1
Lu	0.39	0.33	0.42	0.43	0.36	0.40	0.37	0.24	0.33	0.30	0.60
Hf	6.6	5.2	8.7	8.5	9.6	9.3	8.4	4.3	6.2	7.1	7.4
Ta	1.80	1.70	1.10	1.80	1.40	1.60	1.60	0.60	1.00	0.90	7.1
Pb	16	29	137	10	17	11	28	4.0	6.9	46	36
Th	17	18	17	16	16	17	17	6.1	11	13	30
U	3.4	4.4	3.5	3.9	3.5	3.7	4.0	1.30	2.10	3.4	9.1

Table 2: continued

Region	Tapajos									
Sample	Np405	Np406	NP - 039B	NP - 073	NP - 114	NP - 121	NP - 173*	NP - 175B	NP - 182C	
Class	R	R	R	R	R	R	R	R	R	
Type	A	A	A	A	A	A	I	I	I	
XRF (%)										
SiO ₂	73.67	69.79	65.32	72.82	63.80	75.09	75.58	75.03	74.44	
TiO ₂	0.33	0.45	0.86	0.31	0.74	0.27	0.20	0.22	0.22	
Al ₂ O ₃	13.09	14.72	16.61	13.84	17.99	13.16	12.96	13.46	13.50	
Cr ₂ O ₃	b.d.l.	b.d.l.	b.d.l.	b.d.l.	b.d.l.	b.d.l.	b.d.l.	b.d.l.	b.d.l.	
FeOt	1.33	1.78	3.27	1.29	3.30	1.01	0.99	0.96	1.23	
MnO	0.05	0.05	0.09	0.04	0.05	0.03	0.07	0.09	0.02	
MgO	0.26	0.30	0.51	0.28	0.70	0.10	0.19	0.19	0.14	
CaO	0.53	0.76	2.07	0.89	1.54	0.15	0.72	0.42	0.04	
Na ₂ O	2.25	3.87	4.99	3.61	5.02	3.78	3.21	3.69	3.56	
K ₂ O	7.13	5.57	3.88	5.71	5.51	5.19	5.18	5.39	4.92	
P ₂ O ₅	0.03	0.07	0.22	0.04	0.22	0.03	0.02	0.02	0.02	
LOI	0.55	1.26	1.50	0.75	1.45	0.95	1.49	0.83	2.09	
Tot	99.22	98.62	99.32	99.58	100.32	99.76	100.61	100.30	100.18	
Mg#	0.26	0.23	0.22	0.28	0.27	0.15	0.25	0.26	0.17	
ppm										
V	8	<8	55	14	83	18	<8	<8	<8	
Co	1.00	36	19	19	14	52	25	45	100	
Ni	0.40	2.40	2.20	3.60	1.90	0.60	0.70	0.70	1.30	
Zn	30	38	49	21	48	18	16	28	8	
Rb	232	194	96	200	153	190	156	158	133	
Sr	204	229	552	193	377	91	79	63	32	
Y	23	22	20	18	26	34	64	24	18	
Zr	272	336	228	246	265	245	173	191	189	
Nb	14	15	9.2	14	12	17	13	14	13	
Cs	2.20	2.50	2.10	2.30	1.30	3.1	4.1	3.5	1.10	
Ba	1634	1965	1615	534	1918	583	485	413	569	
La	63	62	50	57	58	62	48	41	41	
Ce	120	117	96	101	107	112	76	80	80	
Pr	12	12	11	11	13	13	10	10	10	
Nd	43	42	38	38	49	45	34	32	32	
Sm	6.6	6.9	6.4	5.6	7.5	8.4	5.4	5.8	5.4	
Eu	0.93	1.27	1.68	0.68	1.70	0.87	0.69	0.53	0.66	
Gd	5.2	5.3	5.1	4.5	5.8	7.0	5.0	4.6	3.8	
Tb	0.73	0.74	0.69	0.55	0.80	1.02	0.80	0.76	0.58	
Dy	3.9	4.0	3.8	3.0	4.4	6.1	5.2	4.2	3.6	
Ho	0.82	0.79	0.79	0.58	0.94	1.25	1.17	0.80	0.66	
Er	2.21	2.31	2.31	1.76	2.64	3.4	3.8	2.42	2.02	
Tm	0.35	0.34	0.34	0.27	0.39	0.52	0.56	0.36	0.31	
Yb	2.47	2.28	2.01	1.83	2.43	3.3	3.1	2.43	2.03	
Lu	0.39	0.37	0.30	0.26	0.35	0.53	0.54	0.36	0.33	
Hf	8	9.3	5.9	7.3	6.3	7.6	5.5	6.0	5.3	
Ta	1.00	4.5	1.00	1.50	0.80	2.30	1.60	2.20	1.50	
Pb	10	11	10	19	8.6	16	13	9.2	2.70	
Th	20	17	12	24	14	23	19	17	17	
U	4.5	3.9	2.90	5.4	3.2	6.9	5.0	4.2	2.70	

